



National Library
of Canada

Acquisitions and
Bibliographic Services Branch

395 Wellington Street
Ottawa, Ontario
K1A 0N4

Bibliothèque nationale
du Canada

Direction des acquisitions et
des services bibliographiques

395, rue Wellington
Ottawa (Ontario)
K1A 0N4

Your file / votre référence

Our file / notre référence

NOTICE

The quality of this microform is heavily dependent upon the quality of the original thesis submitted for microfilming. Every effort has been made to ensure the highest quality of reproduction possible.

If pages are missing, contact the university which granted the degree.

Some pages may have indistinct print especially if the original pages were typed with a poor typewriter ribbon or if the university sent us an inferior photocopy.

Reproduction in full or in part of this microform is governed by the Canadian Copyright Act, R.S.C. 1970, c. C-30, and subsequent amendments.

AVIS

La qualité de cette microforme dépend grandement de la qualité de la thèse soumise au microfilmage. Nous avons tout fait pour assurer une qualité supérieure de reproduction.

S'il manque des pages, veuillez communiquer avec l'université qui a conféré le grade.

La qualité d'impression de certaines pages peut laisser à désirer, surtout si les pages originales ont été dactylographiées à l'aide d'un ruban usé ou si l'université nous a fait parvenir une photocopie de qualité inférieure.

La reproduction, même partielle, de cette microforme est soumise à la Loi canadienne sur le droit d'auteur, SRC 1970, c. C-30, et ses amendements subséquents.

Canada

UNIVERSITY OF ALBERTA

Numerical Simulation of Non-Aqueous Phase Liquid Dissolution in Discrete
Rough-Walled Fractures

B^v

Leroy Charles Banack



A thesis submitted to the Faculty of Graduate Studies and Research in partial fulfillment of the requirements for the degree of Masters of Science.

DEPARTMENT OF GEOLOGY

Edmonton, Alberta
Spring 1996



National Library
of Canada

Acquisitions and
Bibliographic Services Branch

395 Wellington Street
Ottawa, Ontario
K1A 0N4

Bibliothèque nationale
du Canada

Direction des acquisitions et
des services bibliographiques

395, rue Wellington
Ottawa (Ontario)
K1A 0N4

Your file / Votre référence

Your file / Notre référence

The author has granted an irrevocable non-exclusive licence allowing the National Library of Canada to reproduce, loan, distribute or sell copies of his/her thesis by any means and in any form or format, making this thesis available to interested persons.

L'auteur a accordé une licence irrévocable et non exclusive permettant à la Bibliothèque nationale du Canada de reproduire, prêter, distribuer ou vendre des copies de sa thèse de quelque manière et sous quelque forme que ce soit pour mettre des exemplaires de cette thèse à la disposition des personnes intéressées.

The author retains ownership of the copyright in his/her thesis. Neither the thesis nor substantial extracts from it may be printed or otherwise reproduced without his/her permission.

L'auteur conserve la propriété du droit d'auteur qui protège sa thèse. Ni la thèse ni des extraits substantiels de celle-ci ne doivent être imprimés ou autrement reproduits sans son autorisation.

ISBN 0-612-10694-2

Canada

UNIVERSITY OF ALBERTA

RELEASE FORM

NAME OF AUTHOR: Leroy Charles Banack

TITLE OF THESIS: Numerical Simulation of Non-Aqueous Phase Liquid Dissolution
in Discrete Rough-Walled Fractures

DEGREE: Master of Science

YEAR THIS DEGREE GRANTED: 1996

Permission is hereby granted to the University of Alberta Library to reproduce single
copies of this thesis and to lend or sell such copies for private, scholarly or scientific
research purposes only.

The author reserves all other publication and other rights in association with the
copyright in the thesis, and except as hereinbefore provided neither the thesis nor any
substantial portion thereof may be printed or otherwise reproduced in any material
form whatever without the author's prior written permission.

(Signed)



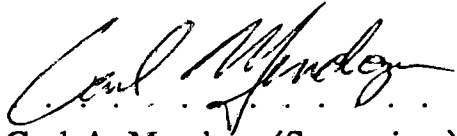
Leroy Charles Banack
12 Montclare Avenue
Camrose, Alberta
Canada, T4V 2K8

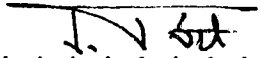
Date: 30/1/96.


UNIVERSITY OF ALBERTA

FACULTY OF GRADUATE STUDIES AND RESEARCH

The undersigned certify that they have read, and recommend to the Faculty of Graduate Studies and Research for acceptance, a thesis entitled **Numerical Simulation of Non-Aqueous Phase Liquid Dissolution in Discrete Rough-Walled Fractures** submitted by Leroy Charles Banack in partial fulfillment of the requirements for the degree of Masters of Science.

...  ...
Dr. Carl A. Mendoza (Supervisor)

...  ...
Dr. József Tóth (Examiner)

...  ...
Dr. Marv Dudas (Examiner)

Date: . 25/1/96.

Abstract

Residual NAPL trapped in fractured geologic media may act as a long-term source for dissolved groundwater contamination that is difficult to remediate. Understanding NAPL dissolution at the scale of a single fracture is the first step to a better representation of this process, as well as other related processes, in larger scale network models. Applying the information from these models will ultimately lead to improved transport predictions and remediation efforts.

The dissolution of NAPL is simulated using a finite-element model with 2-D triangular elements representing a discrete, rough-walled fracture. For fractures that are bounded by a permeable matrix, 1-D elements are used to model diffusion of contaminant into the surrounding matrix. The initial NAPL residual distribution in synthetic correlated aperture fields is created using invasion percolation techniques. Groundwater flow and aqueous-phase transport solutions are then calculated, with a concentration-dependent mass-transfer coefficient being used to represent partitioning between the NAPL and aqueous phase during dissolution. Detailed mass balance calculations are used to determine when individual elements containing residual have been dissolved and should be removed from the system. For comparison, simulations are performed where NAPL is randomly distributed throughout the fracture.

Sensitivity analyses are performed to delineate the qualitative relationships between fracture transmissivity, residual NAPL saturation, and the concentration of dissolved NAPL exiting the fracture. These relationships are very sensitive to not only the initial residual saturation, but also to the initial residual distribution, which is highly dependent on the synthetic aperture field. Because the correlated aperture

field is produced from a random set of aperture segments there is a large uncertainty in the behavior of NAPL dissolution.

At higher initial residual saturations the time for NAPL dissolution increases dramatically because the fracture transmissivity is reduced. This is because at these lower transmissivities less water is flowing through the fracture, the water in the fracture reaches saturation, and the dissolution process slows. In reality, the time for complete dissolution may be even greater since some of the water flow may bypass the fracture containing NAPL.

The effects of the mass-transfer coefficient, groundwater velocity and matrix porosity on remediation are also examined. Increasing groundwater head gradients, such as might occur during a pump and treat operation, are shown to have diminishing returns in terms of removing NAPL from the fracture by dissolution. If the surrounding matrix is permeable, NAPL can quickly diffuse into the matrix; however, after the residual NAPL has disappeared, dissolved NAPL begins to slowly diffuse back into the fracture. This greatly increases remediation times and may render current remediation strategies ineffective.

Acknowledgements

I would like to thank Carl Mendoza, my supervisor, who gave me everything I needed to complete my thesis. When I asked Carl, 'Do you have some time for me?', the answer was always, 'Yes.' It is this type of dedication that makes Carl an extraordinary instructor. The funding he provided me through NSERC was valuable, but not nearly as valuable as his time.

I would also like to thank the people who were in the Hydrogeology group at the University of Alberta during my time there. Thanks to Ben, Kent, Liane, Brent, Debashish, Joe, and John. I would especially like to thank Sheri and Darlene for their support and help; they turned a good experience into a great experience.

Finally, I would like to thank members of my family: my father; my mother; Michelle; Paul; Alexandra; Victoria; and Lorraine. I would also like to thank Lucas and Jason who provided me with numerous distractions, which probably delayed the completion of my thesis. I will always regard them as family.

Contents

| | | |
|----------|---|-----------|
| 1 | Introduction | 1 |
| 1.1 | Previous Studies | 2 |
| 1.2 | Research Outline | 5 |
| 2 | Theory and Methods | 6 |
| 2.1 | Conceptual Model | 6 |
| 2.2 | Fracture Aperture Distributions | 8 |
| 2.3 | Residual Distributions | 9 |
| 2.3.1 | NAPL | 10 |
| 2.3.2 | Capillary Pressure | 10 |
| 2.3.3 | Percolation Theory | 11 |
| 2.4 | Groundwater Flow | 12 |
| 2.5 | Aqueous Phase Transport | 14 |
| 2.6 | Dissolution | 15 |
| 2.6.1 | Mass Transfer Relationships | 15 |
| 2.7 | Numerical Formulation | 17 |
| 2.8 | Model Verification | 20 |
| 3 | Modeling Results and Analysis | 26 |
| 3.1 | General System Behavior | 26 |
| 3.1.1 | Simulation Description | 27 |
| 3.1.2 | Downstream Concentration | 29 |
| 3.1.3 | NAPL Saturation | 29 |

| | | |
|----------|--|-----------|
| 3.1.4 | Relative Transmissivity | 32 |
| 3.1.5 | Mass output | 33 |
| 3.2 | Sensitivity Analyses | 34 |
| 3.2.1 | NAPL Placement | 34 |
| 3.2.2 | Random Field versus Saturation Effects | 39 |
| 3.2.3 | Random Field Variance | 40 |
| 3.2.4 | Higher NAPL Saturations | 43 |
| 3.2.5 | Groundwater Flow and Mass Transfer Coefficient | 52 |
| 3.3 | Monte Carlo Results | 56 |
| 3.3.1 | Mass output | 56 |
| 3.3.2 | Relative Transmissivity | 62 |
| 3.4 | Permeable Matrix | 67 |
| 4 | Conclusions | 69 |
| 4.1 | Implications | 71 |
| | References | 73 |

List of Figures

| | | |
|-----|--|----|
| 2.1 | Conceptual model of a contamination scenario. After <i>Schwille</i> (1988). | 7 |
| 2.2 | An example of different scales of observation at a contaminated site. | 8 |
| 2.3 | A sample log-normal aperture distribution. | 9 |
| 2.4 | Diagram showing the variables used in calculating the volumetric flow rate through a pair of parallel plates. | 13 |
| 2.5 | Conceptualization of processes and boundary conditions for the numerical model for various stages of the modeling. | 19 |
| 2.6 | Numerical model compared to the analytical solution for a simple advection-dispersion problem. | 23 |
| 2.7 | Numerical model compared the analytical solution for a simple advection-dispersion problem. | 24 |
| 3.1 | A series of snapshots showing the dissolution simulation that is discussed in this section. | 28 |
| 3.2 | Concentration versus time curve for a single dissolution simulation. . | 30 |
| 3.3 | NAPL Saturation versus time curve for a single dissolution simulation. | 31 |
| 3.4 | Relative Transmissivity (for water) curve for a single dissolution simulation. | 32 |
| 3.5 | Mass-output curve for a single dissolution simulation. | 33 |
| 3.6 | Mass-output for three saturation levels created with invasion percolation methods for a single fracture with the same aperture distribution. | 35 |
| 3.7 | Mass-output for three saturation levels created with invasion percolation methods for a single fracture with the same aperture distribution. | 37 |

| | | |
|------|--|----|
| 3.8 | Cross-sections through a residual distribution for invasion percolation and random residual assignment. NAPL is shown in grey and water fills the rest of the fracture. | 38 |
| 3.9 | Mass output versus time for two distribution created using invasion percolation on three different random fields. | 40 |
| 3.10 | A cross-section through two fractures that share the same initial aperture distribution; however, the variance of each one has been modified. The black cross-section has a variance of 0.75 while the grey cross-section has a variance of 2.25, but both have a mean aperture of about 30 microns. | 41 |
| 3.11 | Two simulations showing the mass output of the two fractures that differ only by the variance (V) of their aperture distributions. | 42 |
| 3.12 | Mass-output for four saturation levels created with invasion percolation methods for a single fracture (the same aperture distribution). | 43 |
| 3.13 | Mass-output for four saturation levels created with random percolation methods for a single fracture (the same aperture distribution). | 44 |
| 3.14 | Semi-log plot of the relative transmissivity of the fracture versus the volumetric NAPL saturation. The simulations shown here used NAPL distribution created by invasion percolation. | 46 |
| 3.15 | Semi-log plot of the relative transmissivity of the fracture versus the volumetric NAPL saturation. The simulations shown here used NAPL distribution created by random residual assignment. | 48 |
| 3.16 | Semi-log plot of the relative transmissivity of the fracture versus the volumetric NAPL saturation. The simulations shown here used NAPL distribution created by invasion percolation and all distribution have been modified so the initial NAPL saturation is 40% in all cases. | 49 |
| 3.17 | Time for NAPL dissolution versus the initial NAPL saturation. The cross sections show the NAPL position for the invasion percolation case at various points on the curve. | 51 |

| | | |
|------|--|----|
| 3.18 | Areal saturation plots for two similar simulations with different initial areal saturations. Shading indicates NAPL. | 53 |
| 3.19 | Time for NAPL dissolution versus the gradient across the fracture. | 55 |
| 3.20 | Downstream mass output versus time. Black and grey lines shown an arbitrary separation. | 58 |
| 3.21 | Downstream mass output versus volumetric saturation of the wetting phase. Black and grey lines shown an arbitrary separation. | 60 |
| 3.22 | Two conceptual cases on how NAPL is located within a fracture. The bottom grid shows what the areal saturation would look like in plan view. | 61 |
| 3.23 | Downstream mass output versus volumetric saturation of the wetting phase. Two example realizations are highlighted. | 62 |
| 3.24 | Downstream mass output versus time. Two example realizations are highlighted. | 63 |
| 3.25 | Initial residual distribution for cases A and B. | 63 |
| 3.26 | Cross sections taken through cases A and B. | 64 |
| 3.27 | The relative transmissivity curve from the Monte Carlo analysis. The same black and grey separation of the curves is used. | 65 |
| 3.28 | Relative transmissivity curves where the groundwater velocity and the mass transfer coefficients are varied. | 66 |
| 3.29 | Plot of NAPL dissolution time versus matrix porosity. | 67 |

List of Tables

| | | |
|-----|---|----|
| 2.1 | Physical properties of the NAPL used. | 10 |
| 2.2 | Parameters used in numerical model for comparison with the LINE2D analytical solution. | 22 |
| 2.3 | Parameters used in numerical model for comparison with example from <i>Powers et. al.</i> (1991). | 25 |
| 3.1 | Parameters used in numerical model for the example simulation. . . . | 27 |
| 3.2 | Parameters used for Monte Carlo simulations | 57 |

Chapter 1

Introduction

The use of non-aqueous phase liquids (NAPLs) by industry following World War II has become very common. Unfortunately, contamination of geologic material with these chemicals has also become common. The spilling of NAPL onto the ground surface leading to subsurface contamination can occur during NAPL production, transport, storage and disposal.

Common NAPLs, such as chlorinated solvents, have low aqueous solubilities. For example, trichloroethene (TCE) has a solubility of 1100 *mg/l* (Flick, 1985). However, the maximum allowable limits imposed by government agencies tend to be much lower. The drinking water quality standard in the United States for TCE is 0.005 *mg/l* (VanderLeeden *et al.*, 1990). Like TCE, many of these liquids are extremely toxic. This toxicity, combined with the fact that they can contaminate large volumes of water because of their low solubilities, makes NAPLs a serious threat to ground water resources.

When a NAPL is spilled a portion of the liquid may percolate down through the unsaturated zone. If it reaches the saturated zone the NAPL will continue its downward migration providing that it is denser than water (e.g., a dense NAPL or DNAPL). The NAPL will preferentially travel through highly permeable zones, such as fractures. A certain amount of the NAPL will be left behind in the porous and fractured media following this migration. This residual NAPL may act as a long-term source for groundwater contamination and be difficult to remediate due to slow

dissolution mechanisms and the inaccessible nature of fractures.

The objective of this thesis is to use a numerical model to investigate the theoretical small-scale dissolution behavior of NAPL residual in discrete fractures. The dissolution behavior of NAPL in a discrete, synthetically-generated, rough-walled fracture is simulated. Gaining an understanding of this dissolution process at the small scale will lead to better representations of this process, as well as other related processes such as dissolution in porous media, in larger-scale models. Ultimately this will lead to better predictions at contaminated sites, which could lead to improved remediation efforts. The methodology used for this investigation is given following a review of some previous work in this area.

1.1 Previous Studies

The principles of NAPL migration in the subsurface have been described by *Schwille* (1981; 1988). His theories and laboratory work involving immiscible fluids and porous media are the framework upon which most similar research is based. *Schwille* (1981) does not address the subject of dissolution; he assumes the NAPL is a perfectly immiscible fluid. However, *Schwille* (1988) does discuss aqueous-phase dissolution and migration of NAPLs. Interest in NAPL dissolution as a contamination problem has been growing steadily over the last few years. For some time it has been realized that NAPL in the subsurface can partition to the aqueous phase and be a source for long-term groundwater contamination (*Schwille*, 1988; *Mackay et al.*, 1985). The problem of describing and modeling this dissolution process has been a subject of debate.

Abriola and Pinder (1985) developed a model that describes the transport of a contaminant through porous media in three forms: aqueous phase, non-aqueous phase, and vapour phase. The approach used to describe mass transfer between the non-aqueous phase and aqueous phase is equilibrium phase partitioning, which assumes that by knowing the concentration in one phase, the concentration in the other phase can be calculated using a partition coefficient. This assumption is based

on experimental evidence that suggests equilibrium phase partitioning occurs during the dissolution process (VanderWaarden *et al.*, 1971; Fried *et al.*, 1979).

There is, however, contrary evidence that appears to refute the local equilibrium assumption. For example, laboratory experiments by Lam *et al.* (1983) indicate that these mass transfer processes frequently do not reach a state of equilibrium. This work involved studying residual oil blobs during tertiary oil recovery.

Powers *et al.* (1991) present similar evidence that implies there is a process which limits the rate of NAPL partitioning to the aqueous phase. Powers *et al.* (1994), using laboratory-scale column experiments, showed that the length of time required to dissolve NAPL is greater than predicted by equilibrium phase partitioning calculations. A general correlation for transient dissolution rates in terms of volumetric fractions of NAPL in the porous media and porous media properties was proposed. Similar results were obtained by Imhoff *et al.* (1993) who showed that mass transfer rates for an area of residual NAPL are a function of the NAPL volumetric content, the Darcy water flux through the area and the distance into the contaminated region.

The importance of using equilibrium partitioning versus a rate-limited process becomes particularly evident when trying to predict the effectiveness of remediation schemes. Brusseau (1992) constructed a model that estimates the time required to remediate an aquifer contaminated by residual NAPL. He found if one did not account for a rate-limited mass transfer process the time and volume of water required for remediation would be significantly underestimated.

Hunt *et al.* (1988a; 1988b) found that mass-transfer rate limitations resulted in groundwater extraction at a contaminated site to be ineffective in removing the residual NAPL within a reasonable time frame. They suggested that remobilizing the NAPL, by steam injection for example, would be much more useful in remediation. However, Pennell *et al.* (1994) suggest that this remobilization of NAPL is dangerous because the NAPL can cause previously uncontaminated material to become contaminated. They suggest using surfactants which can increase the rate of mass transfer to the aqueous phase. In theory, if the mass transfer rate is high

enough, NAPL contaminated sites may be remediated using groundwater extraction methods, such as pump and treat. Unfortunately, surfactants may also lower the NAPL's surface tension, which can cause them to remobilize.

Parker et al. (1994) developed a conceptual model for NAPL in parallel plate fractures partitioning to the aqueous phase in the surrounding matrix. They suggest that restoration of contaminated fractured material is extremely difficult. Their findings show that a small amount of time is required for the NAPL to completely partition to the aqueous phase of the surrounding matrix when the matrix is porous.

Recently, *Lowry and Miller* (1995) used pore-scale modeling to describe the formation and removal of NAPL in porous media. These researchers feel that current macroscopic approaches are often unable to capture adequately the complexity of processes such as NAPL invasion and dissolution. They feel that small-scale modeling may provide the necessary conceptual and quantitative basis for constitutive theory development.

VanderKwaak (1993) used a two-dimensional numerical model to simulate the dissolution and transport of NAPL in fractured porous media. Fractures were simulated as high permeability one-dimensional elements that had the propensity to rapidly transport contaminant. The effects of matrix porosity and transport of dissolved NAPL through the porous media were priorities in this research; the small scale effects of dissolution occurring within a fracture were not represented.

Mendoza (1992) developed a model capable of describing the spatial relationship between two separate phases in a discrete fracture during drainage and imbibition processes. Drainage refers to the process whereby NAPL invades the fracture causing water to drain or exit the fracture. Imbibition is the opposite process where water enters the fracture causing NAPL to be displaced. The aperture distribution data and the position of residual within the fracture (i.e. NAPL residual distribution) following the imbibition process is used as starting point for the dissolution modeling for this thesis.

1.2 Research Outline

The work presented in this thesis has similarities to previous research in the area; however, this study examines the dissolution process at a much finer, more detailed scale. These finer details include using rough-walled fractures, accounting for advective-dispersive transport in the fracture and modeling the process of matrix diffusion across the entire fracture. In addition, phase transfer across explicit water-NAPL interfaces is accounted for.

The numerical model is a finite-element simulator coded in FORTRAN. Major inputs for the model, taken from the *Mendoza* (1992) model, include aperture distributions representing a rough-walled fracture and the initial location of NAPL residual within the fracture. The numerical model simulates the dissolution of this NAPL residual in the single fracture. The model calculates water flow caused by a head gradient along the fracture. Also, it simulates advective-dispersive transport within the fracture and diffusion of NAPL into the surrounding fracture matrix. As documented later, the model compares favorably to analytical solutions and results obtained by other researchers.

The modeling was carried out on a fracture of an arbitrary size (1.25m by 1.25m). Relationships between the NAPL residual distribution, the mass output of the fracture, groundwater flow rates, and mass transfer coefficients were studied. Also, changes in fracture transmissivity during dissolution were recorded and then compared to the mass-output results. A few simulations that included diffusion into a surrounding porous matrix were also performed. Approximately 60 separate aperture and residual distributions were investigated, although some of the more detailed investigations used a single aperture field and corresponding residual distribution.

Details of the theory involved and implementation of that theory is given in Chapter 2. The results and analysis of the numerical simulations are presented in Chapter 3. Conclusions and a discussion of their implications are presented in Chapter 4.

Chapter 2

Theory and Methods

This chapter describes the theory and conceptual model behind the numerical model used for later simulations. The chapter also addresses the implementation and some features and limitations of the numerical model.

2.1 Conceptual Model

Figure 2.1 shows a conceptual model of a contaminated site where a spill on or near the ground surface has released some NAPL contaminant. This NAPL could be made up of a single component such as trichloroethene (TCE) or a mixture of several NAPLs. The NAPL migrates down through the unsaturated zone. The mechanism driving this downward migration is pressure due to the overlying column of NAPL. Because the NAPL in this scenario is denser than water (a DNAPL), it continues its downward migration through the saturated zone. The NAPL may subsequently invade and travel through fractures in the underlying fractured material.

The NAPL will preferentially enter a fracture only if the capillary entry pressure of the fracture is lower than the surrounding material and the capillary pressure exceeds the entry pressure. The capillary entry pressure is simply the pressure required to force NAPL into a fracture or pore space. The larger the opening of the fracture, the lower the capillary entry pressure required for the NAPL to occupy that space. The extent to which the fracture becomes filled depends on the fracture aperture

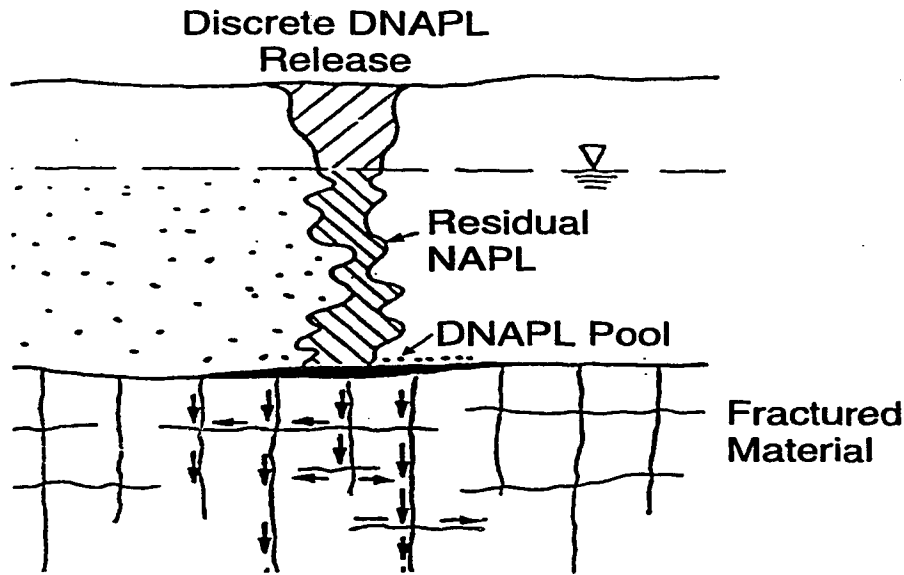


Figure 2.1: Conceptual model of a contamination scenario. After *Schwille* (1988).

distribution, the porosity of the surrounding matrix and the height of the column of NAPL.

Once the source of NAPL has been exhausted or removed, the NAPL will begin to drain out of the fractured material; this is the imbibition process. Following this imbibition process will be a certain amount of NAPL residual left in the fractured material. It is this residual that will be immobile and can cause the long-term contamination as it slowly dissolves over time.

Figure 2.2 shows a detailed example of fractured material. Studying the migration and subsequent dissolution of NAPL in this material can be accomplished on different scales of observation. Case 1 would involve studying the fracture network and the surrounding matrix material. Case 2 would involve studying a single fracture. A single fracture study would include more detail than a larger-scale study. These small scale details include the aperture distribution of the fracture and position of NAPL within the fracture. It will be shown in the following chapter that these details can have a large effect on the dissolution process. Understanding the effect of these small-scale details can improve the accuracy of modeling at larger scales, such as case 1.

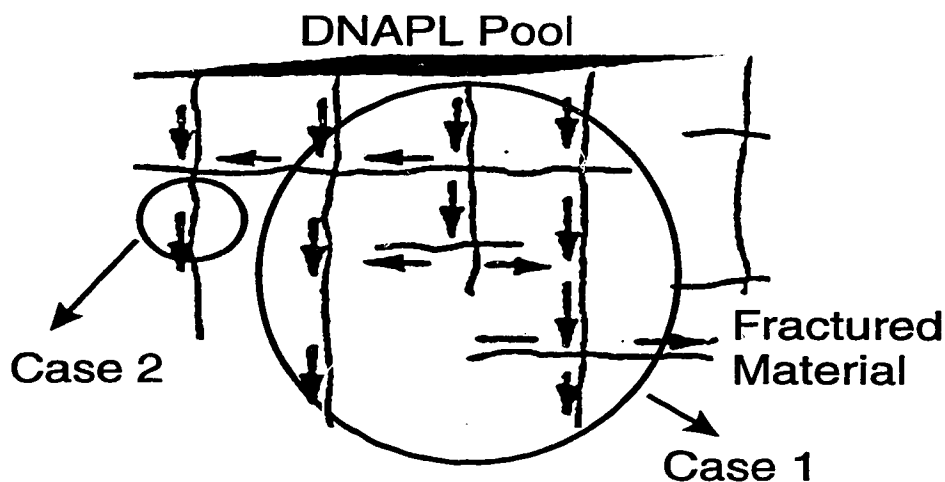


Figure 2.2: An example of different scales of observation at a contaminated site.

The conceptual model for this thesis is limited to a region within a single fracture (i.e., case 2). This single fracture is assumed to contain some NAPL residual contaminant that will dissolve into the groundwater flowing through the fracture. For the purposes of a single fracture this groundwater is assumed to have no dissolved NAPL in it prior to entering the fracture. The superposition of results from several such fractures where groundwater may have some dissolved NAPL prior to entering the fracture is left for further study.

2.2 Fracture Aperture Distributions

Fractures are often represented as two parallel plates, with the distance between these two plates being the fracture aperture. For the model used in this thesis a synthetic aperture distribution is used to simulate a discrete, rough-walled fracture (i.e., the aperture will vary spatially throughout the fracture). These synthetic distributions are created using a Fast Fourier Transform spectral technique developed by *Robin* (1993). The aperture field is assumed to be log-normally distributed and to exhibit isotropic, exponential correlation structure. Research by *Snow* (1970) has shown

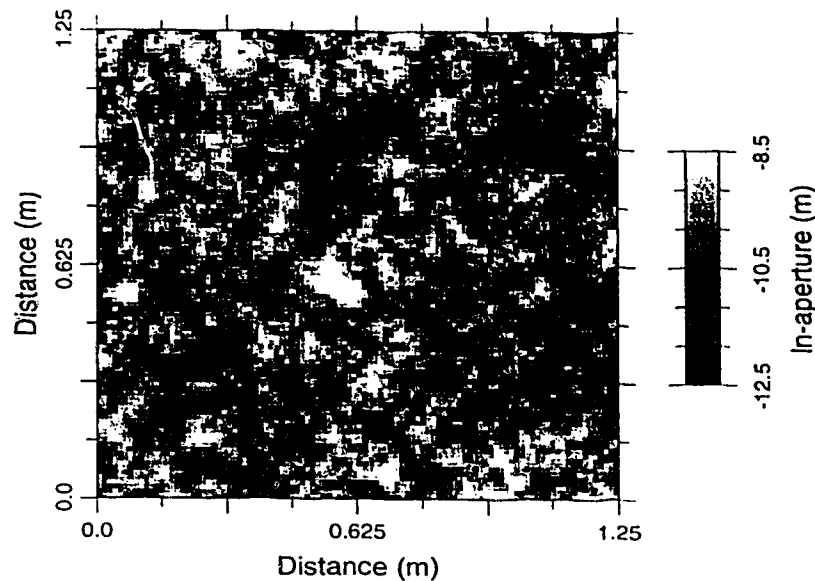


Figure 2.3: A sample log-normal aperture distribution.

that a log-normal aperture field is a reasonable representation of naturally occurring discrete fractures in various geologic materials.

The aperture field is discretized onto a two-dimensional square grid. The grid used for modeling contains 2500 cells (50 by 50 squares). Simulations for this work use a natural log-aperture mean of -10.5 (aperture in metres). The size of individual cells are 2.5cm^2 . Figure 2.3 shows an example of one of the fracture aperture fields used.

2.3 Residual Distributions

The spatial position of NAPL in a discrete fracture following the invasion process (both drainage and imbibition) will be referred to as the residual distribution or residual saturation. The controlling factors in determining the pattern of the residual distribution are the size and distribution of apertures, the pressure history, the invasion history, properties of the NAPL and fracture walls, and the physical limitations of the percolation system.

| | |
|------------------------------------|--------------------------|
| Density, ρ_{NAPL} | 1460 kg/m^3 |
| Aqueous Solubility at 20°C, C_s | 1100 mg/L |
| Coefficient of mass transfer, k | $2.0 \times 10^{-6} m/s$ |
| Viscosity, μ | 0.57 cp |
| Interfacial Tension, γ | 34.5 dyn/cm |
| Water Diffusion Coefficient, D^* | $1.0 \times 10^{-9} m/s$ |

Table 2.1: Physical properties of the NAPL used.

2.3.1 NAPL

A generic NAPL has been selected for use in the dissolution modeling. Numerous variations in NAPL properties makes it unfeasible to conduct simulations on many different NAPLs. This situation becomes increasingly complex when the NAPL is a mixture of more than one NAPL (which is, unfortunately, often the case). For this study the NAPL is denser than water (DNAPL); however, similar results can be expected with a NAPL that is less dense than water (LNAPL) (Hardisty *et al.*, 1995).

The physical properties of the NAPL have been chosen to be similar to Trichlorethene (TCE). TCE is a common chlorinated solvent, and consequently is also a common subsurface contaminant. The physical properties for the NAPL are given in Table 2.1. For this thesis the water is assumed to be perfectly wetting and the NAPL is considered to be the non-wetting phase.

2.3.2 Capillary Pressure

For a cell to become occupied by NAPL during the invasion process the capillary pressure of the NAPL must exceed the capillary entry pressure (P_c^*) of that cell. Each cell in the fracture model is represented by two parallel plates with the aperture being the distance between the two plates. The capillary entry pressure for a set of two parallel plates is:

$$P_c^* = \frac{2\gamma}{b} \cos \theta \quad (2.1)$$

where b is the distance between the two plates, γ is the interfacial tension between the two fluids and θ is the contact angle between the interface of the two fluids and the fracture wall. For this study water is assumed to be perfectly wetting and thus the contact angle will equal zero.

As pressure of the NAPL at the inlet boundary increases during invasion it may invade cells with progressively smaller apertures. At any given pressure there is a minimum aperture that the NAPL can enter. The value, called the critical aperture (b^*), is defined by:

$$b^* = \frac{2\gamma \cos \theta}{P_c} \quad (2.2)$$

Hence, all cells where b is greater than b^* can be invaded by the NAPL. The concept of critical aperture used in this context is known as the occupancy criterion.

2.3.3 Percolation Theory

The invasion of NAPL into a fracture is accomplished by using a modified form of percolation theory. For traditional percolation the only criterion used to determine the position of the NAPL during the invasion process would be the occupancy criterion. Using traditional percolation theory to place NAPL into the fracture ignores physical constraints of the system such as phase contacts, phase positions, and the nature of the fracture walls¹. Invasion percolation theory (Mendoza, 1992) is used to account for these physical constraints by constraining the fluid to entering and exiting at discrete points. This leads to the introduction of the accessibility and the trapping criteria.

The accessibility criterion restricts NAPL from invading a cell unless it is physically connected with the rest of the invading NAPL. This prevents the invading fluid

¹A fracture in a permeable material is considered to have permeable fracture walls. A fracture in an impermeable material is considered to have impermeable fracture walls.

from occurring everywhere the occupancy criterion is satisfied, as would occur in the traditional percolation case. For the fracture model the surrounding matrix is considered inaccessible to the invading NAPL phase; therefore, NAPL can only appear at the inlet boundary and travel through the fracture as a continuous phase.

The trapping criterion restricts the removal of NAPL during the imbibition process. If a section becomes isolated from the rest of the continuous phase then it is considered to be trapped. The water (i.e., wetting phase) is subject to the same trapping criteria if the fracture walls are impermeable. On the other hand, permeable fracture walls will allow water to exit freely. NAPL is trapped whether the walls are permeable or impermeable.

2.4 Groundwater Flow

Groundwater flow through fractured media has commonly been approximated using a parallel plate model. Each cell within the fracture has a constant aperture value; therefore, a parallel plate model is applied to each cell. The equation that describes the volumetric flow rate through two parallel plates is given by the following:

$$Q = -\frac{b^3 \rho g}{12\mu} w \Delta h \quad (2.3)$$

where Q is the volumetric flow rate through the fracture, μ is the viscosity, w is the distance along the fracture and Δh is the hydraulic head difference along the plates ($h_1 - h_2$). Figure 2.4 shows how the variables in Equation 2.3 pertain to the physical system.

From Equation 2.3 the permeability, k , of each aperture segment can be defined:

$$k = \frac{b^2}{12} \quad (2.4)$$

and the transmissivity, T , for each segment:

$$T = \frac{b^3 \rho g}{12\mu} \quad (2.5)$$

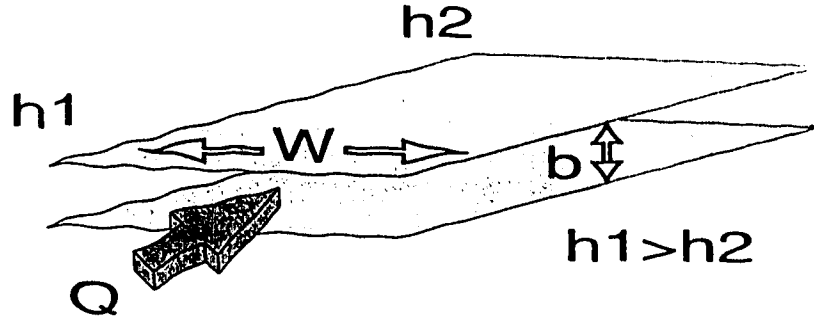


Figure 2.4: Diagram showing the variables used in calculating the volumetric flow rate through a pair of parallel plates.

The fluid continuity equation for a pair of parallel plates is given by:

$$\nabla \left(\frac{b^3 \rho g}{12\mu} \nabla h \right) = 0 \quad (2.6)$$

The fracture plane can be represented on a two-dimensional grid. The spatially varying aperture in the fracture corresponds to a spatially varying heterogeneous transmissivity distribution on this two-dimensional grid. Using this information and the relation defined in Equation 2.5 the fluid continuity equation for the two-dimensional plate representing a rough-walled fracture can be written as:

$$\nabla (T(x, y) \nabla h) = 0 \quad (2.7)$$

where x and y represent coordinates in the fracture plane.

Capillary Number

During the dissolution modeling the NAPL residual is considered to be immobile. For this approach to be valid the viscous forces resulting from the flowing groundwater must be insignificant relative to the capillary forces. The dimensionless capillary number (N_c) measures the ratio of these viscous effects compared to the capillary effects. The capillary number is expressed as:

$$N_c = \frac{\mu v}{\gamma} \quad (2.8)$$

where v is the average linear groundwater velocity.

When the capillary number is “small” capillary forces will dominate. Experimental evidence in porous media (Larson *et al.*, 1981) and numerical simulations conducted using rough-walled fractures (Mendoza, 1992) suggest that $N_c < 10^{-4}$ is an appropriate cut off value. Using this value for the capillary number and the parameters stated in Table 2.1 a minimum average linear velocity can be calculated. This minimum velocity is the point above which the viscous forces will dominate resulting in the remobilization of the NAPL. Using Equation 2.8 an expression for this minimum linear velocity, q , can be derived:

$$q_{min} = \frac{N_c \gamma}{\mu} \quad (2.9)$$

Solving for q_{max} leads to:

$$q_{min} = 500 \frac{m}{day} \quad (2.10)$$

The maximum values for q during the dissolution modeling are at least one order of magnitude below this minimum value; therefore, the NAPL is treated as immobile.

2.5 Aqueous Phase Transport

During dissolution mass from the NAPL is transferred to the aqueous phase. The aqueous phase mass is transported through the fracture by groundwater advection and hydrodynamic dispersion. The two-dimensional advection-dispersion equation governing aqueous phase transport in a rough-walled fracture (Sudicky and Frind, 1982) is:

$$b \frac{\partial C}{\partial t} + b v_i \frac{\partial C}{\partial x_i} - \frac{\partial}{\partial x_i} b D_{ij} \frac{\partial C}{\partial x_j} = 0 \quad i, j = x, y \quad (2.11)$$

where C is the aqueous phase concentration of the NAPL and V is the advective groundwater velocity. The hydrodynamic dispersion term, D , is a function of the dispersivity value assigned to the fracture, the groundwater velocity, and the effective diffusion coefficient.

2.6 Dissolution

There have been several models developed which describe the partitioning of NAPL to the aqueous phase. Several of these models use the assumption of “local equilibrium”. This approach assumes that the concentration of a component in one phase will be in equilibrium with its concentration in the other phase and that the concentrations may be related by a “partition coefficient” (Abriola and Pinder, 1985).

Despite frequent use in the modeling of NAPL-phase water relationships, local equilibrium has yet to be adequately demonstrated as being valid (Powers *et al.*, 1991). The local equilibrium relationship has been inferred from many lab scale experimental studies ((Fried *et al.*, 1979),(VanderWaarden *et al.*, 1971),(Hunt *et al.*, 1988a)); however, these studies have been carried out over a limited range of matrix material, organic compounds, and velocities. Also, there is laboratory evidence to support a non-equilibrium relationship for NAPL dissolution. Studies for tertiary oil recovery involving the use of surfactants have indicated that the rate of mass transfer of oil blobs is frequently not fast enough to reach a state of phase equilibrium (Lam *et al.*, 1983). Geller and Hunt (1988) showed that the concentration of some organic chemicals were below the equilibrium concentration levels immediately downstream of a NAPL source.

This study assumes NAPL dissolution is a rate-limited process. The details of this rate-limit process are discussed in the following section.

2.6.1 Mass Transfer Relationships

As previously mentioned, the transfer of NAPL from the non-aqueous to the aqueous phase is represented here as a rate-limited, mass-transfer process. Powers *et al.* (1991) have defined a rate-limited mass flux across a two-dimensional interface. This flux, F_a , is expressed as:

$$F_a = -k_t(C - C_s) \quad (2.12)$$

where k_t is an effective mass transfer coefficient, and C_s is the equilibrium concentration of the NAPL in the aqueous phase. The equilibrium concentration for a pure NAPL species is the solubility of that NAPL in water.

The rate of mass transfer from the non-aqueous to the aqueous phase is considered to be limited primarily by diffusion across a boundary layer. The mass transfer coefficient is thus directly proportional to the diffusion coefficient of the NAPL and inversely proportional to the thickness of the boundary layer. For simplicity, the mass transfer coefficient is assumed to be constant; that is, neither the thickness of the boundary layer nor the diffusion coefficient change during the dissolution process.

The mass flux (F_a), however, will be non-linear with respect to time. As NAPL dissolves, the aqueous concentration (C) increases. This increase will result in decrease in the $(C - C_s)$ term and therefore, a decrease in the mass flux across the NAPL-water contact boundary.

Fracture

To calculate a mass flux of NAPL into the fracture, Equation 2.12 must be modified to include the interfacial area of the NAPL/water contact. The resulting equation is

$$F_a = -bwk_t(C - C_s) \quad (2.13)$$

where w is the width of the aperture segment and b is the height of the aperture segment. During dissolution the value for b will change whenever a grid block of NAPL has been removed by dissolution. This will increase the non-linearity of the F_a with respect to time. Since the grid is square, the value of w does not change during the dissolution process.

Matrix

If the fracture walls are permeable, NAPL will also diffuse into the surrounding matrix. To calculate the mass flux from the NAPL to the matrix, equation 2.12 is

again modified. The resulting equation is:

$$F_a = -\phi w^2 k_t (C - C_s) \quad (2.14)$$

where ϕ is the matrix porosity. As the matrix porosity is increased, the flux into the matrix will also increase.

2.7 Numerical Formulation

A single discrete fracture is represented on a two-dimensional grid at the micro-scale. The governing flow and transport equations are discretized using the standard Galerkin finite-element formulation (Huyakorn and Pinder, 1983). Flow and transport are modeled using a triangular finite-element grid. A comparison was made between using square and triangular finite-elements grids; the triangular grid provided the least amount of numerical error so it was chosen for the flow and transport modeling. For models that incorporate matrix diffusion the surrounding matrix is modeled using one-dimensional line elements at every node on the fracture grid. This one-dimensional line element will simulate the diffusion process into the third dimension (out of the fracture plane). For simplicity, no lateral advection or diffusion takes place in the matrix. This would be reasonable where the matrix permeability is much less than that of the fracture, which is often the case.

Grid

The original aperture field and residual distribution were generated on 200x200 square grids. Using grids of coarser resolution to simulate the drainage and imbibition processes produced results that are statistically dissimilar. However, modeling flow, dissolution, and transport on 200x200 square grids was infeasible due to the amount of computing time required. For example, a single transport simulation on a 200x200 grid could take up to a week to complete. To solve this problem initial residual distributions were generated on a 200x200 grid and then scaled to a 50x50 grid for dissolution modeling.

Sixteen cells from the 200x200 distribution (4x4 segment) were reduced to one cell in the 50x50 distribution. The geometric mean of the sixteen aperture segments was used to calculate the new aperture of the smaller distribution. If seven or more of the sixteen cells contained residual, then the new cell in the 50x50 distribution would also contain residual. By experimenting with different values it is found that seven cells as the cutoff value provides the closest match in NAPL saturation to the original distribution.

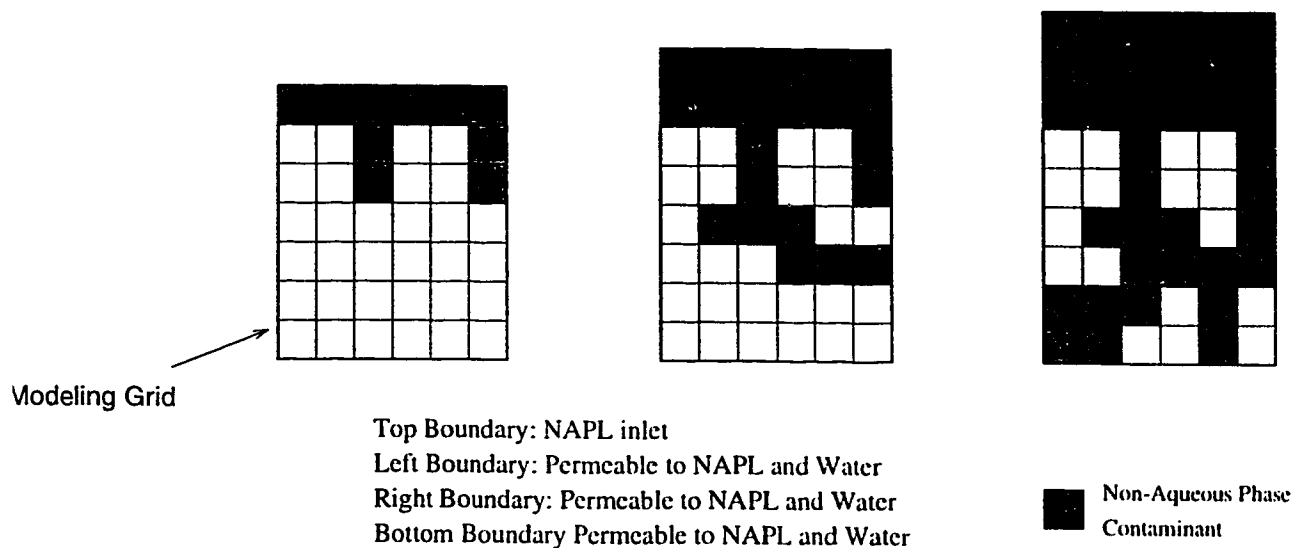
Boundary Conditions

The boundary conditions for the model change from the NAPL invasion process to the dissolution process. The invasion process is conceptualized as a separate event from the dissolution process. That is, the residual NAPL is in place before the groundwater begins to flow and dissolution takes place. The separation of these two events is physically unrealistic; however, the separation is required to perform the modeling. The invasion percolation process is not performed in discrete temporal steps; it is based on discrete capillary pressure steps. Also, starting with in NAPL residual already in place makes the dissolution model easier to construct.

Figure 2.5 illustrates the various boundary conditions used in different stages of the numerical modeling. The NAPL enters the fracture from the inlet boundary located at the top of the fracture. During the creation of the initial residual distribution the driving mechanism of the NAPL, which is the head of NAPL at the inlet boundary, is the dominating force. For drainage the NAPL enters only at the top. For imbibition the NAPL exits only at the top and bottom. The permeability of the fracture walls depends on whether the surrounding matrix is porous.

Following the invasion process, the boundary conditions are changed to simulate groundwater flow through the fracture. The left and right boundaries are specified head boundaries. The specified head boundaries are setup of so that flow is from left to right. The top and bottom boundaries now become impermeable to water flow. They can be thought of as symmetry boundaries.

NAPL Invasion Modeling



NAPL Dissolution Modeling

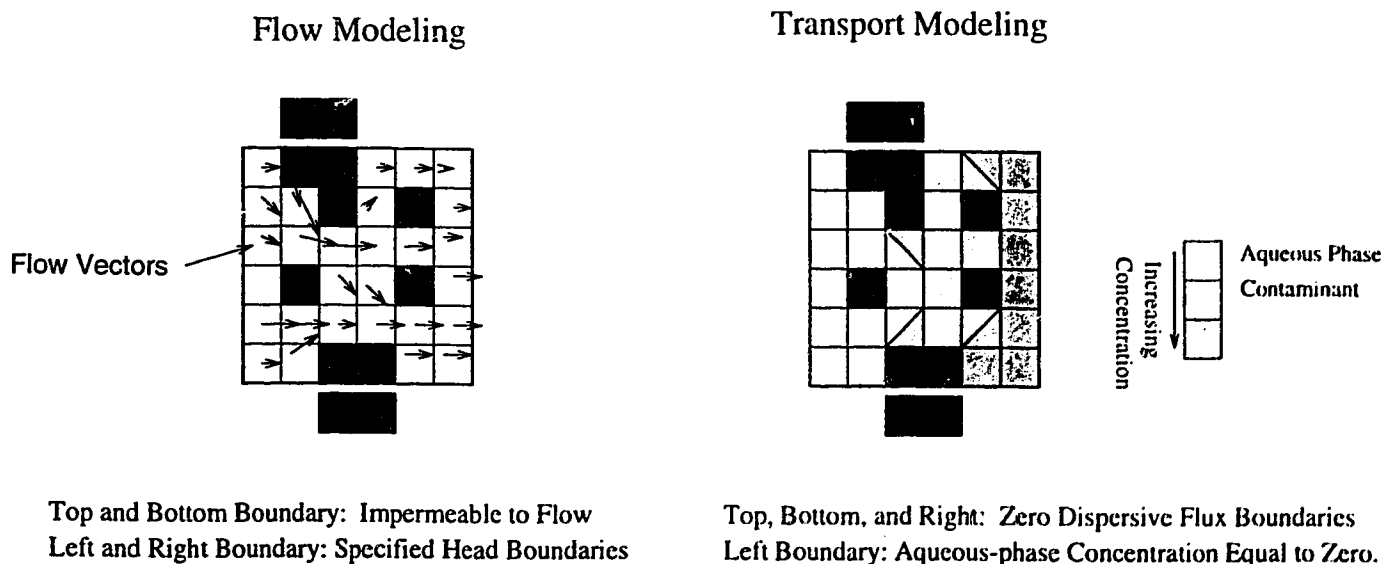


Figure 2.5: Conceptualization of processes and boundary conditions for the numerical model for various stages of the modeling.

For the transport solution the top, bottom and right boundaries are considered impermeable for dispersive transport; mass exits the right hand boundary via advective transport only. The left-hand boundary is constrained to a zero concentration, which assumes that only clean water (i.e. no aqueous-phase NAPL) is entering the system.

Dissolution Modeling

The model first calculates a groundwater flow solution through the fracture with no NAPL residual. This information is used for calculating the effective aperture and relative transmissivities during dissolution.

The residual is placed into the fracture using invasion percolation techniques and the flow solution is recalculated. The contact area between the NAPL and water for every cell is computed. The mass flux of NAPL across that interface is calculated and applied to the nodes associated with that interface. The mass fluxes at these nodes represent the dissolution process. The model now begins stepping through time, accounting for advective-dispersive transport and NAPL dissolution. The amount of NAPL removed from each cell due to dissolution is calculated. When the mass of NAPL originally in the cell is equal to the mass of NAPL that has been removed via dissolution, the cell becomes free for water to flow through. A new flow solution is then calculated and the NAPL dissolution boundaries (i.e. the nodal mass fluxes) are changed to reflect the change in the NAPL residual distribution. The transport solution now continues with the modified grid. The dissolution modeling continues until all the NAPL has been removed from the system.

2.8 Model Verification

Due to the complexity of the numerical model there is no single analytical solution that can be used to verify it. Several comparisons were made to test various aspects the numerical model. For example, comparing flow through the fracture or matrix

diffusion out of the fracture were compared to analytical solutions to verify the numerical implementation of the flow and transport equations. Following a short review of mass balance, the two most complex verifications, advective-dispersive transport and NAPL dissolution are presented.

Mass Balance

To determine whether the model is accurate and stable, a mass balance calculation is performed. A mass error term is used to quantify the amount of mass that cannot be accounted for due to numerical problems. The mass error term is defined as the mass transferred into the aqueous phase subtracted from the mass change at the boundaries and the ending aqueous phase mass in the system. A percent error is calculated by normalizing this mass error term with the original NAPL mass in the system.

Since this problem is non-linear the Peclet and Courant criteria are only used as a guide because significant errors may arise even if the criteria are fully satisfied. Increased values for longitudinal and transverse dispersivities also help increase accuracy and numerical stability without having a dramatic effect on the mass output results.

Advective-Dispersive Transport

The numerical model was used to perform a transport solution to compare with an analytical model to verify the accuracy of the advective-dispersive transport equation implementation. The simulations were performed on grids of various sizes. Parameters such as potential difference and source conditions were varied to test the robustness of the solution.

For flow calculations the left and right boundaries had constrained head values, while top and bottom boundaries were impermeable. Flow was from left to right. A uniform aperture was specified for the entire domain. A single constrained source (concentration = 1.0) in the middle of the left side boundary provided the input

| | Test 1 | Test 2 | Test 3 |
|---------------------------------------|----------------------|-----------------------|----------------------|
| Potential Difference, Δh | 9.0 | 9.0 | 99.0 |
| Grid Size (x) | 10 | 20 | 10 |
| Grid Size (y) | 10 | 20 | 10 |
| Source Thickness | 1.0 | 0.5 | 1.0 |
| Length of Model, L | 10.0 | 10.0 | 10.0 |
| Grid Spacing, ΔL | 1.0 | 0.5 | 1.0 |
| Groundwater Velocity, v | 0.075 | 0.075 | 0.825 |
| Longitudinal Dispersivity, α_l | 0.5 | 0.5 | 0.5 |
| Transverse Dispersivity, α_t | 0.5 | 0.5 | 0.5 |
| Diffusion Coefficient, D^* | 1.0×10^{-9} | 1.0×10^{-9} | 1.0×10^{-9} |
| Time Step, Δt | 1.0 | 1.0 | 1.0 |
| Total Time, t | 100.0 | 100.0 | 100.0 |
| Peclet Number(x) | 2.0 | 1.0 | 2.0 |
| Peclet Number(y) | 0.013 | 0.013 | .123 |
| Courant Number(x) | 0.075 | 0.15 | .825 |
| Courant Number(y) | 1.3×10^{-9} | 5.4×10^{-11} | 1.3×10^{-9} |
| %Error | -0.00190 | -0.00024 | -0.00588 |

Table 2.2: Parameters used in numerical model for comparison with the LINE2D analytical solution.

mass. Parameters used for these tests are shown in Table 2.2.

Each of these tests was compared to an analytical solution, LINE2D (Sudicky, 1986). The results of these comparisons are shown in Figure 2.6. The solution attained by the numerical model and analytical solution are essentially identical. Small differences result from the effects of boundary conditions and being unable to represent source conditions exactly between the two codes.

Dissolution

The numerical dissolution process was compared to an example given by Powers *et al.* (1991). Their work involved studying the dissolution of NAPLs in porous media. The NAPL in their work is represented by “blobs” in the porous media. The blobs are quantified by the interfacial contact area with the surrounding saturated media. The NAPL is dissolved using a rate-limited process. The effects of groundwater flow, transport (including dispersion), and diffusion are also included.

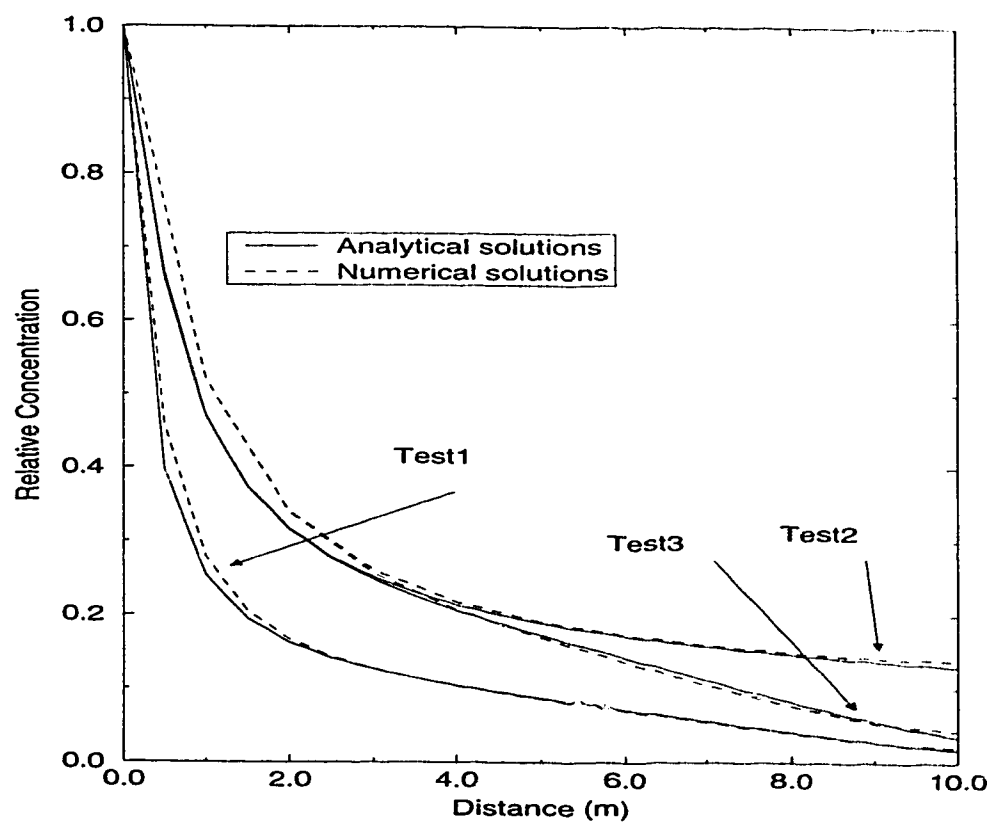


Figure 2.6: Numerical model compared to the analytical solution for a simple advection-dispersion problem.

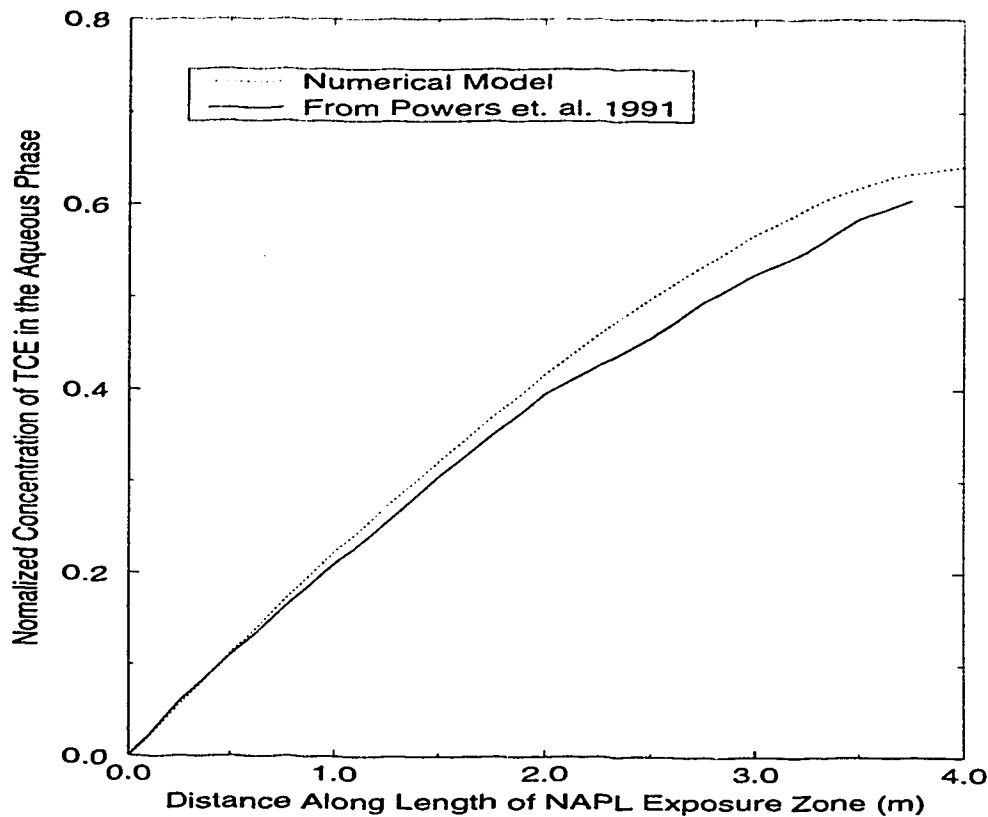


Figure 2.7: Numerical model compared the analytical solution for a simple advection-dispersion problem.

The fracture model is setup to closely resemble the scenario presented above. NAPL is distributed evenly within a fracture that has a constant aperture (i.e. for a 10% saturation every tenth cell contains NAPL residual). Parameter values such as porosity and interfacial area are matched exactly between the simulations (see Table 2.3); however, due to numerical constraints such as the effects that the boundaries have, the results cannot be matched perfectly. The results of this comparison are presented in Figure 2.7.

| | |
|---------------------------------------|-------------------|
| Aquifer Dispersivity, α | .10 <i>m</i> |
| Darcy velocity, q | 10.0 <i>m/d</i> |
| Porosity, θ | .25 |
| Residual saturation of TCE | .10 |
| Lateral extent of contaminated region | 4.0 <i>m</i> |
| Coefficient of Mass Transfer, k_t | 2.4e-6 <i>m/s</i> |

Table 2.3: Parameters used in numerical model for comparison with example from *Powers et. al.* (1991).

Chapter 3

Modeling Results and Analysis

The numerical model described in the previous chapter was applied to a number of theoretical scenarios to elucidate the dissolution behavior of NAPLs in rough-walled fractures. Most simulations were conducted using impermeable fractures walls; however, some example simulations were also run using a permeable matrix. The impermeable matrix simulations demonstrate the essential character of the dissolution process, including what factors control the dissolution process. Through comparison to the previous results, the permeable matrix simulations illustrate the potential significance of matrix diffusion on the dissolution process.

3.1 General System Behavior

This section examines the general behavior of a fracture containing NAPL residual undergoing dissolution. First, the overall character of NAPL aqueous concentration and saturation in space and time are illustrated. These are followed by an examination of changes in the mass output of the fracture, aqueous phase concentration of the NAPL, NAPL saturation and relative transmissivity of the fracture.

The small-scale perturbations in some of the curves presented here are a direct result of the discrete representation of the dissolution process whereby NAPL-occupied cells are converted to water-occupied cells. For example, when residual is removed from the fracture two effects combine to affect the dissolution process: the flow pat-

| Parameter | Value |
|---------------------------------------|----------------------------|
| Gradient Across Fracture | 0.08 m/m |
| Fracture Width, (x) | 1.25 m |
| Fracture Height, (y) | 1.25 m |
| NAPL Solubility Limit | 1100 ppm |
| Coefficient of Mass Transfer, k_t | 2.0e-6 m/s |
| Initial Mass of NAPL | 59.9 grams |
| Longitudinal Dispersivity, α_l | 0.5 m |
| Transverse Dispersivity, α_t | 0.5 m |
| Diffusion Coefficient, D^* | $1.0 \times 10^{-9} m^2/s$ |
| Time Step, Δt | 1000.0 sec |
| Total Time for NAPL Dissolution, t | 7.9 years |
| Total Mass Error, % | .13 |

Table 3.1: Parameters used in numerical model for the example simulation.

tern is changed and the amount of NAPL in contact with water changes. In most cases, removing a block of NAPL residual only marginally affects the flow pattern, yet it might dramatically increase or decrease the contact area between the water and the NAPL. This change in contact area affects the output concentration. Occasionally removing a block of NAPL may dramatically affect the fracture's transmissivity and thus change the total flow of water through the fracture. The combination of these micro-scale changes may then lead to either a spike or drop in parameters that characterize the dissolution process, such as the total downstream mass-output.

3.1.1 Simulation Description

The results in this section are from a single dissolution simulation conducted using a fracture with impermeable walls (i.e., no matrix porosity). The parameters and some basic output characteristics for this simulation are presented in Table 3.1.

The pattern of NAPL dissolution in this simulation is typical of most simulations presented later in this chapter. Figure 3.1 shows representative snapshots of the NAPL distribution and the aqueous-phase concentration within the fracture as dissolution proceeds.

Early in the dissolution process the groundwater within the fracture, which is

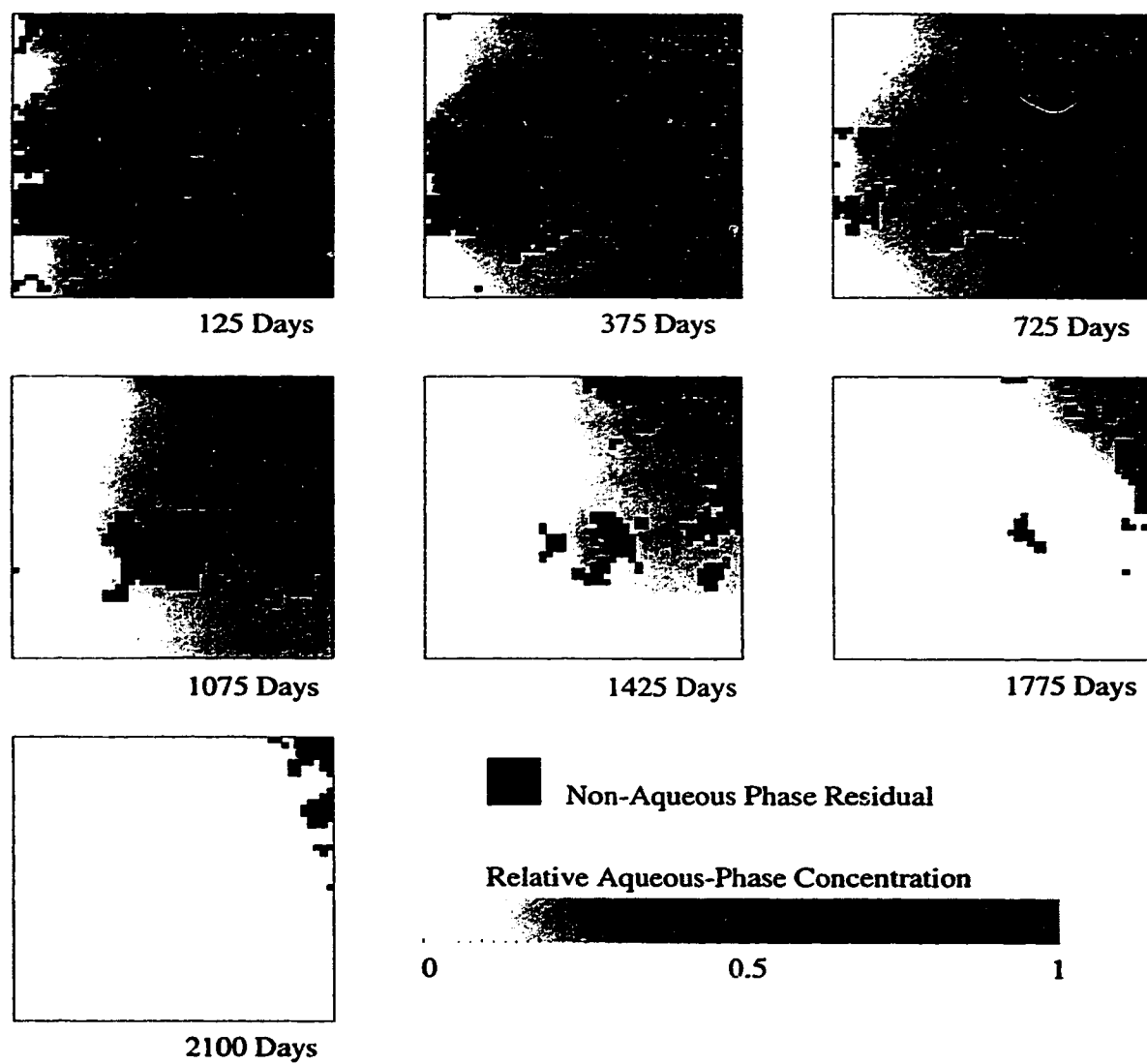


Figure 3.1: A series of snapshots showing the dissolution simulation that is discussed in this section.

moving from left to right in Figure 3.1, becomes nearly saturated with NAPL. There is a general increase in NAPL concentration from left to right; clean groundwater enters the fracture at the left and the NAPL concentration increases as water comes into contact with more NAPL residual as it passes through the fracture. The rate of NAPL dissolution at the downstream end of the fracture is slower than the upstream end because NAPL concentrations are higher near the downstream end; higher NAPL concentrations result in a slower rate of mass transfer from the non-aqueous to the aqueous phase.

3.1.2 Downstream Concentration

As shown above, the aqueous-phase concentration of NAPL varies spatially throughout the fracture. Thus, the aqueous-phase concentration in water exiting the fracture will also differ along the downstream boundary (Figure 3.1). To calculate a representative concentration of the water exiting the fracture the mass flux of NAPL at the boundary is divided by the volumetric water flux.

The average concentration of NAPL in the aqueous phase exiting the fracture falls steadily during the dissolution process (Figure 3.2). The concentration is initially close to the solubility limit and declines almost immediately. This decline is associated with the disappearance of NAPL and a greater amount of water flowing through the fracture. In other simulations where the groundwater velocity is lower than this example case, the downstream concentration may be at the solubility limit for a long period of time before the concentration begins decreasing.

3.1.3 NAPL Saturation

The amount of NAPL in the fracture is expressed in terms of its saturation. NAPL saturation is measured using both volumes and areas which are referred to as volumetric or areal saturation respectively. The specific values for volumetric and areal saturations differ because of the varying aperture distribution; however, general trends

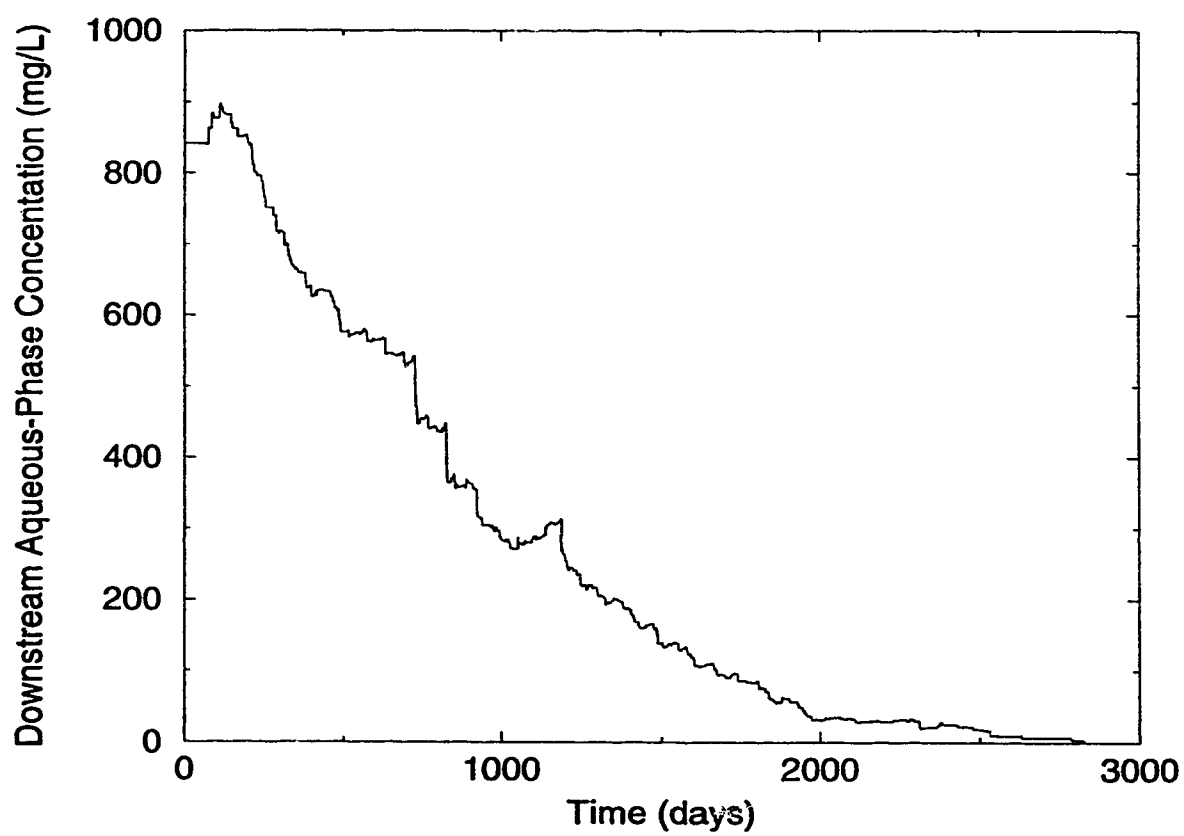


Figure 3.2: Concentration versus time curve for a single dissolution simulation.

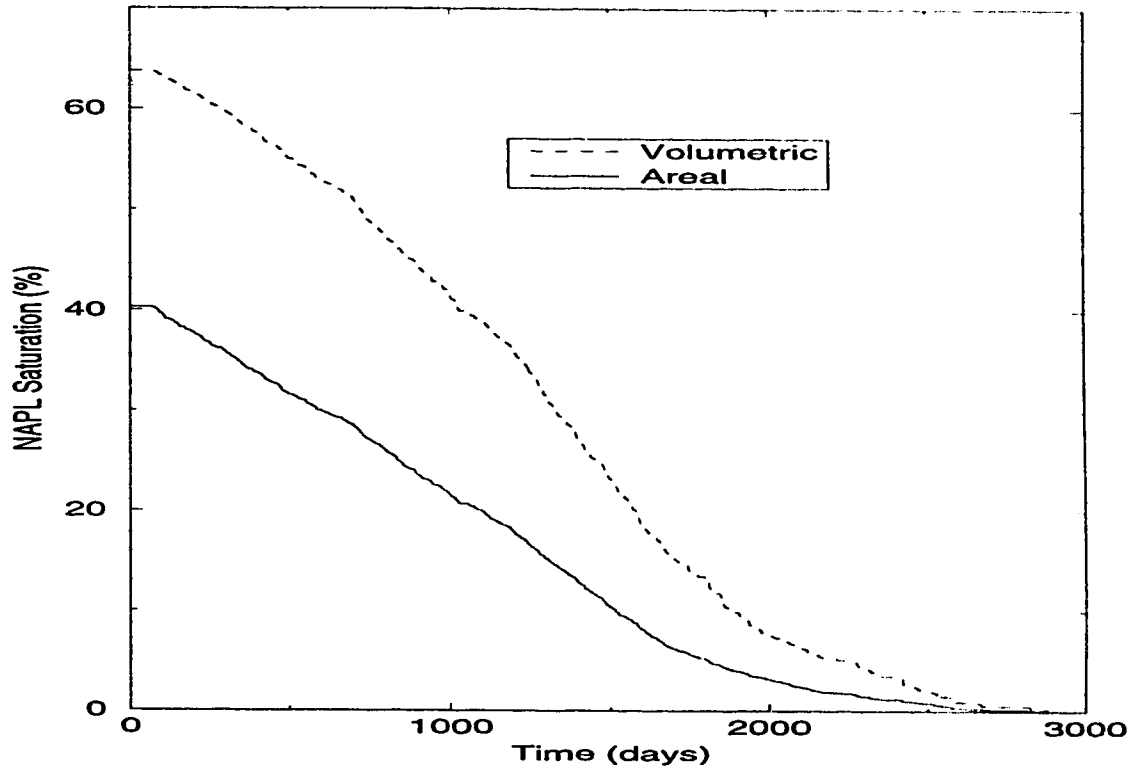


Figure 3.3: NAPL Saturation versus time curve for a single dissolution simulation.

of results are the same when these values are plotted against other parameters, such as time.

The areal saturation (as well as the volumetric saturations) decreases steadily over time during the dissolution process (Figure 3.3). The cells of NAPL disappear at a fairly constant rate; however, this rate slows near the end of the dissolution process. The cells of NAPL at later time in the model are generally the largest cells (i.e. the NAPL occupies the largest aperture segments). Since the cell contains more NAPL, it takes longer for the NAPL to disappear. This phenomenon will be discussed in more detail later.

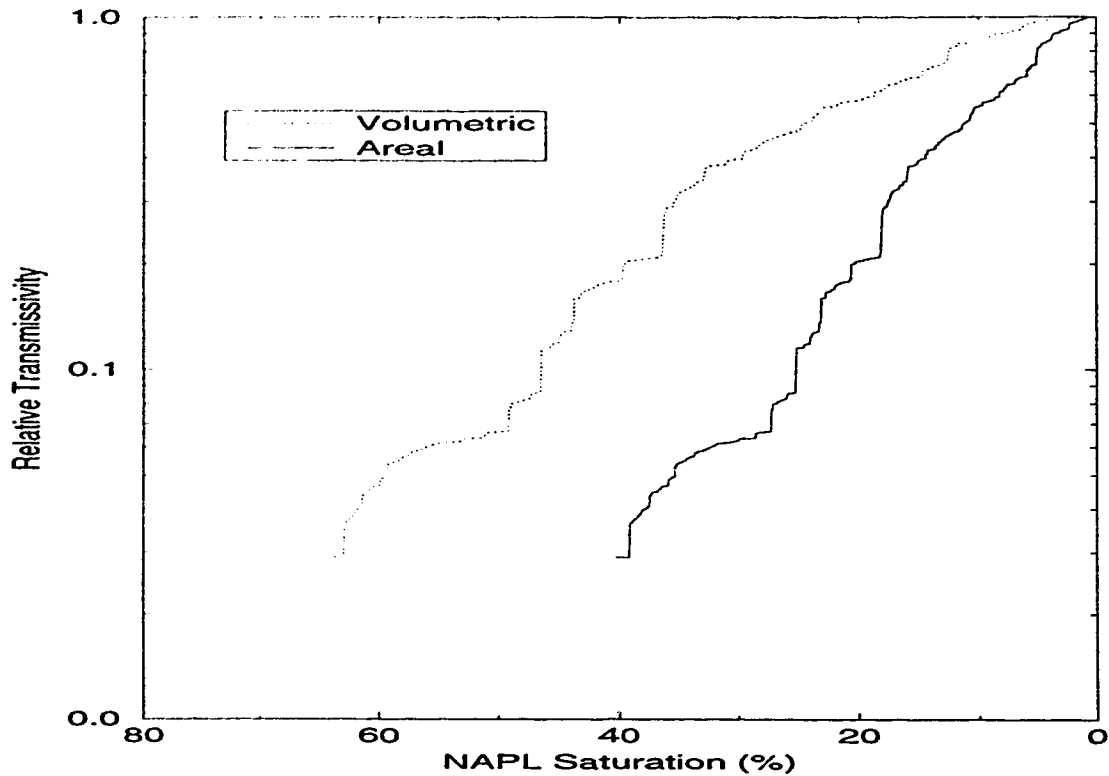


Figure 3.4: Relative Transmissivity (for water) curve for a single dissolution simulation.

3.1.4 Relative Transmissivity

The relative transmissivity of the fracture is plotted versus the areal NAPL saturation; these plots are referred to as relative transmissivity curves. As expected, the relative transmissivity of the fracture increases as the saturation of NAPL decreases (Figure 3.4). Note there are specific “jumps” in the relative transmissivity. The sudden increases occur when a cell is removed that opens a new flow path; this new flow path has a significant effect on the fracture’s relative transmissivity.

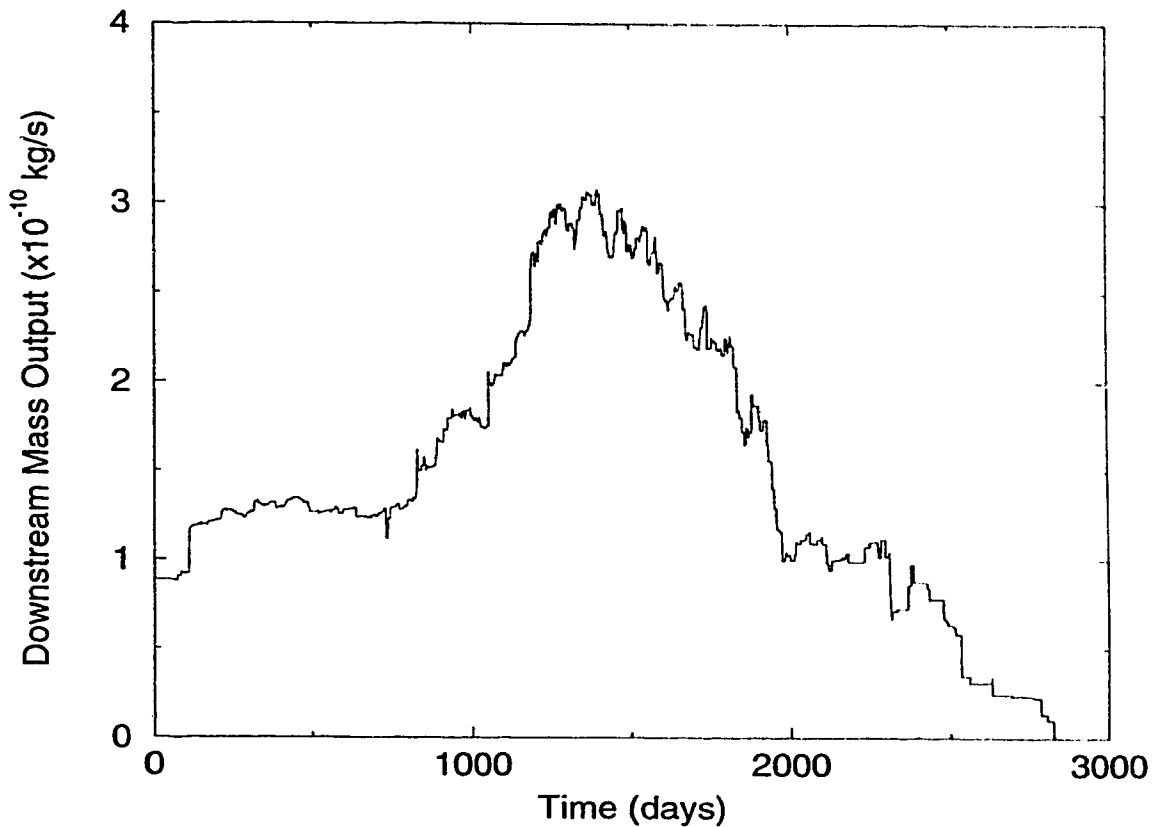


Figure 3.5: Mass-output curve for a single dissolution simulation.

3.1.5 Mass output

Figure 3.5 shows the downstream mass-output relationship versus time for the complete dissolution simulation. The overall pattern presented here is simple and similar for all other simulations: the mass-output increases gradually from an initial value to a maximum and then decreases to zero when all the NAPL has been removed. As mentioned previously, this curve represents the combined effects of variations in mass-output concentration and relative transmissivity. Note also that there is no correlation between the downstream aqueous-phase concentration and the downstream mass output (Figure 3.5) during the dissolution process.

3.2 Sensitivity Analyses

In order to determine the important controls on dissolution, a sensitivity analysis is performed on different simulation parameters. The emphasis for the sensitivity analyses is placed on the physical constraints of the system, such as NAPL location and the fracture aperture distribution.

3.2.1 NAPL Placement

Invasion Percolation

Figure 3.6 shows the mass-output for a single fracture with three different initial NAPL saturation levels created with invasion percolation methods. All other parameters, such as the gradient across the fracture and the coefficient of mass transfer for the NAPL were held constant, and the same random aperture field was used for each of the different simulations. To obtain varying initial saturations, an initial residual distribution was first created using invasion percolation techniques (Mendoza, 1992). This NAPL distribution was then artificially modified by removing or adding residual around the edges of existing NAPL residual clusters.

The curve for the low initial NAPL saturation case (20%) has a high peak or maximum mass output rate. This peak rate occurs relatively early when compared to higher initial NAPL residual saturations. Following this peak, the rate of mass output drops quickly until all the NAPL has disappeared (Figure 3.6).

The curve for the relatively high initial NAPL saturation case (44%) has a low peak mass output rate and the peak rate occurs late when compared to lower initial saturations. As well, the peak rate occurs over a greater interval of time than the lower saturation case (i.e. the curve has more of a “U” shape than a “V” shape). As would be expected, the total time for the NAPL to completely dissolve is much greater than in the lower NAPL saturation cases. This relationship between NAPL saturation and dissolution time will be discussed in more detail later.

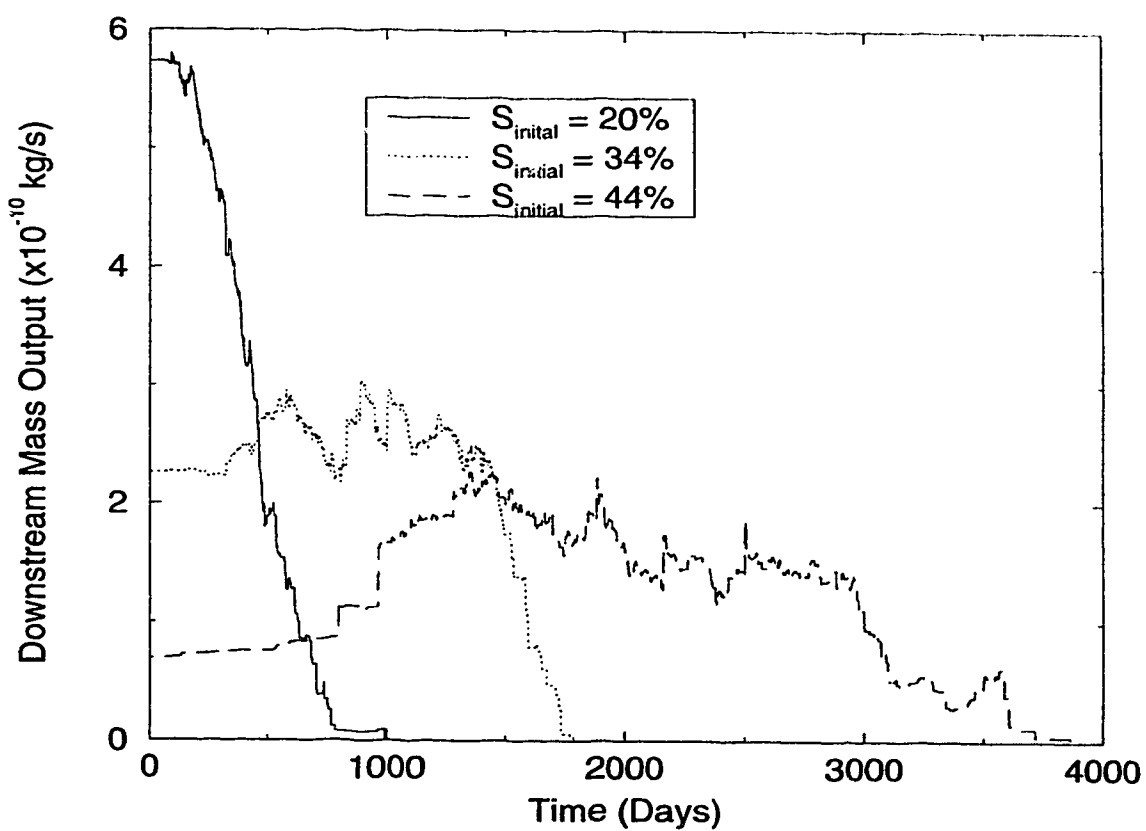


Figure 3.6: Mass-output for three saturation levels created with invasion percolation methods for a single fracture with the same aperture distribution.

Random Residual Assignment

In the previous section it was demonstrated that the initial NAPL saturation affected the mass-output curves. The position of the NAPL within the fracture will also have an effect on the mass-output curves. The location of NAPL in the fracture is controlled by the criteria controlling invasion percolation. To investigate the influence that invasion percolation has on the mass-output curves, simulations were performed where the NAPL was distributed randomly throughout the fracture. To permit direct comparisons to previous results the initial NAPL saturations were forced to be identical to the previous invasion percolation residual distributions.

The random residual assignment is produced by randomly assigning NAPL occupied cells throughout the fracture, with no consideration given to either occupancy (i.e., aperture size) or accessibility (i.e., invasion mechanism) criteria. This random residual assignment distribution of NAPL is not meant to represent any real scenario, nor is it based on an actual physical process, as is the case of invasion percolation. However, the random residual distribution does offer the chance to examine mass output curves that are independent of the process of invasion and that have a greater statistical link to the initial NAPL residual saturation. By comparing the random residual assignment results to those of invasion percolation we can identify features of the mass output curves that are a direct result of the NAPL invasion history and its position in the fracture relative to the random aperture field.

Qualitatively, the general mass-output curve shapes and trends for the random residual distributions are similar to the invasion percolation results (Figure 3.7). That is, initial lower saturations have higher peaks and the NAPL dissolves quickly, whereas higher initial saturations have lower peaks and the NAPL takes a longer time to disappear. Even though the invasion percolation distribution and random NAPL distribution mass output curves have these similarities, differences are strikingly apparent. One major difference is that the residual distributions created with invasion percolation take much longer to dissolve than the random residual distributions (note the different time scales for figure 3.6 and figure 3.7). A second significant

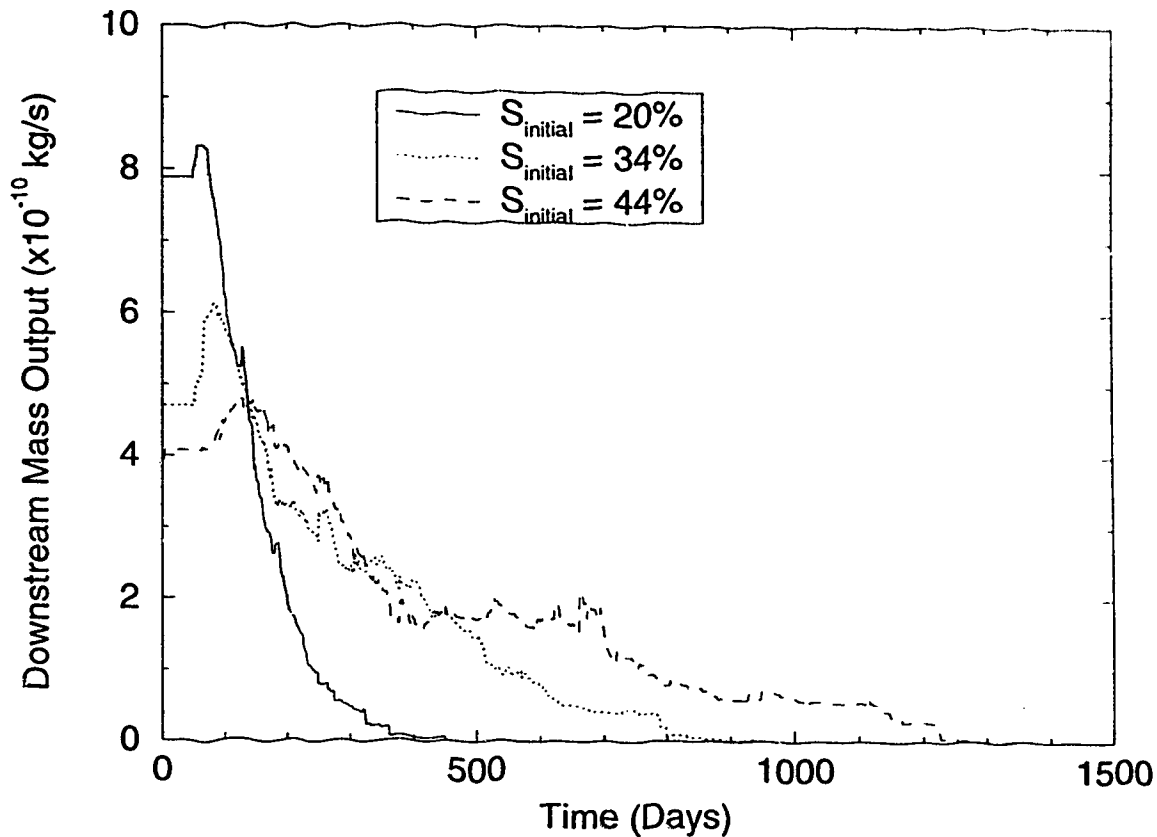


Figure 3.7: Mass-output for three saturation levels created with invasion percolation methods for a single fracture with the same aperture distribution.

difference is that the separation between the maximum peaks for the random residual distribution case is small whereas the time separation for the maximum peaks in the invasion percolation case is relatively large. Thus, invasion percolation curves are skewed far more to the right than the random NAPL distribution curves.

The underlying reason for these differences must be due to the position of NAPL within the fracture, which is directly related to the invasion process controlling the NAPL placement. Further explanation for these differences may be obtained by considering arbitrary cross-sections from both a random residual distribution and a distribution created with using invasion percolation. (Figure 3.8)

The random residual distribution has a high initial dissolution area as compared

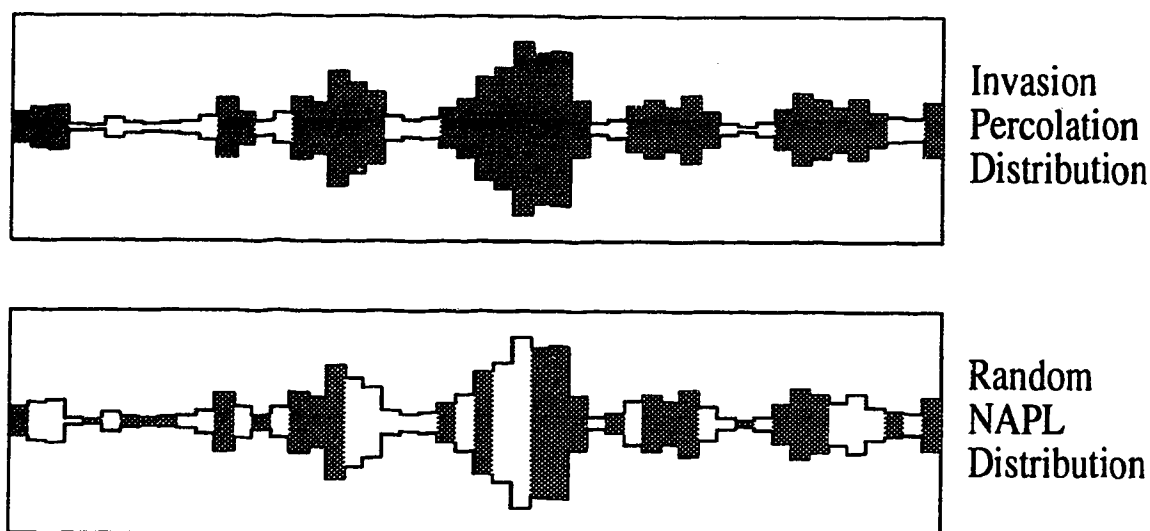


Figure 3.8: Cross-sections through a residual distribution for invasion percolation and random residual assignment. NAPL is shown in grey and water fills the rest of the fracture.

with the invasion percolation distribution. The dissolution area is simply the area of NAPL in contact with water. Even though the cross-section is a simplification of the three-dimensional case, the high initial dissolution area of the random percolation case is visually apparent. It is this high dissolution area that results in random residual distributions having a higher mass output rate than the invasion percolation distributions. Since more of the NAPL is in direct contact with water, the NAPL in random residual distributions dissolves more quickly.

A corollary to this is that the invasion percolation distribution is more continuous. The NAPL is generally located in blobs inside larger aperture spacings. As noted before, these distributions have a smaller initial dissolution area; the NAPL is more likely to be connected in groups. Since there is more NAPL-NAPL contact, there is less NAPL-water contact. Again, this is visually apparent from Figure 3.8. It is the differences in the NAPL distribution patterns that cause the differences between the random residual case and the invasion percolation case in the mass-output curves.

For the invasion scenario, the NAPL begins to dissolve from the edges of the NAPL blobs first. The initial dissolution rates would be low; hence, the initial

mass outputs are low. Once the smaller NAPL-containing cells have been removed the larger ones begin to dissolve. The dissolution of the larger aperture segments containing NAPL yield the peaks seen on the mass output graph. The peaks are generally wider (longer in time) and smaller (lower peak mass-output rate) when compared to the mass output peaks of the random residual distributions. Because of the spatial location of NAPL within the fracture, invasion percolation distributions slow the dissolution process when compared to the random residual distributions.

3.2.2 Random Field versus Saturation Effects

The previous results examined varying NAPL saturations and method of occupation (i.e., random NAPL distribution versus invasion percolation) versus the mass output for a single random aperture distribution. The random aperture distribution will also affect the mass output. To determine whether this effect is significant or predictable further simulations were conducted using a series of statistically similar, but different random aperture fields. Invasion percolation was used to create the initial NAPL residual distribution in each random field investigated. The initial NAPL saturation for every simulation was set at 40% by adding or subtracting NAPL around residual clusters until the target saturation was reached.

Figure 3.9 shows the mass output curves from two separate random field distributions. Even though both begin with an initial NAPL saturation of 40%, the time for total NAPL dissolution varies by over 2000 days. Also, the shapes of the curves vary for each distribution. Curve A has a high initial peak that occurs fairly early. This is similar to the lower saturation curves seen previously. Curve B has a lower peak mass output occurring relatively late. This curve shape is reminiscent of the higher saturations seen previously, yet both mass output curves correspond to the same initial NAPL saturation. Thus, the controlling factor causing the differences in these curves must be the character of the random field and the differences they impose on the residual distributions and flow field.

The random fields are statistically similar. The minor differences in the size

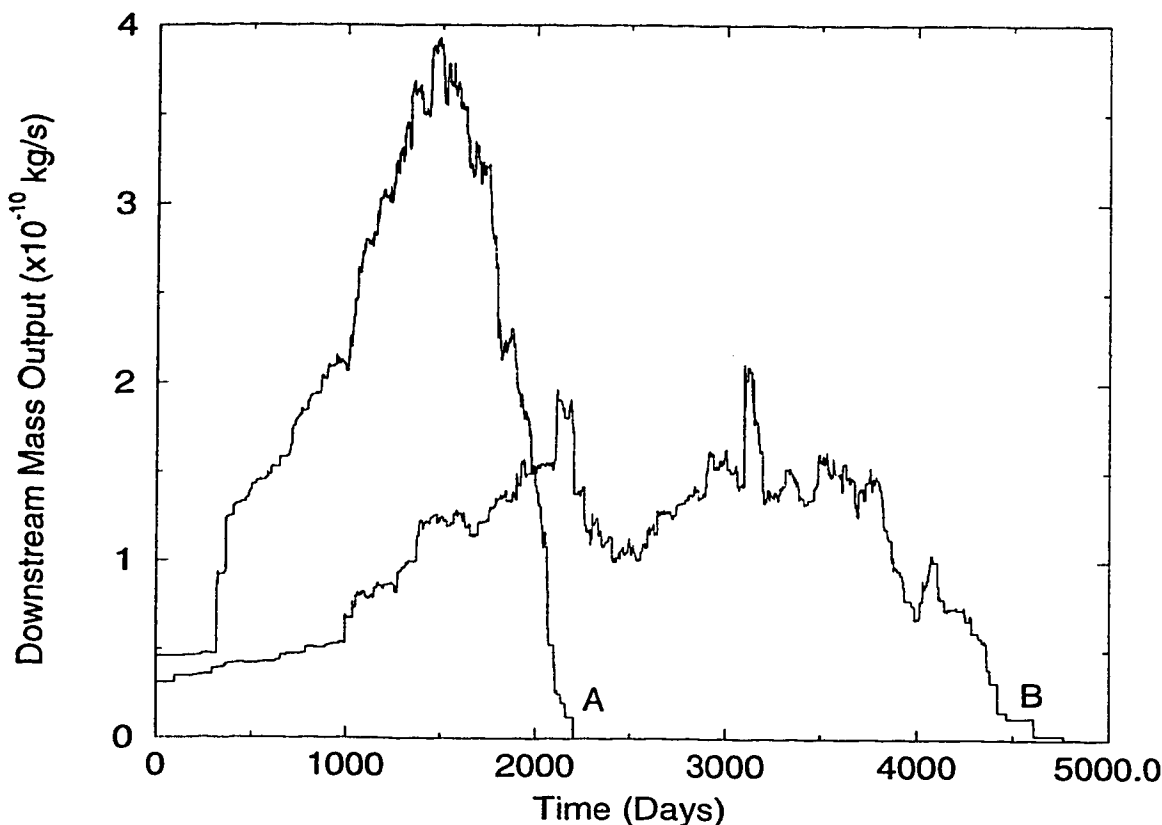


Figure 3.9: Mass output versus time for two distribution created using invasion percolation on three different random fields.

and arrangement of the initial NAPL residual with these fields play a large role in controlling the aqueous-phase mass output. More importantly, it is the series of connected pathways during the invasion process that controls the pattern of the NAPL residual. This effect, even on the conceptual level, is nearly impossible to predict beforehand.

3.2.3 Random Field Variance

The variance of the random field was modified to investigate the type of effect this would have on the mass output curves. Figure 3.10 shows cross-sections of two frac-

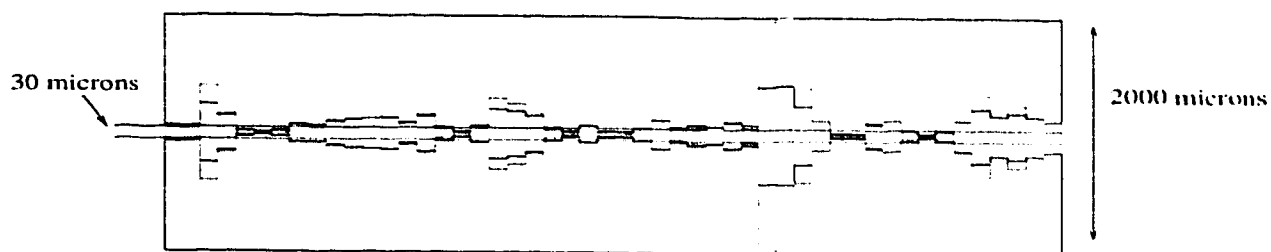


Figure 3.10: A cross-section through two fractures that share the same initial aperture distribution; however, the variance of each one has been modified. The black cross-section has a variance of 0.75 while the grey cross-section has a variance of 2.25, but both have a mean aperture of about 30 microns.

tures. The fractures started with the same aperture distributions and the apertures were modified so the overall variance of the fractures would be different. For the given mean aperture, a fracture aperture distribution with a smaller variance has larger minimum and smaller maximum apertures than a fracture with a larger variance.

The general behavior of the mass output curves after modifying the variance should be predictable. Increasing the variance of the fracture aperture distribution should have two main effects of the mass output curves. First, since the apertures surrounding the NAPL blobs are smaller the initial mass output rates should be smaller for the fractures aperture distributions with larger variances. Also, the time for the mass output peak to occur should be later. Second, the mass output peak should be larger since the peak represents the larger aperture spaces. If the variance of the aperture distribution is larger then the larger apertures space will also be large.

Figure 3.11 shows a two mass output curves for two dissolution simulations. Most of the parameters between the simulations were held constant except for the variance. The result are as exactly as predicted. These results help confirm the importance of the invasion percolation residual (i.e., blobs) in dissolution modeling. It also demonstrates that subtle changes in the nature of the random field can have a dramatic effect on the dissolution of NAPL within the fracture. Also, note that most of the peaks in the output curves can be be correlated with each other. The higher value of variance has the effect of stretching the mass output curve in time.

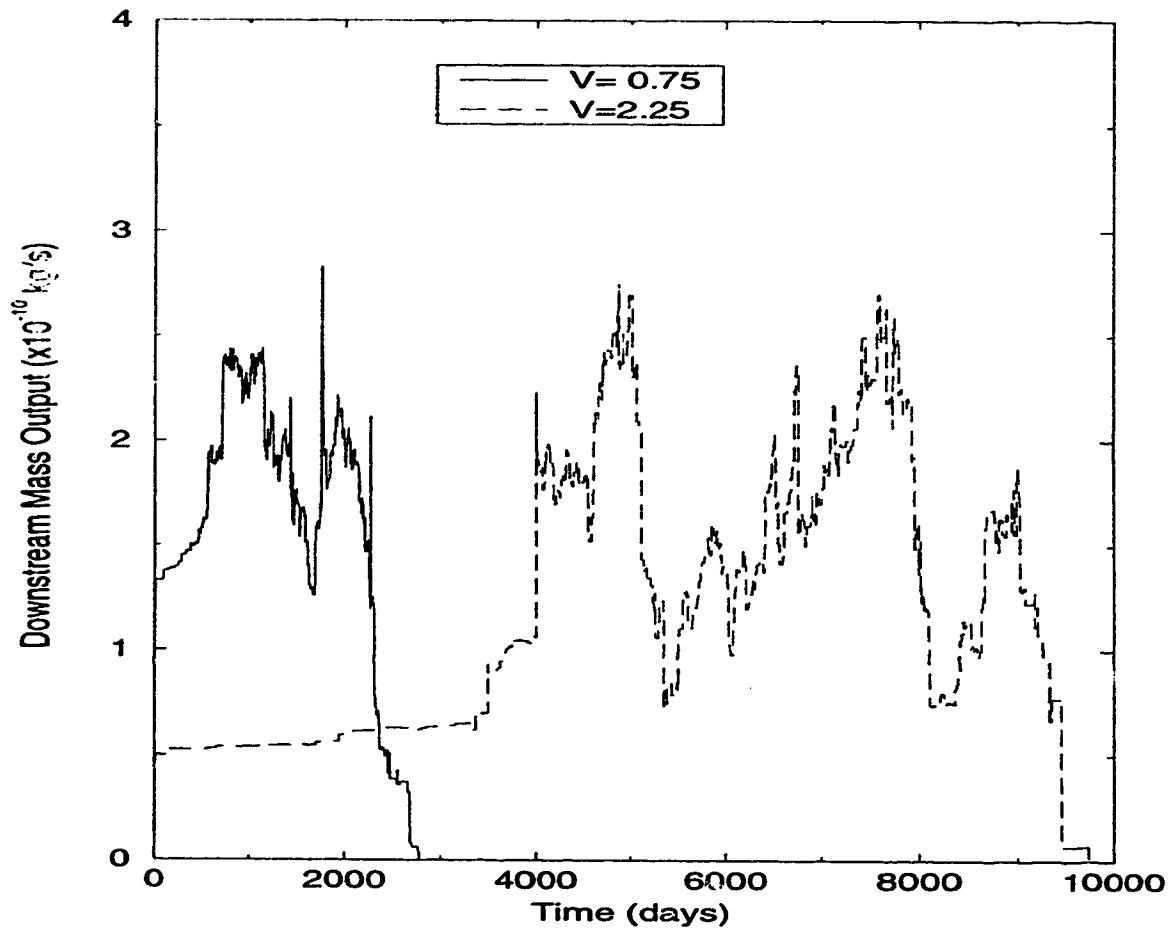


Figure 3.11: Two simulations showing the mass output of the two fractures that differ only by the variance (V) of their aperture distributions.

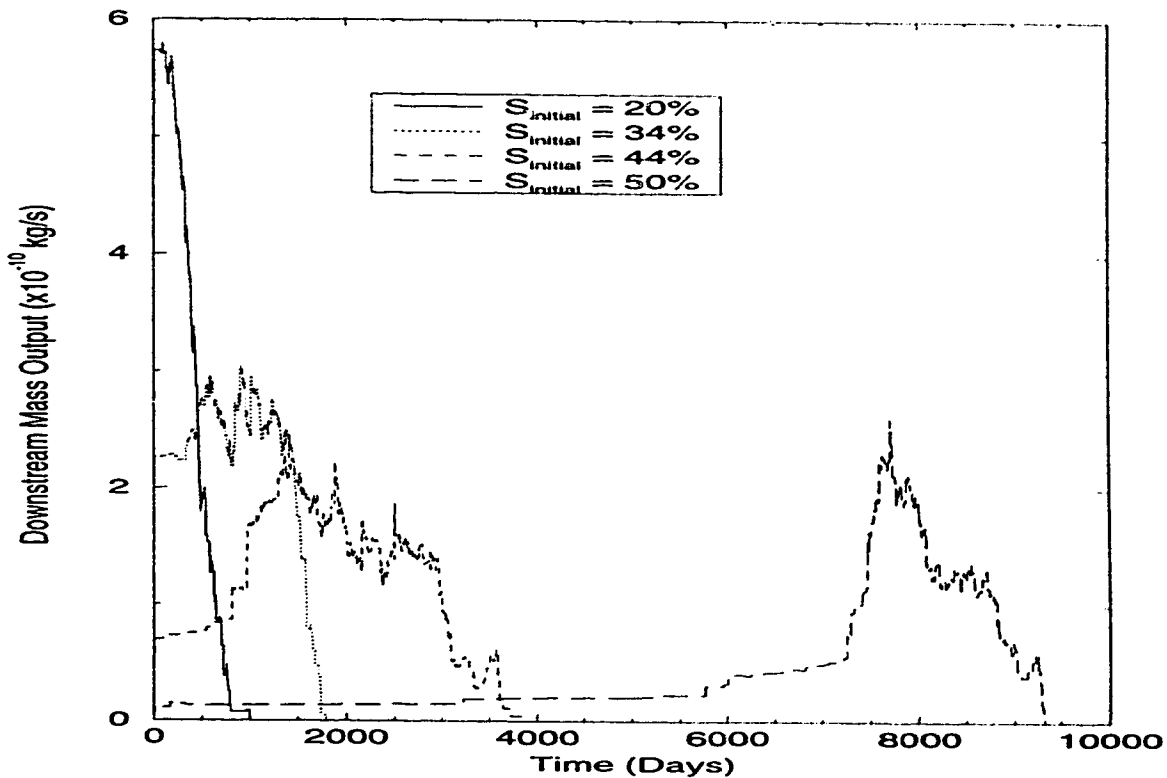


Figure 3.12: Mass-output for four saturation levels created with invasion percolation methods for a single fracture (the same aperture distribution).

3.2.4 Higher NAPL Saturations

The time for the NAPL to completely dissolve can vary by years for fractures with the same initial NAPL saturations, but with different methods of creating the initial residual distribution (e.g., distributions created using invasion percolation versus random NAPL assignment). At even higher initial NAPL saturations the effect becomes further exaggerated as demonstrated by using a NAPL saturation of 50% (compare Figure 3.12 to 3.13).

For the random residual case, increasing the initial saturation this small amount, from 44% to 50%, does not have a dramatic effect on the mass output curve. The peak

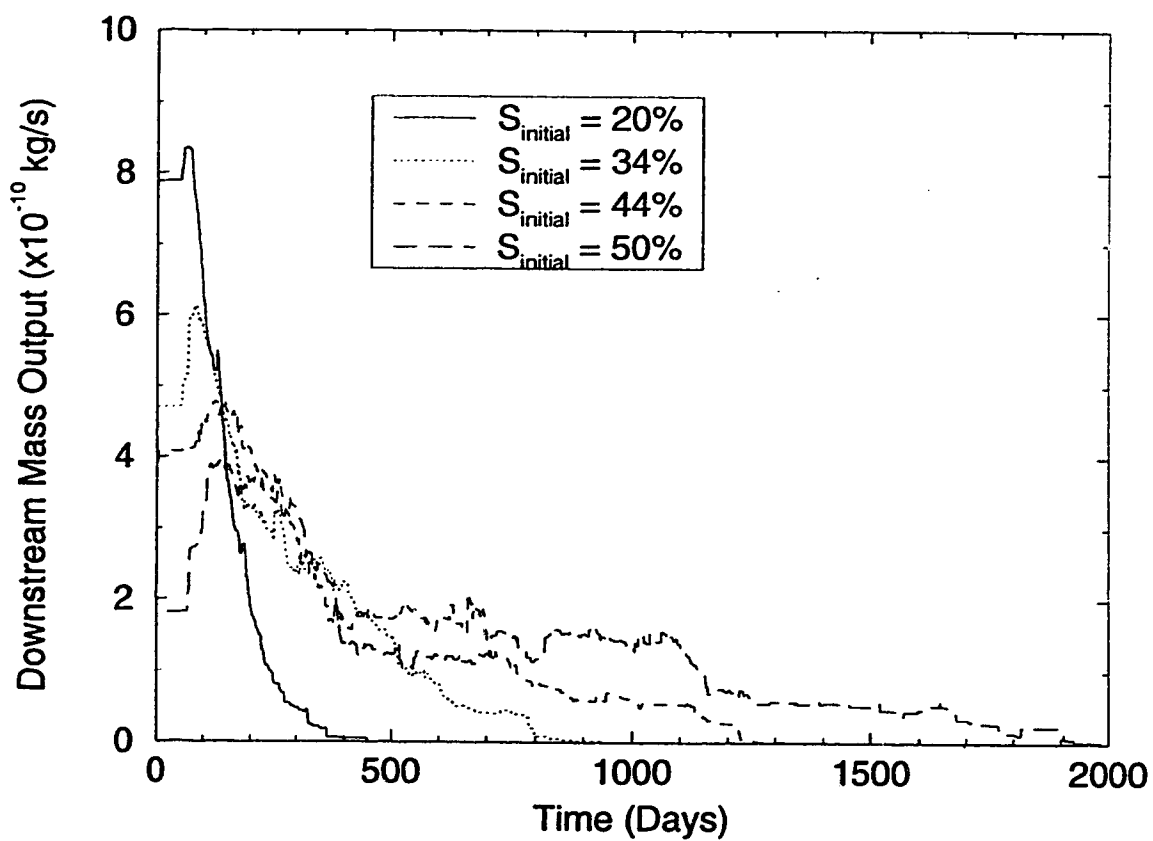


Figure 3.13: Mass-output for four saturation levels created with random percolation methods for a single fracture (the same aperture distribution).

mass output rate has declined and the overall time for complete NAPL dissolution has correspondingly increased. However, for a distribution generated using invasion percolation the mass output peak is delayed significantly where the initial saturation has been increased from 44% to 50%.

At 44% saturation most of the larger aperture segments in the invasion percolation case contain NAPL. When the saturation is increased the only additional space for the NAPL to reside is in the surrounding small aperture spaces. Since the NAPL-water contact area within these aperture cells is very small it takes a very long time for the NAPL to be removed from these smaller aperture cells. Also, the fracture has a low initial relative transmissivity because much of the fracture is filled with immobile and impermeable NAPL. Thus, the volume of water flowing through the fracture is low, which contributes to the slow dissolution rate. Once the smaller cells around the larger ones have dissolved, the mass output increases and the mass output curves have a similar peak rate curve as the lower saturation cases.

For this case there is a significant high saturation point between 44% and 50% initial NAPL saturation. This is the point where the larger aperture segments have been filled with NAPL. Once past this point (i.e. high saturations), the surrounding smaller apertures are filled. This filling of these smaller segments has a large effect on the dissolution time.

Figure 3.14 shows the relative transmissivity curve for four simulations. Each simulation is conducted with the same random aperture distribution. The NAPL residual distribution for these simulations are created using invasion percolation and are then modified to represent varying degrees of NAPL saturation. These four simulations are the same as those presented earlier in Figure 3.12

The 50% initial curve starts with the lowest relative transmissivity. This is to be expected because the NAPL is immobile and impermeable to water flow and is filling much of the fracture. However, this particular simulation continues to have lower relative transmissivities when compared to other curves at the same saturation point. For example, at the 25% NAPL saturation point, the 50% initial NAPL

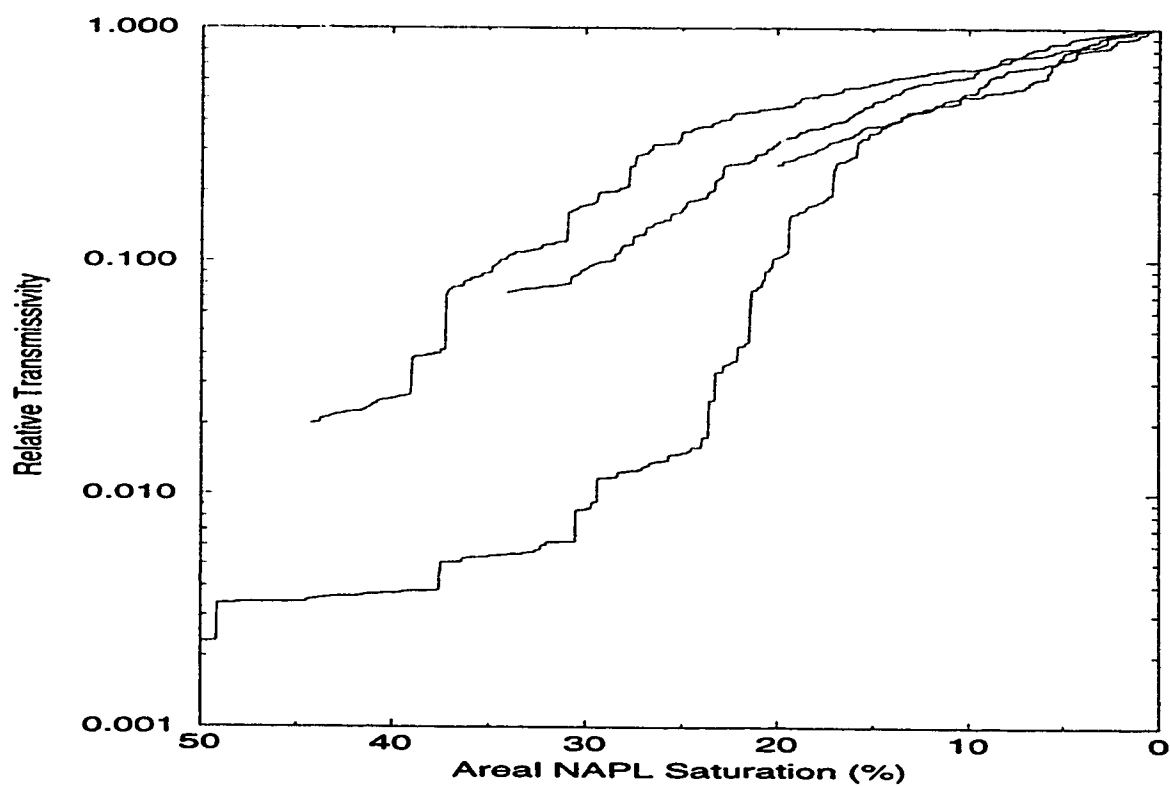


Figure 3.14: Semi-log plot of the relative transmissivity of the fracture versus the volumetric NAPL saturation. The simulations shown here used NAPL distribution created by invasion percolation.

saturation curve has a relative transmissivity of approximately 0.01, yet the curves for initial NAPL saturations of 43% and 33% have relative transmissivities that are over an order of magnitude higher.

The curves produced from the initial NAPL saturations of 20%, 33% and 44% have very similar profiles; however, the 50% saturation curve seems, for the most part, to follow a different path. This curve was differentiated earlier from these other three in the mass-output results. It was considered a “high” saturation case because the dissolution time for the NAPL jumped dramatically. Starting with a higher saturation than the other simulations has had an effect on the path this curve follows. Since the transmissivities are lower for this high saturation case, the dissolution process will take longer.

For comparison, Figure 3.15 shows the relative transmissivity curves for the random residual distributions (Figure 3.13). The overall relative transmissivity of the randomly distributed NAPL is dramatically higher. For example, the initial relative transmissivity for the 43% saturation curve is greater than 0.1. This is over an order of magnitude larger than for the same saturation created using invasion percolation. This trend is apparent throughout all the NAPL saturation levels. The reason for this again has to do with the different position of NAPL relative to the aperture distribution for the invasion percolation case versus the random residual case. The invasion percolation case has the lower relative transmissivities because the larger aperture spaces are preferentially filled. Because the relative transmissivity is directly proportional to the aperture size (Equation 2.5), the invasion percolation distributions have lower transmissivities for equal saturation of random residual distributions.

The other major difference between the invasion percolation and the random residual distribution transmissivity cases is that there is no “high” saturation distinction. The 50% curve in the random percolation case does not show any significant differences from the other curves; just as it did not show any significant differences from the trends in Figure 3.13.

The random aperture field also has an effect on the relative transmissivity curve.

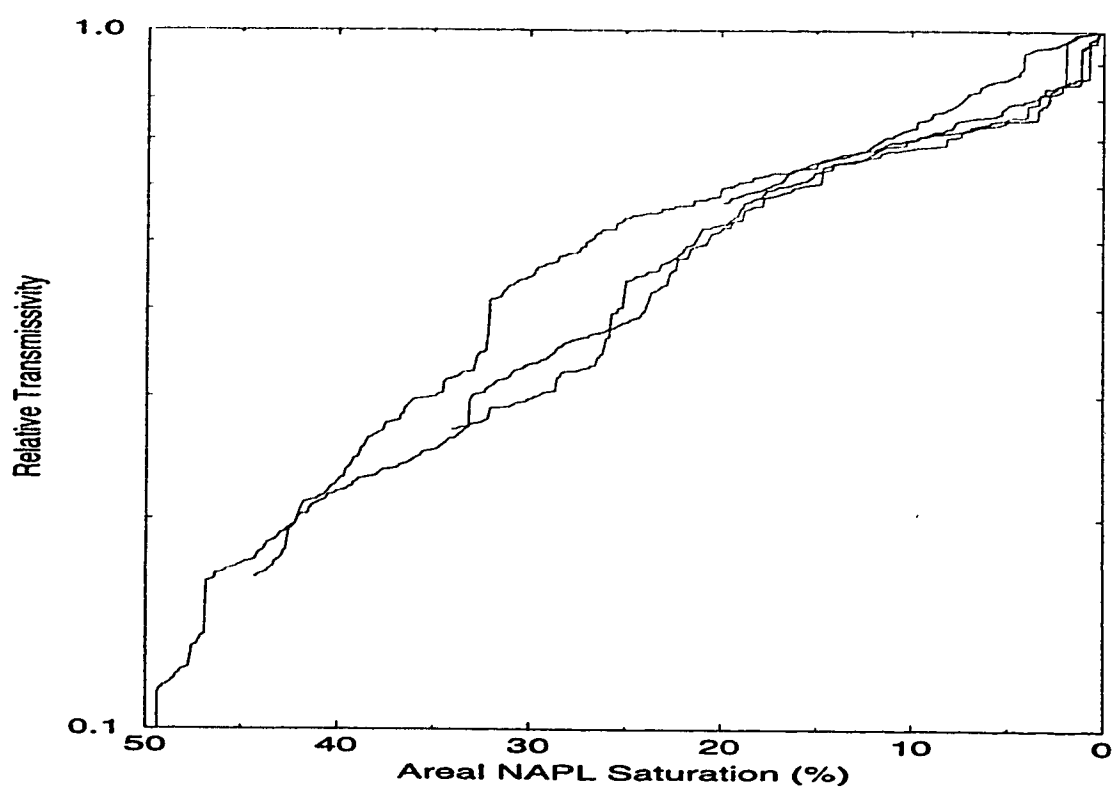


Figure 3.15: Semi-log plot of the relative transmissivity of the fracture versus the volumetric NAPL saturation. The simulations shown here used NAPL distribution created by random residual assignment.

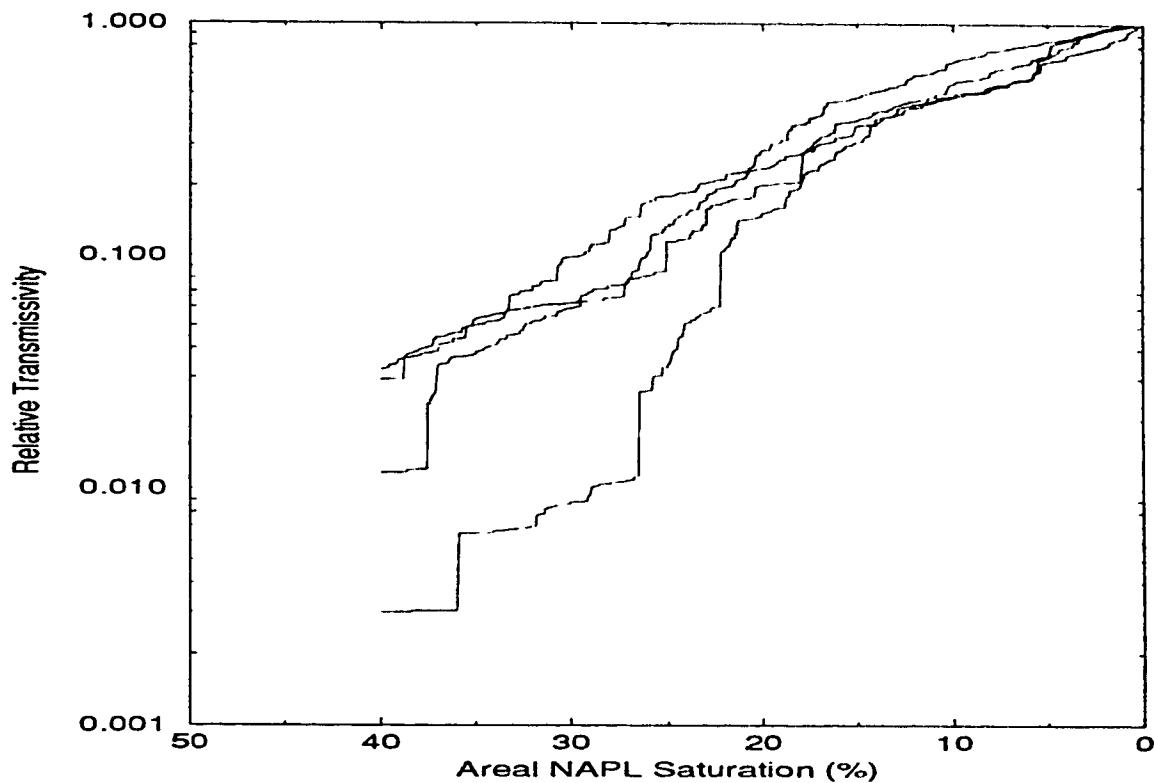


Figure 3.16: Semi-log plot of the relative transmissivity of the fracture versus the volumetric NAPL saturation. The simulations shown here used NAPL distribution created by invasion percolation and all distribution have been modified so the initial NAPL saturation is 40% in all cases.

Figure 3.16 shows the results for 4 simulations conducted with different aperture fields. Initial NAPL saturations of 40% were created using invasion percolation. The transmissivity curve for three of the simulations appear to be similar, however the fourth is lower than the rest. Since these curves are different the pattern of dissolution, and the time it takes for the NAPL to dissolve, will be different. These differences are again related to the unpredictable nature of the random fields.

The relative transmissivity curves converge when the NAPL saturation is less than about 20%. The convergence occurs when the NAPL exists only as disconnected

blobs throughout the fracture. These disconnected blobs do not have a large effect the relative transmissivity of the fracture when compared to higher NAPL saturations. Similar results were presented by *Mendoza* (1992).

NAPL Dissolution Time versus Saturation

Figure 3.17 shows the time for NAPL dissolution versus the initial NAPL saturation. It summarizes many of the concepts that were presented previously. This figure is constructed from the curves in Figures 3.12 and 3.13, and also with information from simulations conducted at lower saturations.

The graph shows two curves, one representing random NAPL distributions and the other representing invasion percolation distributions. The curves are similar for lower saturations (below 30%); however, at higher saturations the NAPL dissolution times for the invasion percolation case begin to increase dramatically. As stated earlier, this is due to the larger pore spaces and the surrounding smaller ones becoming completely occupied with NAPL. The “high saturation point” in this case would be around 46% to 48% where the curve suddenly flattens.

Areal Saturation Plots and Discussion of Boundary Effects

The order in which the NAPL disappears from the fracture is different when comparing the 44% case to the 50% case. This is indicated by the different paths the relative transmissivity curves follow.

Figure 3.18 is a plot of the areal NAPL distribution within the fracture and shows how that distribution changes during the dissolution process. There is little difference between the distribution of the two cases early in the dissolution process; however the 44% case disappears much faster and in a different order. The difference in dissolution time can be explained by the difference in initial relative transmissivities. Since the initial relative transmissivity of the higher saturation case is low, there is little water flowing through the fracture. The aqueous-phase concentration of NAPL within the fracture reaches the solubility limit and the dissolution on NAPL slows

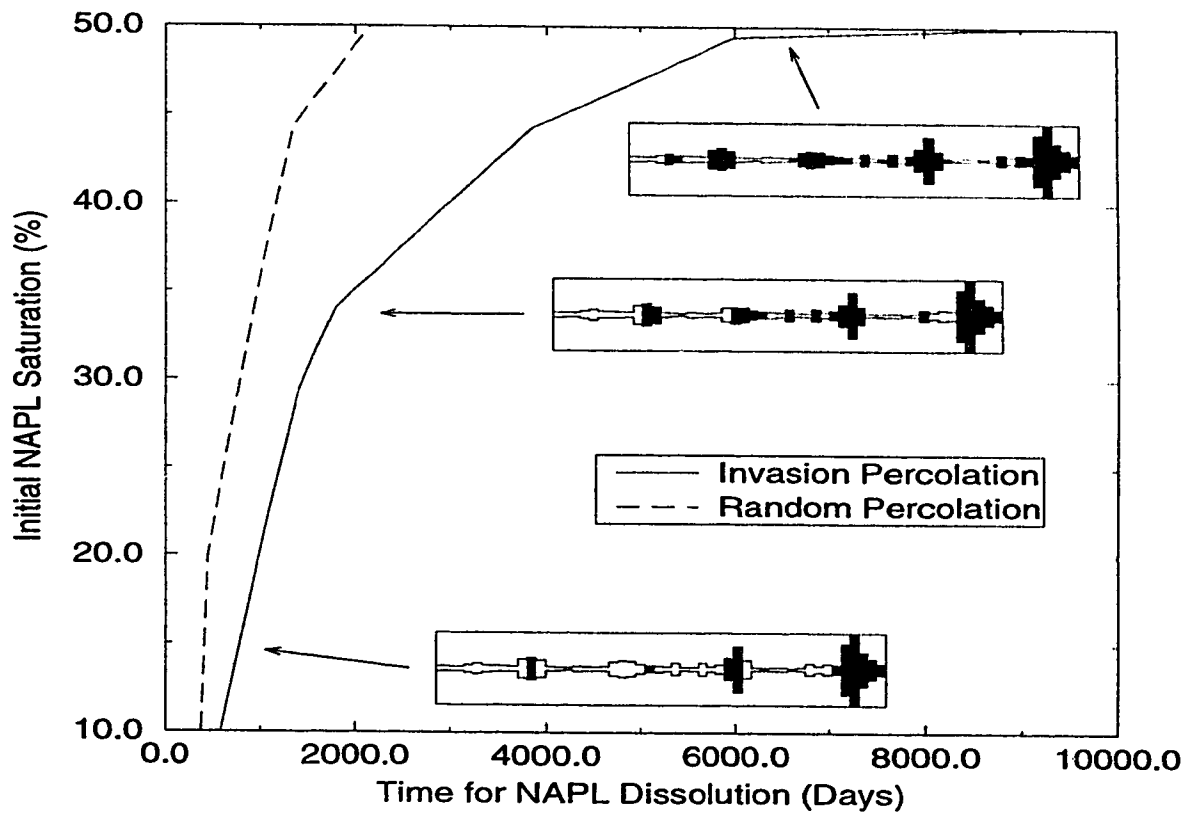


Figure 3.17: Time for NAPL dissolution versus the initial NAPL saturation. The cross sections show the NAPL position for the invasion percolation case at various points on the curve.

dramatically. The dissolution rate increases only when the transmissivity increases to the point where water can move significant amounts of aqueous-phase NAPL out of the fracture.

The pattern in which the NAPL disappears is also different. This results from the boundary conditions imposed on the simulation. For the high saturation case, very little mass is transported out of the downstream boundary, instead the NAPL slowly diffuses out the left-hand side. Until a significant pathway is opened up, this diffusion is the main mechanism for NAPL to exit the fracture. Since this process is very slow, it takes a very long time for the NAPL to dissolve. Also, the NAPL is removed along the left-hand side of the boundary as opposed to along major flow paths (such as in the lower saturation case, see Figure 3.18).

3.2.5 Groundwater Flow and Mass Transfer Coefficient

To this point only the effects of saturation, percolation method and various random fields on dissolution have been investigated. The effect that the mass transfer coefficient and groundwater velocity have on the time for the NAPL to completely dissolve is also important. If the dissolution time is long, then the NAPL residual can act as a long-term source of groundwater contamination that would be difficult or impossible to remediate. If the dissolution time is decreased, the NAPL may be able to be removed using conventional remediation technologies.

To investigate some of the effects of groundwater flow rates and the mass transfer coefficient has on the NAPL dissolution times several additional simulations were conducted. Each simulation used the same random field and the same initial residual distribution created using invasion percolation.

Groundwater Flow

The groundwater velocity through the fracture, which is related to the volume of water coming into contact with the NAPL is a controlling factor in the rate of dissolution. In the discrete fracture there is no single groundwater velocity that can be

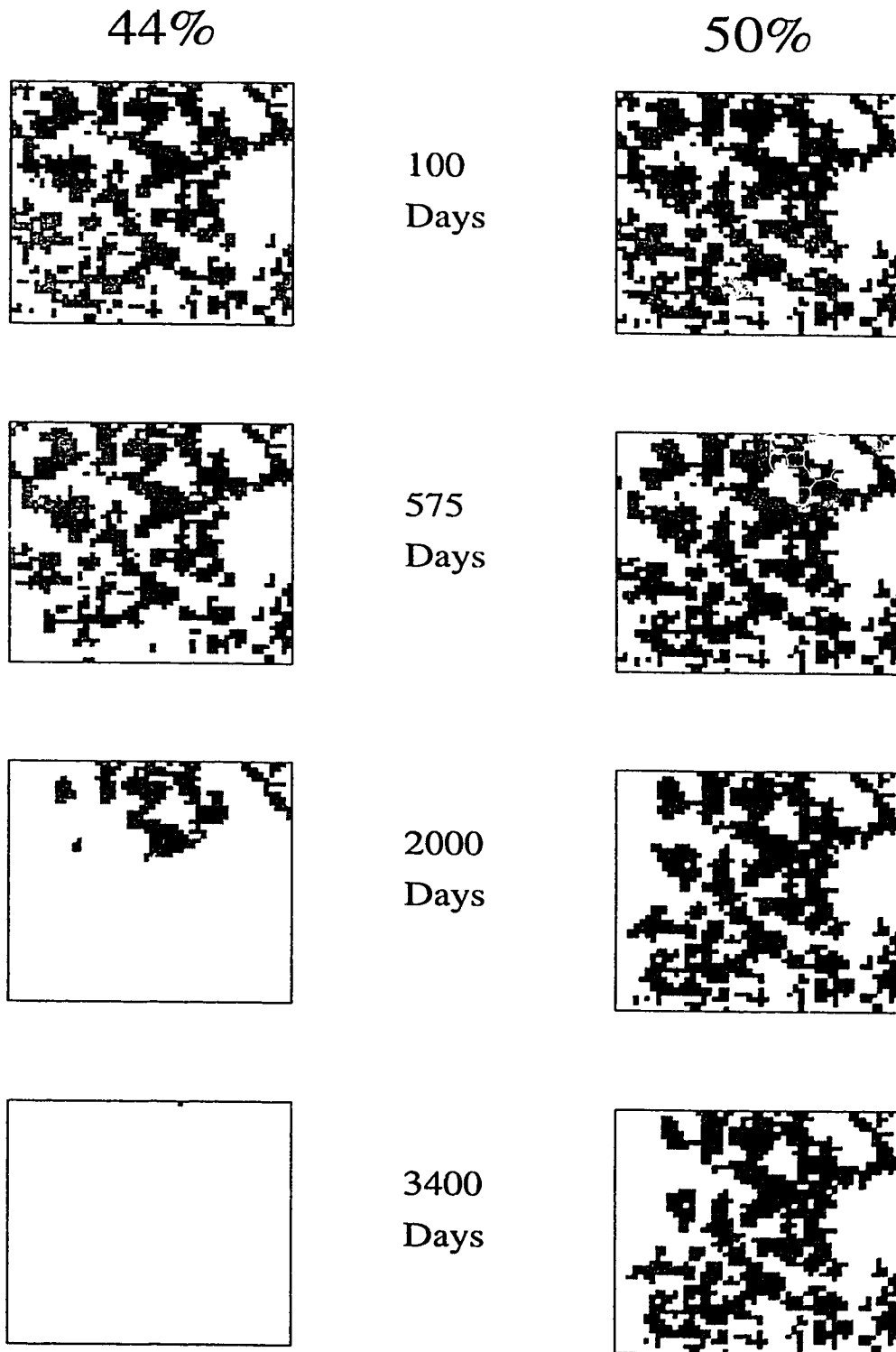


Figure 3.18: Areal saturation plots for two similar simulations with different initial areal saturations. Shading indicates NAPL.

used to characterize the flow through the fracture. Instead, the gradient across the fracture is used. An increase in the gradient directly correlates with an increase in the groundwater velocity. Of course, increasing the gradient across the fracture also increases the volume of water that passes through the fracture for a given amount of time.

Figure 3.19 shows the relationship between the gradient across the fracture versus the time for dissolution for a single residual distribution. Note the flattened part of the curve past about 7000 days. This part of the curve is mainly controlled by diffusion out of the fracture at the left-hand side. Due to the constraints of the boundary conditions for the transport model, mass can only exit via diffusion through the left hand boundary; therefore, the slope at this point in the graph may be less than expected under “real” conditions.

The effect that the groundwater flow rate has on dissolution is most dramatic in the neighbourhood of 5000 days. Here the groundwater velocity is still relatively small and the dissolution time is relatively long. However, only the smallest change in groundwater velocity produces over a 2000 day difference in the time required for NAPL dissolution. This effect is mainly a result of the right-hand boundary condition. Mass that was previously building up at the boundary and not exiting the system is now being carried across the boundary by advection. Moving this mass across the boundary lowers the concentration in the system, which increases the rate of dissolution and decreases the dissolution time.

Figure 3.19 shows that if the gradient across the fracture is increased to about 0.2 m/m , the dissolution time is around 2500 days. This difference in dissolution time is not as dramatic as in the previous step. The rate of groundwater flow is being increased; however, the rate of mass transfer from the non-aqueous to the aqueous phase remains the same. The controlling factor in the flux term controlling the dissolution is the mass-transfer coefficient (k_t) instead of the difference between the maximum solubility and the actual concentration ($C_s - C$).

When looking at higher head gradient values, such as 0.4, increasing the water

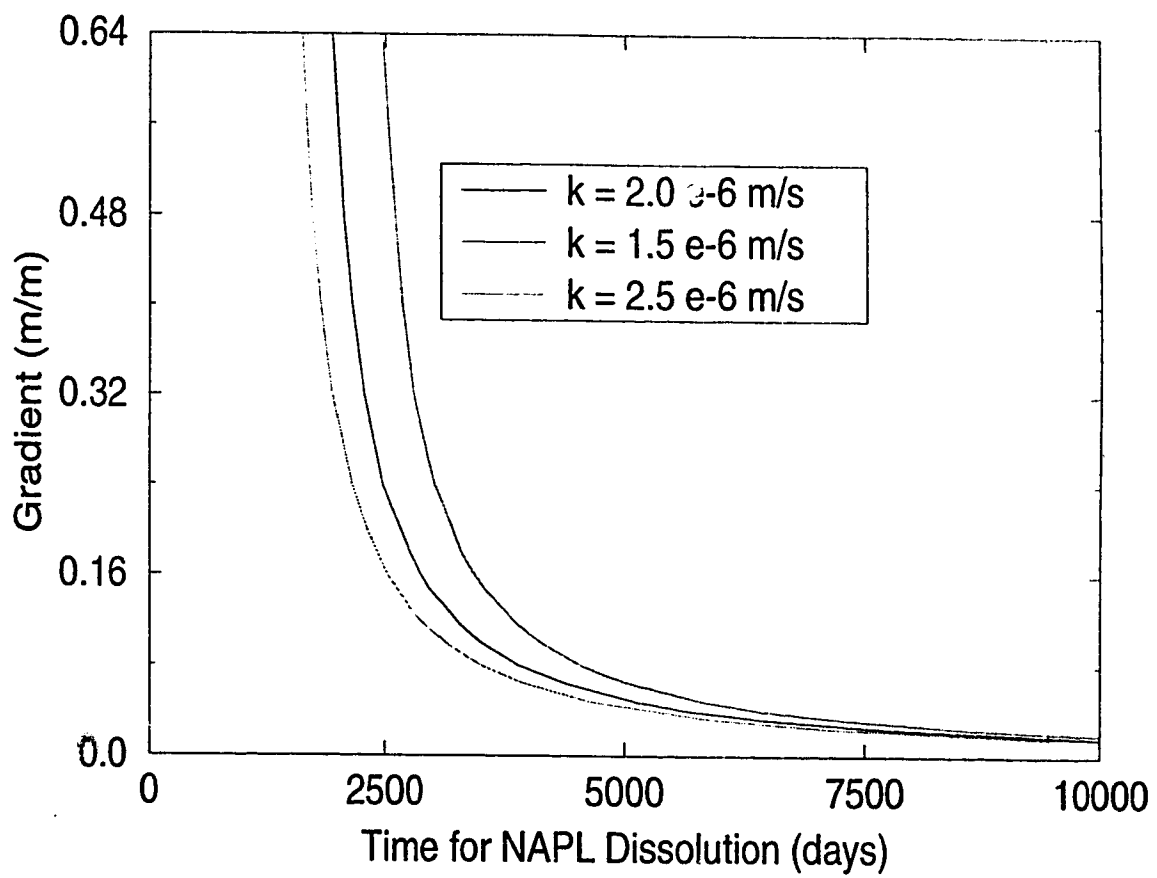


Figure 3.19: Time for NAPL dissolution versus the gradient across the fracture.

flow rate has nearly lost its effect on dissolution time. Here the water is flowing fast enough to keep mass from building up and concentrations from being high; therefore, the mass transfer coefficient is controlling the dissolution.

Mass Transfer Coefficient

Figure 3.19 also shows the effect that varying the mass transfer coefficient has on dissolution times. At low groundwater flow rates, variation in the mass transfer coefficient has little effect on the rate at which mass will be dissolving because the local concentration difference ($C_s - C$) is the controlling factor. However, when groundwater flow rates are high, differences in dissolution times due to changes in the mass transfer coefficient are more apparent. Obviously, increasing the mass transfer coefficient will result in a shorter dissolution time and vice-versa; the increase in mass transfer rates has a diminishing effect similar to increasing the rate of groundwater flow.

3.3 Monte Carlo Results

Results to this point demonstrate that the aperture field and residual distribution have large affects on the dissolution of the NAPL. However, a precise description of the effect that a certain aperture field will have on dissolution is difficult, if not impossible, to obtain. To better understand the range of dissolution behavior that different, but statistically similar, aperture fields have a Monte Carlo analysis is performed.

3.3.1 Mass output

Multiple simulations are conducted on many different initial residual distributions that were each created from a unique random aperture field. The placement of residual is generated using invasion percolation and the final residual distributions for each random aperture field following the invasion process is left unmodified. The

| | Value Used |
|-----------------------------------|---------------|
| Height/Length of Fracture | 1.25 <i>m</i> |
| Number of Elements | 2500 |
| Average Aperture | 27.5 μ |
| Head Differential Across Fracture | 0.20 <i>m</i> |

Table 3.2: Parameters used for Monte Carlo simulations

initial areal NAPL saturations are all within approximately 20% . The initial statistics used in generating the random aperture field, such as the average aperture, are held constant for every simulation. The random seed used to generate the random aperture distribution is the only parameter that is varied. Changing this seed will cause the random distribution of apertures to be different, which also results in a different residual distribution. Table 3.2 shows the parameters used for the generation of the aperture and residual distributions and some of the parameters used for the dissolution modeling.

Analysis of several simulations shows that the basic pattern is generally the same for all aperture/residual distributions. Figure 3.20 shows the mass output versus time results from 20 simulations. Curves that have a higher maximum mass output have been marked in black, while curves that have a lower maximum mass output have been marked in grey; this arbitrary distinction is useful for further analysis. There are curves that have profiles similar to the low saturation curves in the previous section (black curves). Also some curves have profiles similar to the high saturation curves in the previous section (grey curves). From the previous results we know that the random aperture distribution and NAPL saturation/distribution are controlling the profile of these mass-output curves. The only parameter that has been varied has been the random seed for the generation of the random aperture field. It is obvious from Figure 3.20 that the effect of the different random aperture fields is dramatic.

Figure 3.21 shows the mass-output of the fracture versus the NAPL saturation during dissolution. The curves are from the same simulations that are used in Figure 3.20, with the same black versus grey separation between high and low maximum

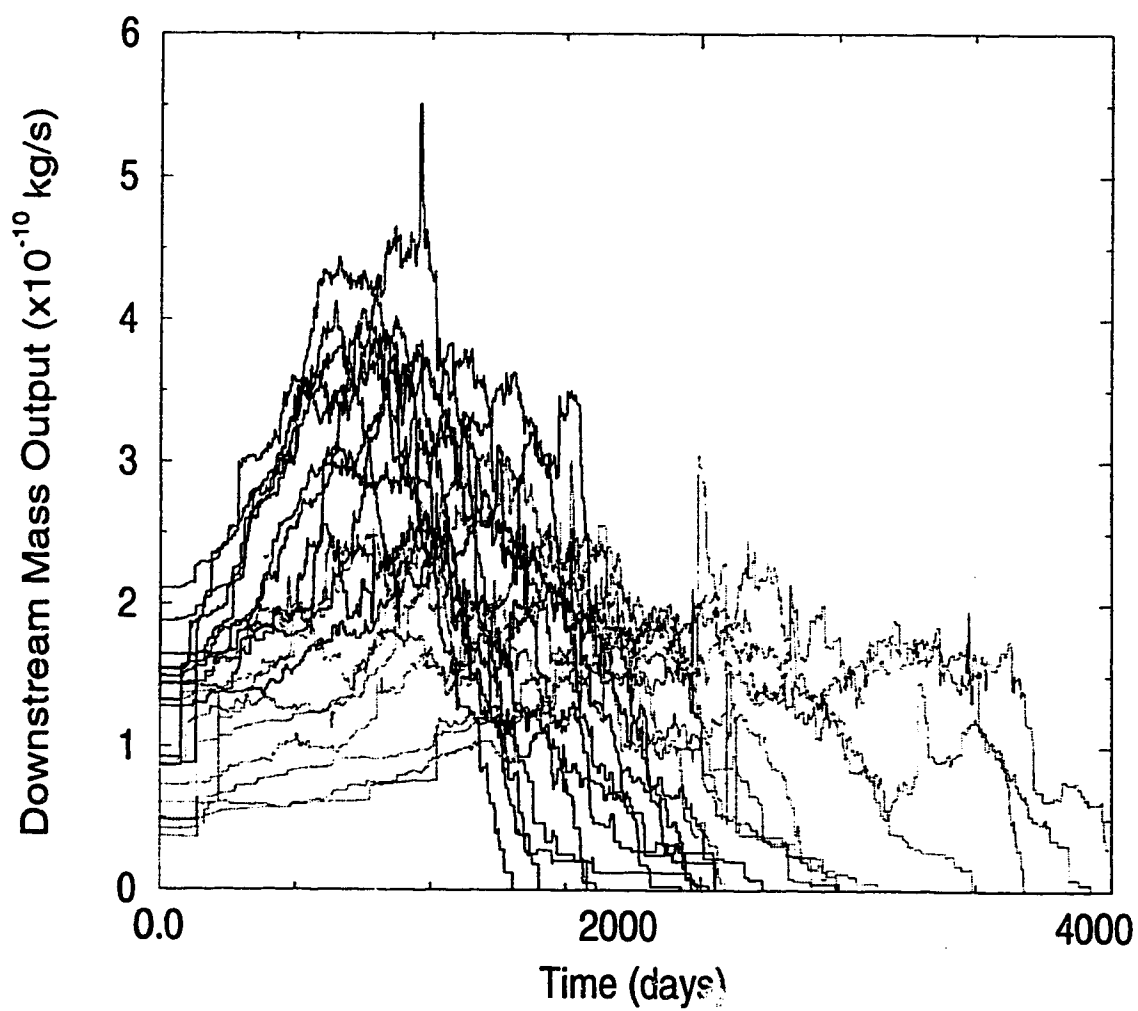


Figure 3.20: Downstream mass output versus time. Black and grey lines shown an arbitrary separation.

output values being used. The curve shape between each simulation is similar except for the maximum mass-output rate. This maximum rate occurs around 20% to 40% volumetric saturation of NAPL. Note that there is a correlation between the initial volumetric saturation of the wetting phase and the maximum downstream mass output; higher initial wetting-phase volumetric saturation (lower NAPL saturation) generally results in higher downstream mass outputs.

The curves that have a high mass output result from NAPL being trapped in larger aperture segments. This results in a larger area of NAPL in contact with water; dissolution time is decreased and the rate of mass output is increased. Curves that have a lower mass output result from NAPL being trapped in small aperture segments. This results in a smaller area of contact with water; dissolution time is increased and the rate of mass output is decreased. This concept, which has been discussed previously, is illustrated in Figure 3.22

Some of the mass-output profiles appear to be produced by saturations similar to case A while some appear to be produced by saturations similar to case B. A high mass output case and a low mass output case will be examined. Figures 3.23 and 3.24 show the previous results with two individual examples of a high output case and a low output case highlighted.

The highlighted residual cluster in the cross-section of case A (Figure 3.26) shows the NAPL in a larger set of aperture segments. The surface area of NAPL in contact with the surrounding water is relatively high. This results in a greater mass flux of NAPL from the non-aqueous to the aqueous phase. Compare this to the highlighted section in the cross-section of case B (Figure 3.26). Here, most of the NAPL is trapped in segments which are relatively small, except for the centre of the residual cluster. The area in contact with water is relatively low, therefore the mass flux during dissolution is also low. Since the mass flux is low, the residual cluster will take a longer time to disappear than the cluster in case A. When the smaller segments around case B cluster have dissolved, the center part will disappear relatively quickly with high mass fluxes into the water leading to the rapid decline in mass output at

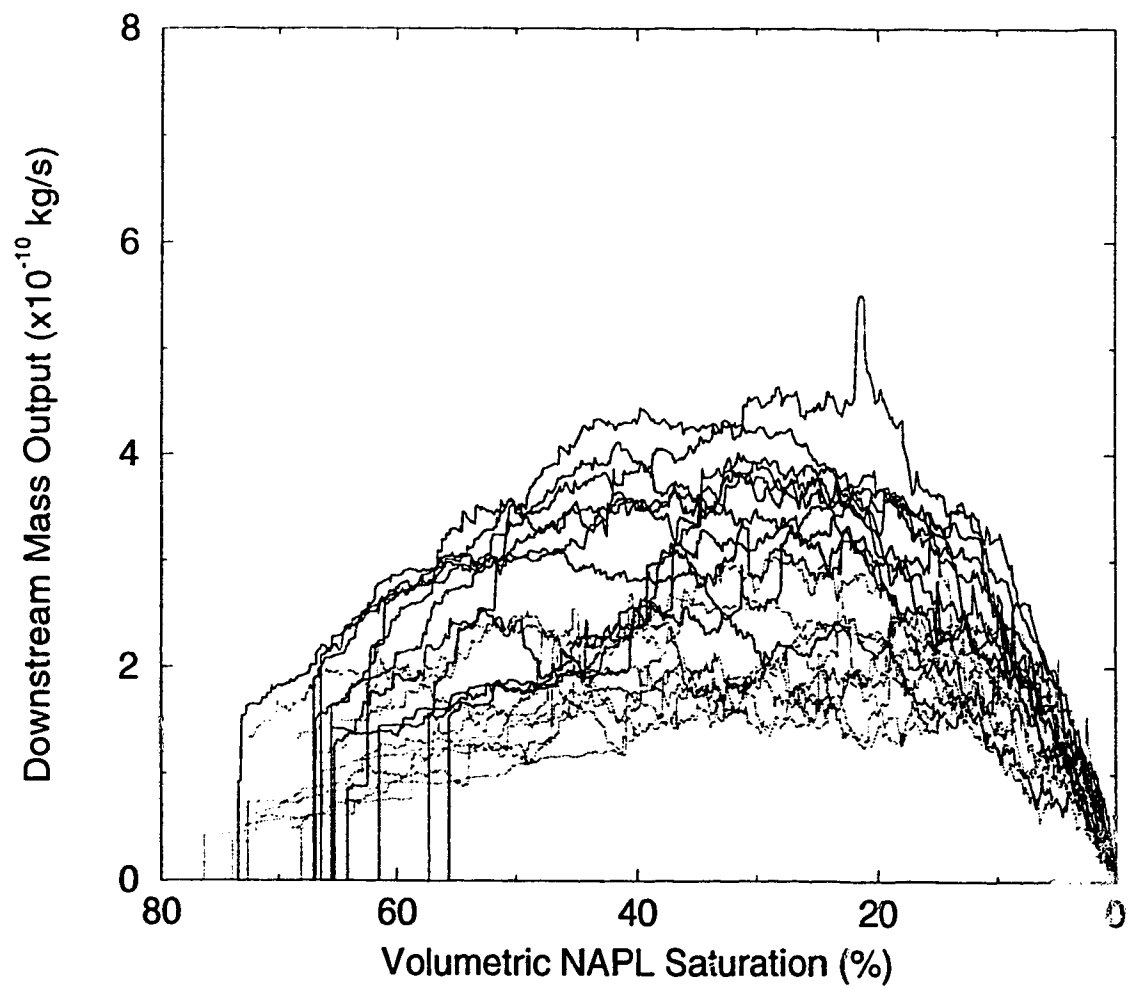


Figure 3.21: Downstream mass output versus volumetric saturation of the wetting phase. Black and grey lines shown an arbitrary separation.

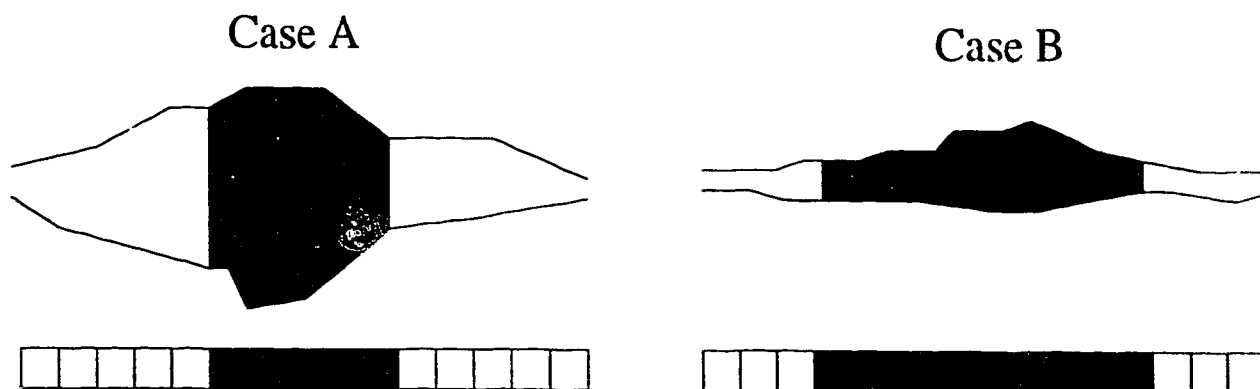


Figure 3.22: Two conceptual cases on how NAPL is located within a fracture. The bottom grid shows what the areal saturation would look like in plan view.

the tail end, similar to case A.

The cluster in case A (Figure 3.26) is surrounded by smaller aperture segments. If these segments were filled with NAPL the pattern of dissolution for the cluster would be more similar to case B. Generally, NAPL is trapped in larger aperture segments. Naturally, these larger aperture segments are surrounded by smaller aperture segments. If these surrounding aperture segments contain no NAPL the dissolution patterns (such as mass output over time) will be similar to case A. If these surrounding aperture segments contain NAPL, then the dissolution pattern will be similar to case B.

The initial residual distribution patterns cannot all be simply identified as case A or case B type initial residual clusters. On the contrary, when looking at other cross-sections of case A, case B type residual cluster distributions can be found and vice-versa. The controlling factor is how many case A residual distributions there are compared to how many case B residual distributions. It is the relative distribution of these two cluster types that will determine which case the mass output will resemble. Because there is a spectrum of distribution types (i.e., some distributions have more case A distributions and some have less) there is a distribution of the mass output curves from type A to type B.

Despite the fact that the above behavior and their causes have been clearly identified, identifying a priori whether a residual pattern will produce a type A or type

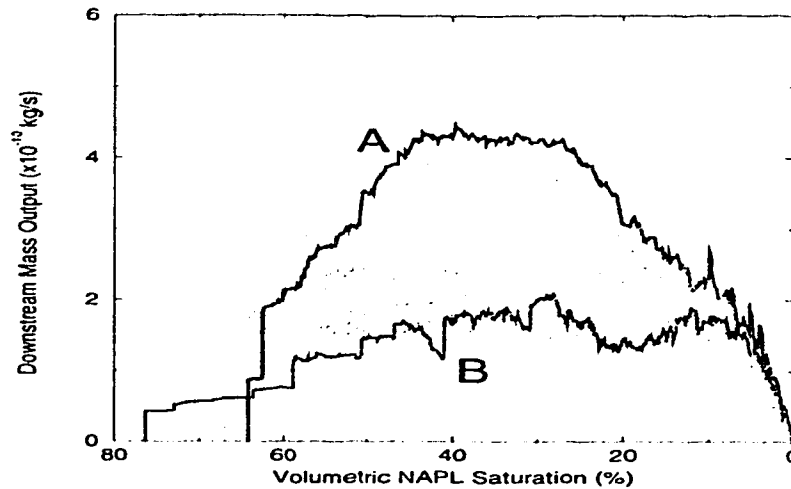


Figure 3.23: Downstream mass output versus volumetric saturation of the wetting phase. Two example realizations are highlighted.

B mass output result is difficult. It is especially difficult in these simulations since the random aperture distribution is the only real variable. There is some indication given by the initial NAPL saturation. For example, Figure 3.25 shows the two initial residual distribution for simulations that produced the A and B mass-output curves. Residual distribution B does have a greater saturation. However, in the scope of these simulations, the effect of the random field is just as important as the areal saturation of the initial residual NAPL.

3.3.2 Relative Transmissivity

Figure 3.27 shows the relative transmissivity curves for the 20 Monte Carlo simulations discussed above. The same distinction between the high mass-output curves and low mass-output curves (black versus grey) has been made. There is no apparent distinction in the paths the relative transmissivity curves follow between these two cases. In general, the grey curves (i.e., corresponding to simulations that have relatively longer dissolution times) have lower starting relative transmissivities similar to the example shown in Figure 3.14.

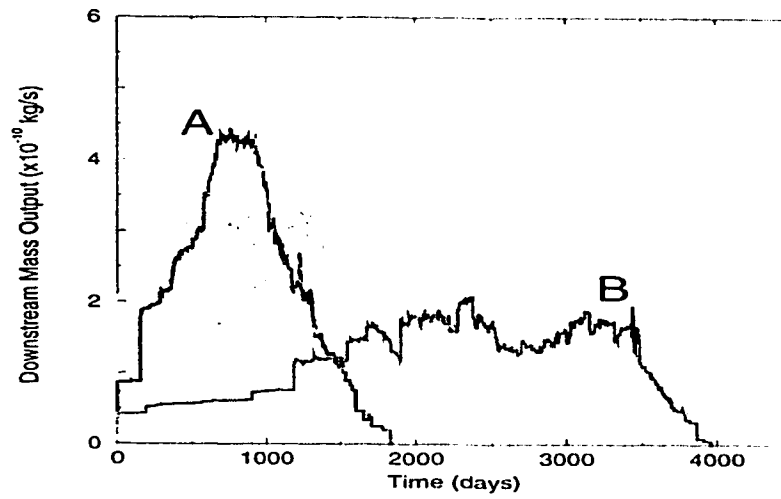


Figure 3.24: Downstream mass output versus time. Two example realizations are highlighted.

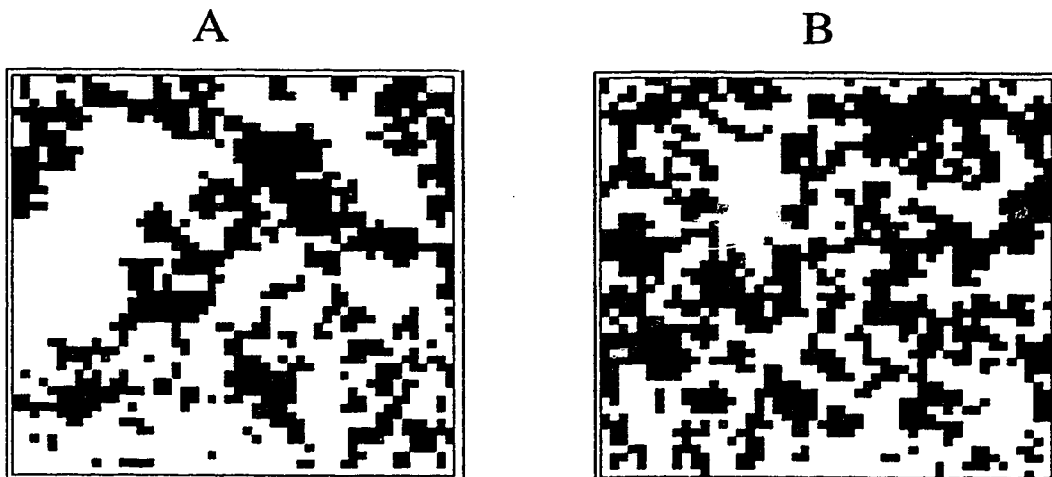


Figure 3.25: Initial residual distribution for cases A and B.

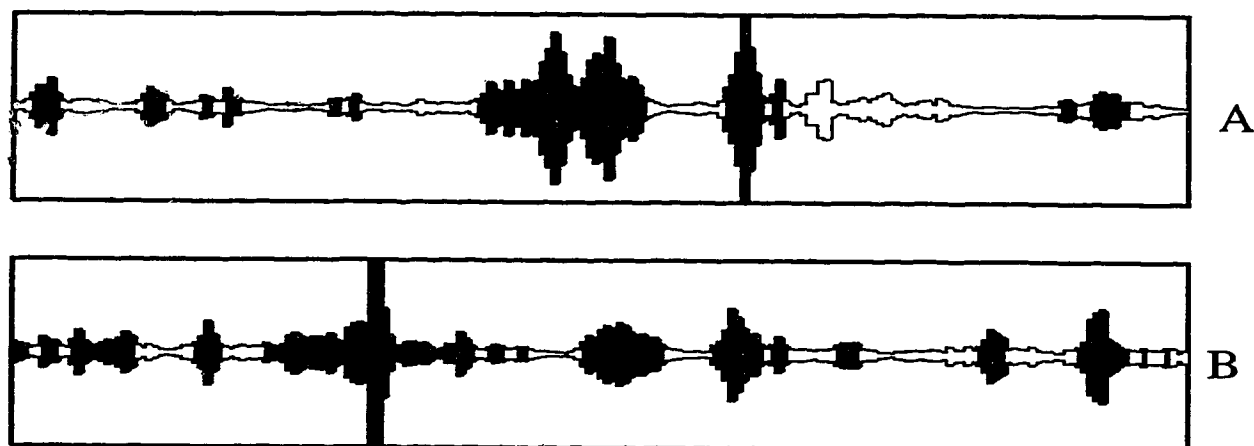


Figure 3.26: Cross sections taken through cases A and B.

These curves depend not only on the original placement of the NAPL as the mass output results do but, they also depend on the order of disappearance of NAPL. That is, when one cell containing NAPL is removed the transmissivity of the entire fracture will change accordingly. A cell may be right near a flow channel and affect the transmissivity dramatically when it disappears or it may have little effect on the relative transmissivity when it is removed.

Figure 3.28 shows the effect of varying the mass transfer coefficient and the average groundwater velocity on the relative transmissivity curves. Simulations were conducted on one random aperture field with the same initial invasion percolation distribution. The gradient was modified from $8 \times 10^{-5} m/m$ of water head to about $0.4 m/m$ of water head across the fracture. The mass transfer coefficient was modified from $1.5 cm/s$ to $2.5 cm/s$. The results show very little difference in the relative transmissivity curves which suggests that the NAPL is being dissolved in nearly the same order for every case, even though dissolution times can vary dramatically.

The one dotted curve in Figure 3.28 corresponds to a very low gradient case. Here the NAPL does dissolve in a slightly different order. This is due to the limiting right-hand boundary condition. The limitation of this boundary is that mass can only cross that boundary via groundwater advection. Because the groundwater velocity is low, more NAPL diffuses out the left hand-side boundary than exits at the right.

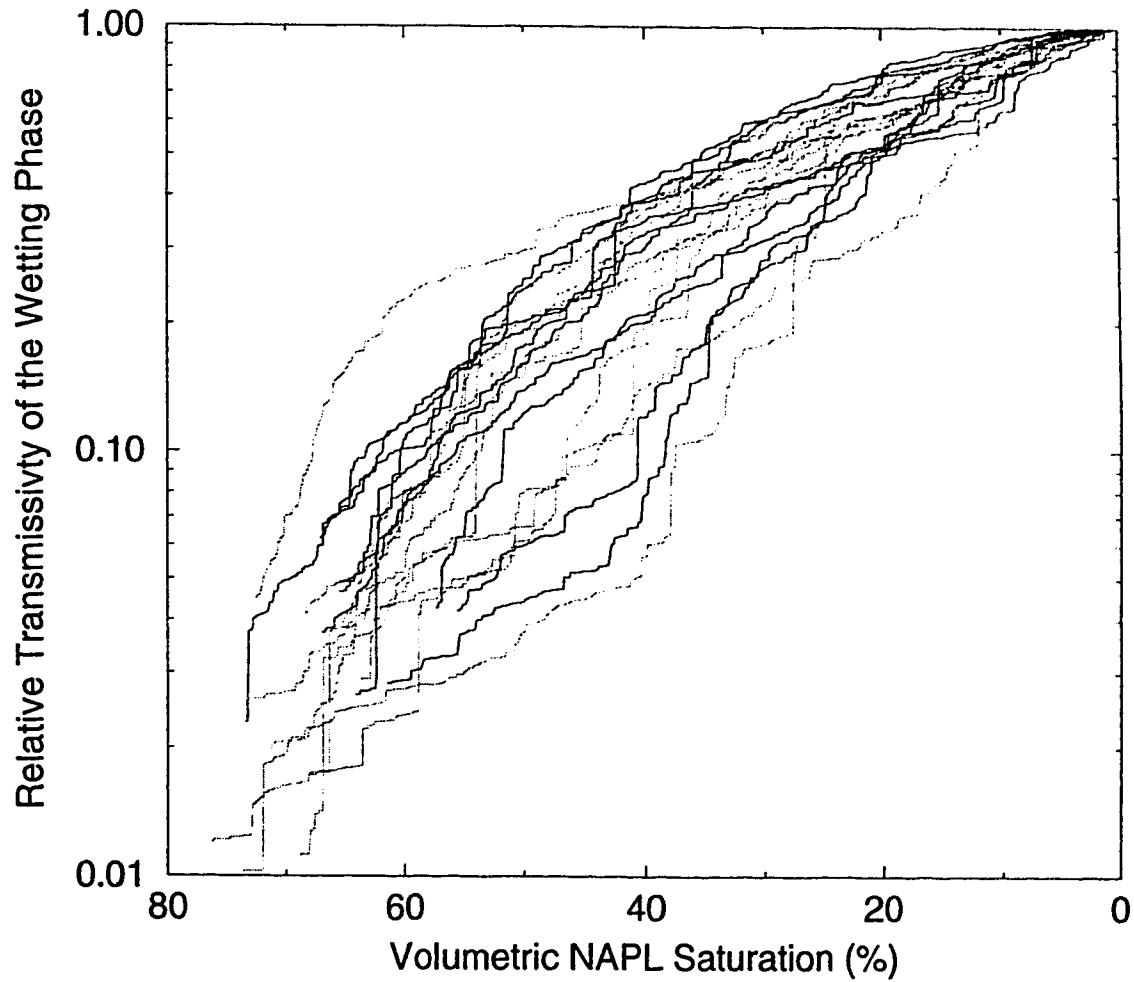


Figure 3.27: The relative transmissivity curve from the Monte Carlo analysis. The same black and grey separation of the curves is used.

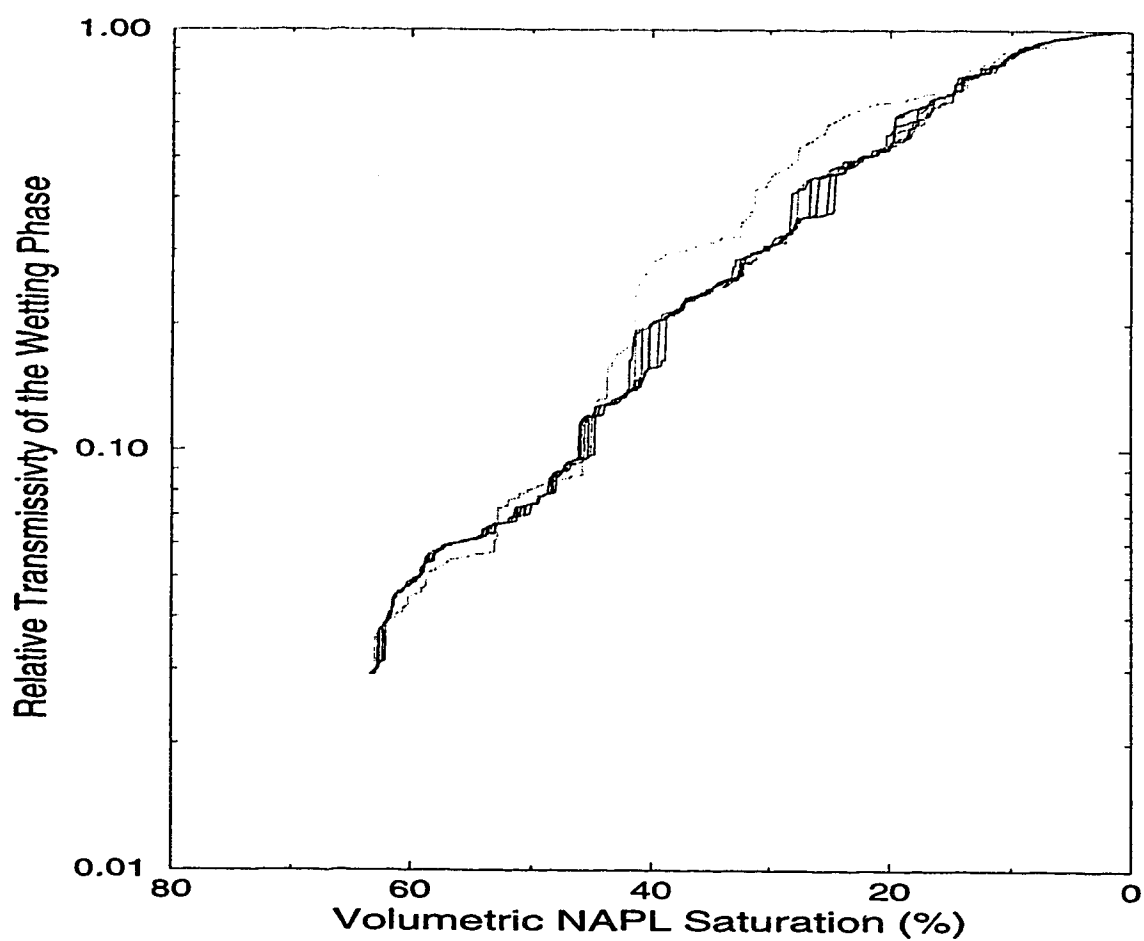


Figure 3.28: Relative transmissivity curves where the groundwater velocity and the mass transfer coefficients are varied.

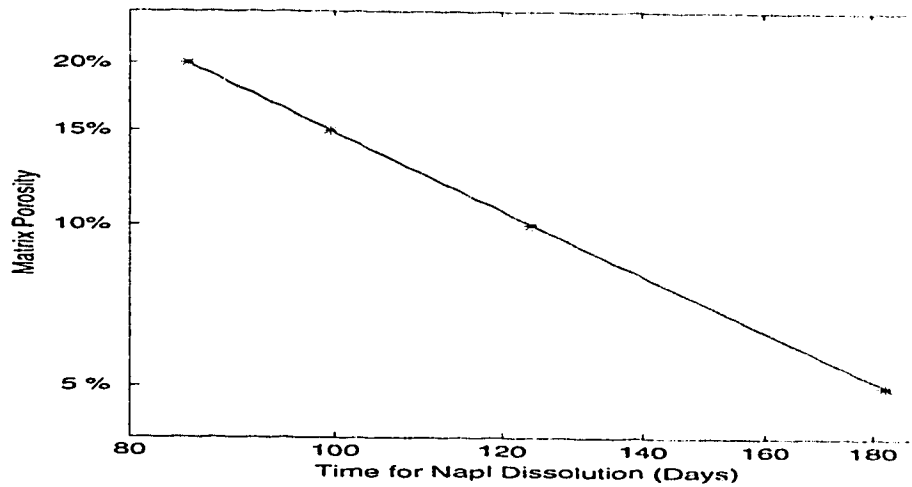


Figure 3.29: Plot of NAPL dissolution time versus matrix porosity.

3.4 Permeable Matrix

The results presented to this point have all dealt with fractures that have impermeable walls (i.e., the surrounding matrix has no porosity). However, recent research (Parker *et al.*, 1994) has indicated that a permeable matrix can have a large effect on NAPL dissolution time; a sample of this effect on dissolution is presented here.

Figure 3.29 shows a plot of the NAPL dissolution time versus the matrix porosity (note the plot is on a log-log scale). The simulations represented on this plot are conducted on a constant aperture field with the same invasion percolation NAPL distribution. The grid used is smaller (25X25) than the previous sections; this was necessary because of the extra computational requirements involving in modeling both the fracture and the matrix. Each simulation was conducted with a different value for matrix porosity. The overall effect on the dissolution time is dramatic.

Matrix porosity is critical because the surface area available for NAPL-water contact with matrix water is much greater than the NAPL-water contact area within the fracture. Even though diffusion is a relatively slow process, much of the NAPL can migrate into the surrounding matrix. If the matrix is porous then the predictions

of the dissolution time and output concentrations become even more complex. Mass that is stored in the matrix will begin to slowly diffuse back into the fracture and act as a low-level, long-term source of groundwater contamination.

Chapter 4

Conclusions

This study modeled physical processes at the micro scale to investigate the dissolution of non-aqueous phase liquids in single, discrete, rough-walled fractures. The results indicate that micro-scale features, in particular the random aperture distribution of the rough-walled fracture, have large effects on the dissolution process.

Predicting NAPL dissolution times and concentrations for fractured material has been extremely elusive. A porous media analogue can be used to represent the contaminated fractured material. A conceptual porous media scenario usually involves blobs of NAPL (usually spheres) distributed through the porous media (e.g. *Powers* (1991)). However, porous media analogues do not account for the effects that the fractures have on the distribution and dissolution of NAPL. For accurate simulation of dissolution in field scale models, effects that the fracture system has on dissolution must be incorporated into the models. Because these effects are generally ignored (not to mention difficult or impossible to predict) accurate dissolution estimates may be difficult to produce.

In general, the results of the dissolution modeling are very sensitive to the aperture distribution within a rough-walled fracture. This sensitivity is particularly evident from examining the aqueous-phase mass output over time and the time necessary for complete dissolution of the residual NAPL: simulations using aperture distributions that are statistically similar can produce very different results. These results are closely related to the amount and spatial distribution of NAPL within the frac-

ture; however, the NAPL distribution is the result of invasion percolation which is ultimately controlled by the random aperture distribution. Because the results are extremely sensitive to an essentially random parameter (i.e., random aperture distribution) there is appreciable uncertainty.

As a result of the invasion percolation process, blobs of NAPL are located in the larger aperture spaces and are surrounded by smaller aperture spaces. The control this spatial arrangement has on the dissolution process is particularly evident in the mass-output curves, which in turn are a function of the output concentration and average relative transmissivity. A low dissolution rate occurs initially when the smaller NAPL cells are dissolving, while a mass output peak occurs when the larger, inner NAPL cells begin dissolving. The mass output then decreases at later time when only a few isolated zones of residual are present. Comparisons with random NAPL distributions further emphasize the importance of modeling the NAPL position within the fracture using a physically realistic scenario (i.e., invasion percolation). Low initial NAPL saturations will produce high rates of mass output over a short period of time whereas high initial NAPL saturations will produce low rates of mass output over a much longer period of time. The random aperture field and the NAPL distribution within the field also can have a significant effect on the mass-output results. Fractures with similar characteristics and initial NAPL saturations can have very different mass-output curves.

Following an initial rapid buildup, the average concentration exiting the fracture generally decreases steadily during the dissolution process. This decrease correlates with a decrease in the NAPL saturation, which decreases the water-NAPL contact area and an increase in the relative transmissivity, which increases the water flow rate through the fracture. In the field, low concentrations are generally interpreted to mean there is little or no NAPL free-phase contaminant present. Results from this study support this interpretation; however, it is important to acknowledge that even though the NAPL concentration is decreasing, the mass output of NAPL out of the fracture may be increasing due to increased water flow rates.

Relative to an assumption of phase equilibrium, the use of a rate-limited mass transfer process reduces the effect that increased groundwater velocity has on the time for NAPL dissolution. Remediation schemes using dissolution to remove residual contaminant may be improved by studying this relationship between the mass-transfer coefficient and the groundwater velocity.

The initial relative transmissivity of a fracture is highly dependent on the initial NAPL residual distribution; however, the change in relative transmissivity during the dissolution process is generally insensitive to the groundwater velocity and mass-transfer coefficient. In other words the NAPL disappears in roughly the same sequence regardless of the groundwater gradient or the mass-transfer coefficient.

An exception occurs for cases with very high initial saturations. In this case the initial effective transmissivities are so low that diffusion is the primary transport mechanism. The consequences of this are that the dissolution process is initially very slow and the relative transmissivity curve may follow a different path than for initial residual saturations in the same fracture. Of course, because transport by diffusion is generally very slow the dissolution time for the NAPL in the fracture increases substantially.

NAPL can rapidly diffuse into the surrounding matrix if it is porous. This matrix diffusion process adds to the complexity in predictions involving NAPL and fractured material. Aqueous-phase NAPL that is stored in the matrix can begin to diffuse back into the fracture once the original NAPL residual has completely dissolved. This reverse matrix diffusion would cause the fracture to continue to output low concentrations of NAPL over a long period of time; this is consistent with field observations (Kennedy and Lennox, 1995).

4.1 Implications

Results here have shown that predicting the dissolution character of a single fracture may be very difficult, or even impossible, given the usual lack of specific information about the fracture aperture distributions and corresponding NAPL saturation.

However, the general prediction of NAPL dissolution over an entire site still may be possible. By using a fracture network model, the individual mass outputs of single fractures may become less important and an average value of mass output and dissolution rate may be enough to make general predictions. This may be particularly true in fractured, porous media where the uptake of the dissolved-phase into the matrix will tend to integrate and smooth results.

The time required for NAPL in a fracture to completely dissolve is quite long; simulations conducted for the impermeable case averaged about seven years for the NAPL to completely dissolve (with clean water flowing into a 1 *m* square fracture). Extrapolating this to the field scale (i.e., a network model) would be difficult; however, it would be expected that NAPL dissolution at this scale would take a much longer time, possibly tens of years.

One limitation of the approach taken here, where only a single fracture is considered, is that the model does not account for flow bypassing the fracture containing NAPL. If the fracture has an appreciable NAPL saturation it will have a low transmissivity. Thus, water may bypass the fracture through either the surrounding matrix or adjacent fractures that do not contain NAPL. If this occurs then the mass output of the fracture system would be over-predicted, leading to a gross under-prediction of the required dissolution time. Another limiting feature of the modeling is that the water flowing into the fracture is assumed to be clean: that is, it contains no aqueous-phase NAPL. If it does contain some aqueous-phase NAPL then the dissolution time for the fracture segment under consideration would be increased since the mass transfer rate from the non-aqueous to the aqueous phase would be lower. Thus, the overall dissolution time for a fracture network would increase since water entering fractures downstream contains aqueous NAPL.

References

- Abriola, L. M., and Pinder, G. F. 1985. A Multiphase Approach to the Modeling of Porous Media Conamination by Organic Compounds 1. Equation Development. *Water Resources Research*, 21(1), 11-18.
- Brusseau, M. L. 1992. Rate-Limited Mass Transfer and Transport of Organic Solutes in Porous Media that Contains Immobile Immiscible Organic Liquid. *Water Resources Research*, 28(1), 33-45.
- Flick, E. W. 1985. *Industrial Solvents Handbook*. Third edn. Park Ridge, New Jersey, USA: Noyes Data Corporation.
- Fried, J. J., Muntzer, P., and Zillox, L. 1979. Groundwater pollution by transfer of oil hydrocarbons. *Ground Water*, 17(6), 586-594.
- Geller, J. T., and Hunt, J R. 1988 (July). *Non-aqueous phase organic liquids in the subsurface: dissolution kinetics in the saturaed zone*. Presented at the International Symposium on Processes Governing the Fate of Contaminants in the Subsurface Environment, Int. Assoc. of Water Pollut. Res. and Control, Stanford, Calif.
- Hardisty, P. E., Ross, S. D., Dabrowski, T.L., and Brown, A. 1995. Remediation of LNAPL in Fractured Rock: Theory and Application. In: *Solutions '95 International Congress XXVI*. International Association of Hydrogeologists, Edmonton, Alberta, Canada.

- Hunt, J. R., Sitar, N., and Udell, K. S. 1988a. Nonaqueous Phase Liquid Transport and Cleanup 1. Analysis of Mechanisms. *Water Resources Research*, 24(8), 1247–1258.
- Hunt, J. R., Sitar, N., and Udell, K. S. 1988b. Nonaqueous Phase Liquid Transport and Cleanup 2. Experimental studies. *Water Resources Research*, 24(8), 1259–1269.
- Huyakorn, P.S., and Pinder, G.F. 1983. *Computational Methods in Subsurface Flow*. San Diego, California, USA: Academic.
- Imhoff, P. T., Jaffe, P. R., and Pinder, G. F. 1993. An experimental study of complete dissolution of a nonaqueous liquid in a saturated porous media. *Water Resources Research*, 20(2), 307–320.
- Kennedy, C. A., and Lennox, W. C. 1995. A control volume model of solute transport in a single fracture. *Water Resources Research*, 31(2), 313–322.
- Lam, A. C., Schechter, R. S., and Wade, W.H. 1983. Mobilization of residual oil under equilibrium and non-equilibrium conditions. *Soc. Petrol. Enq. J.*, 23(6), 781–790.
- Larson, R. G., Davis, H. T, and Scriven, L. E. 1981. Displacement of residual non-wetting fluid from porous media. *Chemical Engineering Science*, 36, 75–85.
- Lowry, M. I., and Miller, C. T. 1995. Pore-scale modeling of nonwetting-phase residual in porous media. *Water Resources Research*, 31(3), 455–494.
- Mackay, D. M., Roberts, P. V., and Cherry, J. A. 1985. Transport of organic contaminants in groundwater. *Environ. Sci. Technol.*, 19(5), 364–392.
- Mendoza, C. A. 1992. *Capillary Pressure and Relative Transmissivity Relationships Describing Two-Phase Flow Through Rough-Walled Fractures in Geologic Materials*. Ph.D. thesis, University of Waterloo, Waterloo, Ontario, Canada.

- Parker, B. L., Gillham, R. W., and Cherry, J. A. 1994. Diffusive Disappearance of Immiscible-Phase Organic Liquids in Fractured Geologic Media. *Ground Water*, 32(5), 805–820.
- Pennell, K. D., Jin, M., Abriola, L. M., and Pope, G. A. 1994. Surface enhanced remediation of soil columns contaminated by residual tetrachloroethylene. *Journal of Contaminant Hydrogeology*, 16, 35–53.
- Powers, S. E., Loureiro, C. O., Abriola, L. M., and W. J. Weber, Jr. 1991. Theoretical Study of the Significance of Nonequilibrium Dissolution of Nonaqueous Phase Liquids in Subsurface Systems. *Water Resources Research*, 20(4), 463–477.
- Powers, S. E., Abriola, L. M., and W. J. Weber, Jr. 1994. An experimental investigation of nonaqueous phase liquid dissolution in saturated subsurface systems: Transient mass transfer rates. *Water Resources Research*, 30(2), 321–332.
- Robin, M. J. L., Gutjahr, A. L., Sudicky, E. A., and Wilson, J. L. 1993. Cross-Correlated Random Field Generation With the Direct Fourier Transform Method. *Water Resources Research*, 29(7), 2385 – 2397.
- Schwille, F. 1981. Groundwater Pollution in Porous Media by Fluids Immiscible with Water. *The Science of the Total Environment*, 21, 173–185.
- Schwille, F. 1988. *Dense Chlorinated Solvents in Porous and Fractured Media*. Chelsea, Michigan, USA: Lewis Publishers. Translated by James F. Pankow.
- Snow, D. T. 1970. The frequency and apertures of fractures in rock. *Int. J. Rock Mech. Min. Sci.*, 7(23).
- Sudicky, E. A., and Frind, E. O. 1982. Solute Transport in Fractured Porous Media. *Water Resources Research*, 18(6).
- Sudicky, E.A. 1986. *LINE2D*. Institute for Groundwater Research, University of Waterloo, Canada. Unpublished FORTRAN code.

- VanderKwaak, J. E. 1993. *Numerical Simulation of DNAPL Dissolution and Aqueous Phase Contaminant Transport in Discretely Fractured Porous Media*. M.Phil. thesis, University of Waterloo, Waterloo, Ontario, Canada.
- VanderLeeden, F., Troise, F.L., and Todd, D.K. 1990. *The Water Encyclopedia*. Second edn. Chelsea, Michigan, USA: Lewis Publishers.
- VanderWaarden, M., Bridie, L. A. M., and Groenewoud, W. M. 1971. Transport of mineral oil components to groundwater. *Water Res.*, 5, 213–226.



National Library
of Canada

Acquisitions and
Bibliographic Services Branch

395 Wellington Street
Ottawa, Ontario
K1A 0N4

Bibliothèque nationale
du Canada

Direction des acquisitions et
des services bibliographiques

395, rue Wellington
Ottawa (Ontario)
K1A 0N4

Your file / votre référence

Our file / notre référence

NOTICE

The quality of this microform is heavily dependent upon the quality of the original thesis submitted for microfilming. Every effort has been made to ensure the highest quality of reproduction possible.

If pages are missing, contact the university which granted the degree.

Some pages may have indistinct print especially if the original pages were typed with a poor typewriter ribbon or if the university sent us an inferior photocopy.

Reproduction in full or in part of this microform is governed by the Canadian Copyright Act, R.S.C. 1970, c. C-30, and subsequent amendments.

AVIS

La qualité de cette microforme dépend grandement de la qualité de la thèse soumise au microfilmage. Nous avons tout fait pour assurer une qualité supérieure de reproduction.

S'il manque des pages, veuillez communiquer avec l'université qui a conféré le grade.

La qualité d'impression de certaines pages peut laisser à désirer, surtout si les pages originales ont été dactylographiées à l'aide d'un ruban usé ou si l'université nous a fait parvenir une photocopie de qualité inférieure.

La reproduction, même partielle, de cette microforme est soumise à la Loi canadienne sur le droit d'auteur, SRC 1970, c. C-30, et ses amendements subséquents.

Canada

UNIVERSITY OF ALBERTA

Numerical Simulation of Non-Aqueous Phase Liquid Dissolution in Discrete
Rough-Walled Fractures

B^v

Leroy Charles Banack



A thesis submitted to the Faculty of Graduate Studies and Research in partial fulfillment of the requirements for the degree of Masters of Science.

DEPARTMENT OF GEOLOGY

Edmonton, Alberta
Spring 1996



National Library
of Canada

Acquisitions and
Bibliographic Services Branch

395 Wellington Street
Ottawa, Ontario
K1A 0N4

Bibliothèque nationale
du Canada

Direction des acquisitions et
des services bibliographiques

395, rue Wellington
Ottawa (Ontario)
K1A 0N4

Your file / Votre référence

Your file / Notre référence

The author has granted an irrevocable non-exclusive licence allowing the National Library of Canada to reproduce, loan, distribute or sell copies of his/her thesis by any means and in any form or format, making this thesis available to interested persons.

L'auteur a accordé une licence irrévocable et non exclusive permettant à la Bibliothèque nationale du Canada de reproduire, prêter, distribuer ou vendre des copies de sa thèse de quelque manière et sous quelque forme que ce soit pour mettre des exemplaires de cette thèse à la disposition des personnes intéressées.

The author retains ownership of the copyright in his/her thesis. Neither the thesis nor substantial extracts from it may be printed or otherwise reproduced without his/her permission.

L'auteur conserve la propriété du droit d'auteur qui protège sa thèse. Ni la thèse ni des extraits substantiels de celle-ci ne doivent être imprimés ou autrement reproduits sans son autorisation.

ISBN 0-612-10694-2

Canada

UNIVERSITY OF ALBERTA

RELEASE FORM

NAME OF AUTHOR: Leroy Charles Banack

TITLE OF THESIS: Numerical Simulation of Non-Aqueous Phase Liquid Dissolution
in Discrete Rough-Walled Fractures

DEGREE: Master of Science

YEAR THIS DEGREE GRANTED: 1996

Permission is hereby granted to the University of Alberta Library to reproduce single copies of this thesis and to lend or sell such copies for private, scholarly or scientific research purposes only.

The author reserves all other publication and other rights in association with the copyright in the thesis, and except as hereinbefore provided neither the thesis nor any substantial portion thereof may be printed or otherwise reproduced in any material form whatever without the author's prior written permission.

(Signed)



Leroy Charles Banack
12 Montclare Avenue
Camrose, Alberta
Canada, T4V 2K8

Date: 30/1/96.

UNIVERSITY OF ALBERTA

FACULTY OF GRADUATE STUDIES AND RESEARCH

The undersigned certify that they have read, and recommend to the Faculty of Graduate Studies and Research for acceptance, a thesis entitled **Numerical Simulation of Non-Aqueous Phase Liquid Dissolution in Discrete Rough-Walled Fractures** submitted by Leroy Charles Banack in partial fulfillment of the requirements for the degree of Masters of Science.

.....
Dr. Carl A. Mendoza (Supervisor)

.....
Dr. József Tóth (Examiner)

.....
Dr. Marv Dudas (Examiner)

Date: . 25/1/96 .

Abstract

Residual NAPL trapped in fractured geologic media may act as a long-term source for dissolved groundwater contamination that is difficult to remediate. Understanding NAPL dissolution at the scale of a single fracture is the first step to a better representation of this process, as well as other related processes, in larger scale network models. Applying the information from these models will ultimately lead to improved transport predictions and remediation efforts.

The dissolution of NAPL is simulated using a finite-element model with 2-D triangular elements representing a discrete, rough-walled fracture. For fractures that are bounded by a permeable matrix, 1-D elements are used to model diffusion of contaminant into the surrounding matrix. The initial NAPL residual distribution in synthetic correlated aperture fields is created using invasion percolation techniques. Groundwater flow and aqueous-phase transport solutions are then calculated, with a concentration-dependent mass-transfer coefficient being used to represent partitioning between the NAPL and aqueous phase during dissolution. Detailed mass balance calculations are used to determine when individual elements containing residual have been dissolved and should be removed from the system. For comparison, simulations are performed where NAPL is randomly distributed throughout the fracture.

Sensitivity analyses are performed to delineate the qualitative relationships between fracture transmissivity, residual NAPL saturation, and the concentration of dissolved NAPL exiting the fracture. These relationships are very sensitive to not only the initial residual saturation, but also to the initial residual distribution, which is highly dependent on the synthetic aperture field. Because the correlated aperture

field is produced from a random set of aperture segments there is a large uncertainty in the behavior of NAPL dissolution.

At higher initial residual saturations the time for NAPL dissolution increases dramatically because the fracture transmissivity is reduced. This is because at these lower transmissivities less water is flowing through the fracture, the water in the fracture reaches saturation, and the dissolution process slows. In reality, the time for complete dissolution may be even greater since some of the water flow may bypass the fracture containing NAPL.

The effects of the mass-transfer coefficient, groundwater velocity and matrix porosity on remediation are also examined. Increasing groundwater head gradients, such as might occur during a pump and treat operation, are shown to have diminishing returns in terms of removing NAPL from the fracture by dissolution. If the surrounding matrix is permeable, NAPL can quickly diffuse into the matrix; however, after the residual NAPL has disappeared, dissolved NAPL begins to slowly diffuse back into the fracture. This greatly increases remediation times and may render current remediation strategies ineffective.

Acknowledgements

I would like to thank Carl Mendoza, my supervisor, who gave me everything I needed to complete my thesis. When I asked Carl, 'Do you have some time for me?', the answer was always, 'Yes.' It is this type of dedication that makes Carl an extraordinary instructor. The funding he provided me through NSERC was valuable, but not nearly as valuable as his time.

I would also like to thank the people who were in the Hydrogeology group at the University of Alberta during my time there. Thanks to Ben, Kent, Liane, Brent, Debashish, Joe, and John. I would especially like to thank Sheri and Darlene for their support and help; they turned a good experience into a great experience.

Finally, I would like to thank members of my family: my father; my mother; Michelle; Paul; Alexandra; Victoria; and Lorraine. I would also like to thank Lucas and Jason who provided me with numerous distractions, which probably delayed the completion of my thesis. I will always regard them as family.

Contents

| | | |
|----------|---|-----------|
| 1 | Introduction | 1 |
| 1.1 | Previous Studies | 2 |
| 1.2 | Research Outline | 5 |
| 2 | Theory and Methods | 6 |
| 2.1 | Conceptual Model | 6 |
| 2.2 | Fracture Aperture Distributions | 8 |
| 2.3 | Residual Distributions | 9 |
| 2.3.1 | NAPL | 10 |
| 2.3.2 | Capillary Pressure | 10 |
| 2.3.3 | Percolation Theory | 11 |
| 2.4 | Groundwater Flow | 12 |
| 2.5 | Aqueous Phase Transport | 14 |
| 2.6 | Dissolution | 15 |
| 2.6.1 | Mass Transfer Relationships | 15 |
| 2.7 | Numerical Formulation | 17 |
| 2.8 | Model Verification | 20 |
| 3 | Modeling Results and Analysis | 26 |
| 3.1 | General System Behavior | 26 |
| 3.1.1 | Simulation Description | 27 |
| 3.1.2 | Downstream Concentration | 29 |
| 3.1.3 | NAPL Saturation | 29 |

| | | |
|----------|--|-----------|
| 3.1.4 | Relative Transmissivity | 32 |
| 3.1.5 | Mass output | 33 |
| 3.2 | Sensitivity Analyses | 34 |
| 3.2.1 | NAPL Placement | 34 |
| 3.2.2 | Random Field versus Saturation Effects | 39 |
| 3.2.3 | Random Field Variance | 40 |
| 3.2.4 | Higher NAPL Saturations | 43 |
| 3.2.5 | Groundwater Flow and Mass Transfer Coefficient | 52 |
| 3.3 | Monte Carlo Results | 56 |
| 3.3.1 | Mass output | 56 |
| 3.3.2 | Relative Transmissivity | 62 |
| 3.4 | Permeable Matrix | 67 |
| 4 | Conclusions | 69 |
| 4.1 | Implications | 71 |
| | References | 73 |

List of Figures

| | | |
|-----|--|----|
| 2.1 | Conceptual model of a contamination scenario. After <i>Schwille</i> (1988). | 7 |
| 2.2 | An example of different scales of observation at a contaminated site. | 8 |
| 2.3 | A sample log-normal aperture distribution. | 9 |
| 2.4 | Diagram showing the variables used in calculating the volumetric flow rate through a pair of parallel plates. | 13 |
| 2.5 | Conceptualization of processes and boundary conditions for the numerical model for various stages of the modeling. | 19 |
| 2.6 | Numerical model compared to the analytical solution for a simple advection-dispersion problem. | 23 |
| 2.7 | Numerical model compared the analytical solution for a simple advection-dispersion problem. | 24 |
| 3.1 | A series of snapshots showing the dissolution simulation that is discussed in this section. | 28 |
| 3.2 | Concentration versus time curve for a single dissolution simulation. . | 30 |
| 3.3 | NAPL Saturation versus time curve for a single dissolution simulation. | 31 |
| 3.4 | Relative Transmissivity (for water) curve for a single dissolution simulation. | 32 |
| 3.5 | Mass-output curve for a single dissolution simulation. | 33 |
| 3.6 | Mass-output for three saturation levels created with invasion percolation methods for a single fracture with the same aperture distribution. | 35 |
| 3.7 | Mass-output for three saturation levels created with invasion percolation methods for a single fracture with the same aperture distribution. | 37 |

| | | |
|------|--|----|
| 3.8 | Cross-sections through a residual distribution for invasion percolation and random residual assignment. NAPL is shown in grey and water fills the rest of the fracture. | 38 |
| 3.9 | Mass output versus time for two distribution created using invasion percolation on three different random fields. | 40 |
| 3.10 | A cross-section through two fractures that share the same initial aperture distribution; however, the variance of each one has been modified. The black cross-section has a variance of 0.75 while the grey cross-section has a variance of 2.25, but both have a mean aperture of about 30 microns. | 41 |
| 3.11 | Two simulations showing the mass output of the two fractures that differ only by the variance (V) of their aperture distributions. | 42 |
| 3.12 | Mass-output for four saturation levels created with invasion percolation methods for a single fracture (the same aperture distribution). | 43 |
| 3.13 | Mass-output for four saturation levels created with random percolation methods for a single fracture (the same aperture distribution). | 44 |
| 3.14 | Semi-log plot of the relative transmissivity of the fracture versus the volumetric NAPL saturation. The simulations shown here used NAPL distribution created by invasion percolation. | 46 |
| 3.15 | Semi-log plot of the relative transmissivity of the fracture versus the volumetric NAPL saturation. The simulations shown here used NAPL distribution created by random residual assignment. | 48 |
| 3.16 | Semi-log plot of the relative transmissivity of the fracture versus the volumetric NAPL saturation. The simulations shown here used NAPL distribution created by invasion percolation and all distribution have been modified so the initial NAPL saturation is 40% in all cases. | 49 |
| 3.17 | Time for NAPL dissolution versus the initial NAPL saturation. The cross sections show the NAPL position for the invasion percolation case at various points on the curve. | 51 |

| | | |
|------|--|----|
| 3.18 | Areal saturation plots for two similar simulations with different initial areal saturations. Shading indicates NAPL. | 53 |
| 3.19 | Time for NAPL dissolution versus the gradient across the fracture. . . | 55 |
| 3.20 | Downstream mass output versus time. Black and grey lines shown an arbitrary separation. | 58 |
| 3.21 | Downstream mass output versus volumetric saturation of the wetting phase. Black and grey lines shown an arbitrary separation. | 60 |
| 3.22 | Two conceptual cases on how NAPL is located within a fracture. The bottom grid shows what the areal saturation would look like in plan view. | 61 |
| 3.23 | Downstream mass output versus volumetric saturation of the wetting phase. Two example realizations are highlighted. | 62 |
| 3.24 | Downstream mass output versus time. Two example realizations are highlighted. | 63 |
| 3.25 | Initial residual distribution for cases A and B. | 63 |
| 3.26 | Cross sections taken through cases A and B. | 64 |
| 3.27 | The relative transmissivity curve from the Monte Carlo analysis. The same black and grey separation of the curves is used. | 65 |
| 3.28 | Relative transmissivity curves where the groundwater velocity and the mass transfer coefficients are varied. | 66 |
| 3.29 | Plot of NAPL dissolution time versus matrix porosity. | 67 |

List of Tables

| | | |
|-----|---|----|
| 2.1 | Physical properties of the NAPL used. | 10 |
| 2.2 | Parameters used in numerical model for comparison with the LINE2D analytical solution. | 22 |
| 2.3 | Parameters used in numerical model for comparison with example from <i>Powers et. al.</i> (1991). | 25 |
| 3.1 | Parameters used in numerical model for the example simulation. . . . | 27 |
| 3.2 | Parameters used for Monte Carlo simulations | 57 |

Chapter 1

Introduction

The use of non-aqueous phase liquids (NAPLs) by industry following World War II has become very common. Unfortunately, contamination of geologic material with these chemicals has also become common. The spilling of NAPL onto the ground surface leading to subsurface contamination can occur during NAPL production, transport, storage and disposal.

Common NAPLs, such as chlorinated solvents, have low aqueous solubilities. For example, trichloroethene (TCE) has a solubility of 1100 *mg/l* (Flick, 1985). However, the maximum allowable limits imposed by government agencies tend to be much lower. The drinking water quality standard in the United States for TCE is 0.005 *mg/l* (VanderLeeden *et al.*, 1990). Like TCE, many of these liquids are extremely toxic. This toxicity, combined with the fact that they can contaminate large volumes of water because of their low solubilities, makes NAPLs a serious threat to ground water resources.

When a NAPL is spilled a portion of the liquid may percolate down through the unsaturated zone. If it reaches the saturated zone the NAPL will continue its downward migration providing that it is denser than water (e.g., a dense NAPL or DNAPL). The NAPL will preferentially travel through highly permeable zones, such as fractures. A certain amount of the NAPL will be left behind in the porous and fractured media following this migration. This residual NAPL may act as a long-term source for groundwater contamination and be difficult to remediate due to slow

dissolution mechanisms and the inaccessible nature of fractures.

The objective of this thesis is to use a numerical model to investigate the theoretical small-scale dissolution behavior of NAPL residual in discrete fractures. The dissolution behavior of NAPL in a discrete, synthetically-generated, rough-walled fracture is simulated. Gaining an understanding of this dissolution process at the small scale will lead to better representations of this process, as well as other related processes such as dissolution in porous media, in larger-scale models. Ultimately this will lead to better predictions at contaminated sites, which could lead to improved remediation efforts. The methodology used for this investigation is given following a review of some previous work in this area.

1.1 Previous Studies

The principles of NAPL migration in the subsurface have been described by *Schwille* (1981; 1988). His theories and laboratory work involving immiscible fluids and porous media are the framework upon which most similar research is based. *Schwille* (1981) does not address the subject of dissolution; he assumes the NAPL is a perfectly immiscible fluid. However, *Schwille* (1988) does discuss aqueous-phase dissolution and migration of NAPLs. Interest in NAPL dissolution as a contamination problem has been growing steadily over the last few years. For some time it has been realized that NAPL in the subsurface can partition to the aqueous phase and be a source for long-term groundwater contamination (*Schwille*, 1988; *Mackay et al.*, 1985). The problem of describing and modeling this dissolution process has been a subject of debate.

Abriola and Pinder (1985) developed a model that describes the transport of a contaminant through porous media in three forms: aqueous phase, non-aqueous phase, and vapour phase. The approach used to describe mass transfer between the non-aqueous phase and aqueous phase is equilibrium phase partitioning, which assumes that by knowing the concentration in one phase, the concentration in the other phase can be calculated using a partition coefficient. This assumption is based

on experimental evidence that suggests equilibrium phase partitioning occurs during the dissolution process (VanderWaarden *et al.*, 1971; Fried *et al.*, 1979).

There is, however, contrary evidence that appears to refute the local equilibrium assumption. For example, laboratory experiments by Lam *et al.* (1983) indicate that these mass transfer processes frequently do not reach a state of equilibrium. This work involved studying residual oil blobs during tertiary oil recovery.

Powers *et al.* (1991) present similar evidence that implies there is a process which limits the rate of NAPL partitioning to the aqueous phase. Powers *et al.* (1994), using laboratory-scale column experiments, showed that the length of time required to dissolve NAPL is greater than predicted by equilibrium phase partitioning calculations. A general correlation for transient dissolution rates in terms of volumetric fractions of NAPL in the porous media and porous media properties was proposed. Similar results were obtained by Imhoff *et al.* (1993) who showed that mass transfer rates for an area of residual NAPL are a function of the NAPL volumetric content, the Darcy water flux through the area and the distance into the contaminated region.

The importance of using equilibrium partitioning versus a rate-limited process becomes particularly evident when trying to predict the effectiveness of remediation schemes. Brusseau (1992) constructed a model that estimates the time required to remediate an aquifer contaminated by residual NAPL. He found if one did not account for a rate-limited mass transfer process the time and volume of water required for remediation would be significantly underestimated.

Hunt *et al.* (1988a; 1988b) found that mass-transfer rate limitations resulted in groundwater extraction at a contaminated site to be ineffective in removing the residual NAPL within a reasonable time frame. They suggested that remobilizing the NAPL, by steam injection for example, would be much more useful in remediation. However, Pennell *et al.* (1994) suggest that this remobilization of NAPL is dangerous because the NAPL can cause previously uncontaminated material to become contaminated. They suggest using surfactants which can increase the rate of mass transfer to the aqueous phase. In theory, if the mass transfer rate is high

enough, NAPL contaminated sites may be remediated using groundwater extraction methods, such as pump and treat. Unfortunately, surfactants may also lower the NAPL's surface tension, which can cause them to remobilize.

Parker et al. (1994) developed a conceptual model for NAPL in parallel plate fractures partitioning to the aqueous phase in the surrounding matrix. They suggest that restoration of contaminated fractured material is extremely difficult. Their findings show that a small amount of time is required for the NAPL to completely partition to the aqueous phase of the surrounding matrix when the matrix is porous.

Recently, *Lowry and Miller* (1995) used pore-scale modeling to describe the formation and removal of NAPL in porous media. These researchers feel that current macroscopic approaches are often unable to capture adequately the complexity of processes such as NAPL invasion and dissolution. They feel that small-scale modeling may provide the necessary conceptual and quantitative basis for constitutive theory development.

VanderKwaak (1993) used a two-dimensional numerical model to simulate the dissolution and transport of NAPL in fractured porous media. Fractures were simulated as high permeability one-dimensional elements that had the propensity to rapidly transport contaminant. The effects of matrix porosity and transport of dissolved NAPL through the porous media were priorities in this research; the small scale effects of dissolution occurring within a fracture were not represented.

Mendoza (1992) developed a model capable of describing the spatial relationship between two separate phases in a discrete fracture during drainage and imbibition processes. Drainage refers to the process whereby NAPL invades the fracture causing water to drain or exit the fracture. Imbibition is the opposite process where water enters the fracture causing NAPL to be displaced. The aperture distribution data and the position of residual within the fracture (i.e. NAPL residual distribution) following the imbibition process is used as starting point for the dissolution modeling for this thesis.

1.2 Research Outline

The work presented in this thesis has similarities to previous research in the area; however, this study examines the dissolution process at a much finer, more detailed scale. These finer details include using rough-walled fractures, accounting for advective-dispersive transport in the fracture and modeling the process of matrix diffusion across the entire fracture. In addition, phase transfer across explicit water-NAPL interfaces is accounted for.

The numerical model is a finite-element simulator coded in FORTRAN. Major inputs for the model, taken from the *Mendoza* (1992) model, include aperture distributions representing a rough-walled fracture and the initial location of NAPL residual within the fracture. The numerical model simulates the dissolution of this NAPL residual in the single fracture. The model calculates water flow caused by a head gradient along the fracture. Also, it simulates advective-dispersive transport within the fracture and diffusion of NAPL into the surrounding fracture matrix. As documented later, the model compares favorably to analytical solutions and results obtained by other researchers.

The modeling was carried out on a fracture of an arbitrary size (1.25m by 1.25m). Relationships between the NAPL residual distribution, the mass output of the fracture, groundwater flow rates, and mass transfer coefficients were studied. Also, changes in fracture transmissivity during dissolution were recorded and then compared to the mass-output results. A few simulations that included diffusion into a surrounding porous matrix were also performed. Approximately 60 separate aperture and residual distributions were investigated, although some of the more detailed investigations used a single aperture field and corresponding residual distribution.

Details of the theory involved and implementation of that theory is given in Chapter 2. The results and analysis of the numerical simulations are presented in Chapter 3. Conclusions and a discussion of their implications are presented in Chapter 4.

Chapter 2

Theory and Methods

This chapter describes the theory and conceptual model behind the numerical model used for later simulations. The chapter also addresses the implementation and some features and limitations of the numerical model.

2.1 Conceptual Model

Figure 2.1 shows a conceptual model of a contaminated site where a spill on or near the ground surface has released some NAPL contaminant. This NAPL could be made up of a single component such as trichloroethene (TCE) or a mixture of several NAPLs. The NAPL migrates down through the unsaturated zone. The mechanism driving this downward migration is pressure due to the overlying column of NAPL. Because the NAPL in this scenario is denser than water (a DNAPL), it continues its downward migration through the saturated zone. The NAPL may subsequently invade and travel through fractures in the underlying fractured material.

The NAPL will preferentially enter a fracture only if the capillary entry pressure of the fracture is lower than the surrounding material and the capillary pressure exceeds the entry pressure. The capillary entry pressure is simply the pressure required to force NAPL into a fracture or pore space. The larger the opening of the fracture, the lower the capillary entry pressure required for the NAPL to occupy that space. The extent to which the fracture becomes filled depends on the fracture aperture

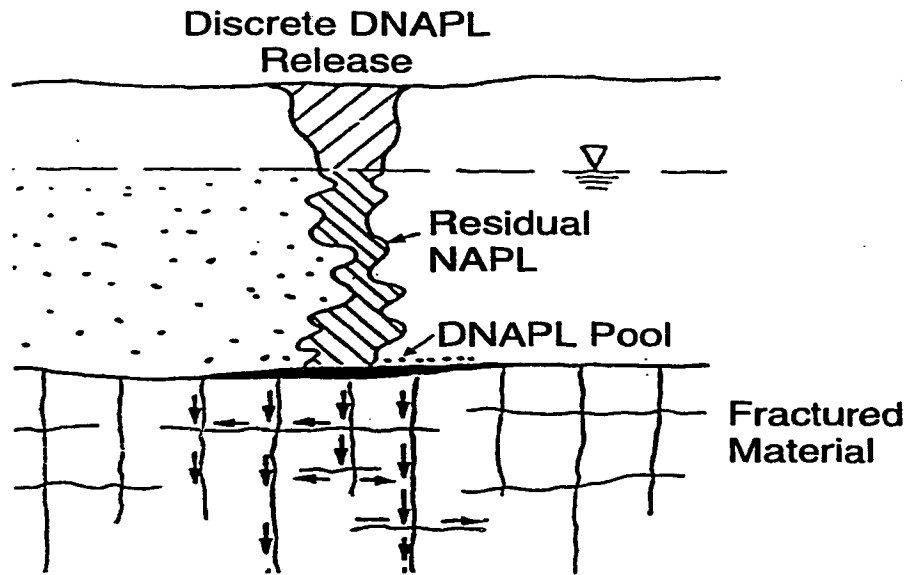


Figure 2.1: Conceptual model of a contamination scenario. After *Schwille* (1988).

distribution, the porosity of the surrounding matrix and the height of the column of NAPL.

Once the source of NAPL has been exhausted or removed, the NAPL will begin to drain out of the fractured material; this is the imbibition process. Following this imbibition process will be a certain amount of NAPL residual left in the fractured material. It is this residual that will be immobile and can cause the long-term contamination as it slowly dissolves over time.

Figure 2.2 shows a detailed example of fractured material. Studying the migration and subsequent dissolution of NAPL in this material can be accomplished on different scales of observation. Case 1 would involve studying the fracture network and the surrounding matrix material. Case 2 would involve studying a single fracture. A single fracture study would include more detail than a larger-scale study. These small scale details include the aperture distribution of the fracture and position of NAPL within the fracture. It will be shown in the following chapter that these details can have a large effect on the dissolution process. Understanding the effect of these small-scale details can improve the accuracy of modeling at larger scales, such as case 1.

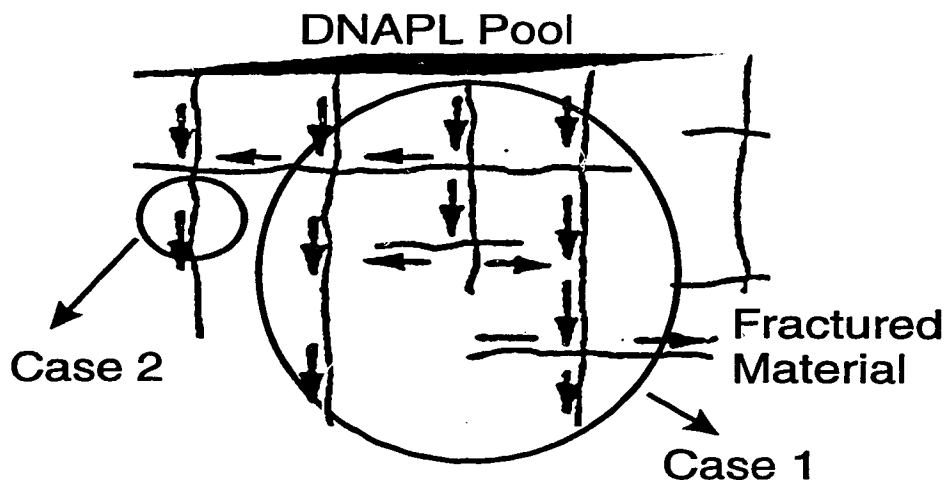


Figure 2.2: An example of different scales of observation at a contaminated site.

The conceptual model for this thesis is limited to a region within a single fracture (i.e., case 2). This single fracture is assumed to contain some NAPL residual contaminant that will dissolve into the groundwater flowing through the fracture. For the purposes of a single fracture this groundwater is assumed to have no dissolved NAPL in it prior to entering the fracture. The superposition of results from several such fractures where groundwater may have some dissolved NAPL prior to entering the fracture is left for further study.

2.2 Fracture Aperture Distributions

Fractures are often represented as two parallel plates, with the distance between these two plates being the fracture aperture. For the model used in this thesis a synthetic aperture distribution is used to simulate a discrete, rough-walled fracture (i.e., the aperture will vary spatially throughout the fracture). These synthetic distributions are created using a Fast Fourier Transform spectral technique developed by *Robin* (1993). The aperture field is assumed to be log-normally distributed and to exhibit isotropic, exponential correlation structure. Research by *Snow* (1970) has shown

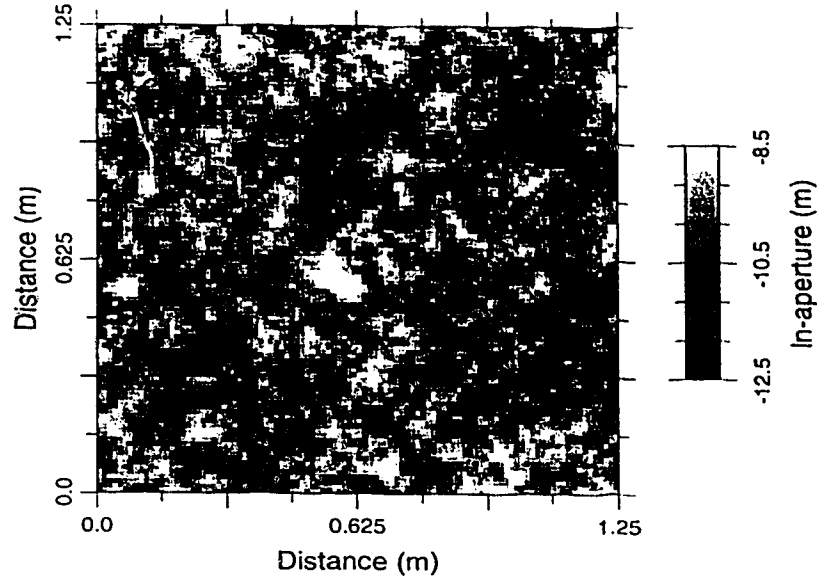


Figure 2.3: A sample log-normal aperture distribution.

that a log-normal aperture field is a reasonable representation of naturally occurring discrete fractures in various geologic materials.

The aperture field is discretized onto a two-dimensional square grid. The grid used for modeling contains 2500 cells (50 by 50 squares). Simulations for this work use a natural log-aperture mean of -10.5 (aperture in metres). The size of individual cells are 2.5cm^2 . Figure 2.3 shows an example of one of the fracture aperture fields used.

2.3 Residual Distributions

The spatial position of NAPL in a discrete fracture following the invasion process (both drainage and imbibition) will be referred to as the residual distribution or residual saturation. The controlling factors in determining the pattern of the residual distribution are the size and distribution of apertures, the pressure history, the invasion history, properties of the NAPL and fracture walls, and the physical limitations of the percolation system.

| | |
|------------------------------------|--------------------------|
| Density, ρ_{NAPL} | 1460 kg/m^3 |
| Aqueous Solubility at 20°C, C_s | 1100 mg/L |
| Coefficient of mass transfer, k | $2.0 \times 10^{-6} m/s$ |
| Viscosity, μ | 0.57 cp |
| Interfacial Tension, γ | 34.5 dyn/cm |
| Water Diffusion Coefficient, D^* | $1.0 \times 10^{-9} m/s$ |

Table 2.1: Physical properties of the NAPL used.

2.3.1 NAPL

A generic NAPL has been selected for use in the dissolution modeling. Numerous variations in NAPL properties makes it unfeasible to conduct simulations on many different NAPLs. This situation becomes increasing complex when the NAPL is a mixture of more than one NAPL (which is, unfortunately, often the case). For this study the NAPL is denser than water (DNAPL); however, similar results can be expected with a NAPL that is less dense than water (LNAPL) (Hardisty *et al.*, 1995).

The physical properties of the NAPL have been chosen to be similar to Trichlorethene (TCE). TCE is a common chlorinated solvent, and consequently is also a common subsurface contaminant. The physical properties for the NAPL are given in Table 2.1. For this thesis the water is assumed to be perfectly wetting and the NAPL is considered to be the non-wetting phase.

2.3.2 Capillary Pressure

For a cell to become occupied by NAPL during the invasion process the capillary pressure of the NAPL must exceed the capillary entry pressure (P_c^*) of that cell. Each cell in the fracture model is represented by two parallel plates with the aperture being the distance between the two plates. The capillary entry pressure for a set of two parallel plates is:

$$P_c^* = \frac{2\gamma}{b} \cos \theta \quad (2.1)$$

where b is the distance between the two plates, γ is the interfacial tension between the two fluids and θ is the contact angle between the interface of the two fluids and the fracture wall. For this study water is assumed to be perfectly wetting and thus the contact angle will equal zero.

As pressure of the NAPL at the inlet boundary increases during invasion it may invade cells with progressively smaller apertures. At any given pressure there is a minimum aperture that the NAPL can enter. The value, called the critical aperture (b^*), is defined by:

$$b^* = \frac{2\gamma \cos \theta}{P_c} \quad (2.2)$$

Hence, all cells where b is greater than b^* can be invaded by the NAPL. The concept of critical aperture used in this context is known as the occupancy criterion.

2.3.3 Percolation Theory

The invasion of NAPL into a fracture is accomplished by using a modified form of percolation theory. For traditional percolation the only criterion used to determine the position of the NAPL during the invasion process would be the occupancy criterion. Using traditional percolation theory to place NAPL into the fracture ignores physical constraints of the system such as phase contacts, phase positions, and the nature of the fracture walls¹. Invasion percolation theory (Mendoza, 1992) is used to account for these physical constraints by constraining the fluid to entering and exiting at discrete points. This leads to the introduction of the accessibility and the trapping criteria.

The accessibility criterion restricts NAPL from invading a cell unless it is physically connected with the rest of the invading NAPL. This prevents the invading fluid

¹A fracture in a permeable material is considered to have permeable fracture walls. A fracture in an impermeable material is considered to have impermeable fracture walls.

from occurring everywhere the occupancy criterion is satisfied, as would occur in the traditional percolation case. For the fracture model the surrounding matrix is considered inaccessible to the invading NAPL phase; therefore, NAPL can only appear at the inlet boundary and travel through the fracture as a continuous phase.

The trapping criterion restricts the removal of NAPL during the imbibition process. If a section becomes isolated from the rest of the continuous phase then it is considered to be trapped. The water (i.e., wetting phase) is subject to the same trapping criteria if the fracture walls are impermeable. On the other hand, permeable fracture walls will allow water to exit freely. NAPL is trapped whether the walls are permeable or impermeable.

2.4 Groundwater Flow

Groundwater flow through fractured media has commonly been approximated using a parallel plate model. Each cell within the fracture has a constant aperture value; therefore, a parallel plate model is applied to each cell. The equation that describes the volumetric flow rate through two parallel plates is given by the following:

$$Q = -\frac{b^3 \rho g}{12\mu} w \Delta h \quad (2.3)$$

where Q is the volumetric flow rate through the fracture, μ is the viscosity, w is the distance along the fracture and Δh is the hydraulic head difference along the plates ($h_1 - h_2$). Figure 2.4 shows how the variables in Equation 2.3 pertain to the physical system.

From Equation 2.3 the permeability, k , of each aperture segment can be defined:

$$k = \frac{b^2}{12} \quad (2.4)$$

and the transmissivity, T , for each segment:

$$T = \frac{b^3 \rho g}{12\mu} \quad (2.5)$$

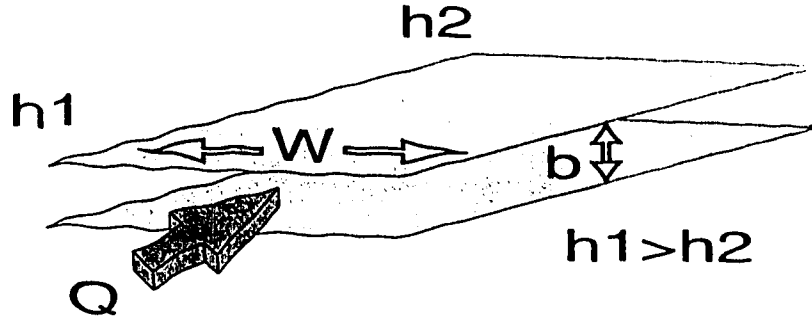


Figure 2.4: Diagram showing the variables used in calculating the volumetric flow rate through a pair of parallel plates.

The fluid continuity equation for a pair of parallel plates is given by:

$$\nabla \left(\frac{b^3 \rho g}{12\mu} \nabla h \right) = 0 \quad (2.6)$$

The fracture plane can be represented on a two-dimensional grid. The spatially varying aperture in the fracture corresponds to a spatially varying heterogeneous transmissivity distribution on this two-dimensional grid. Using this information and the relation defined in Equation 2.5 the fluid continuity equation for the two-dimensional plate representing a rough-walled fracture can be written as:

$$\nabla (T(x, y) \nabla h) = 0 \quad (2.7)$$

where x and y represent coordinates in the fracture plane.

Capillary Number

During the dissolution modeling the NAPL residual is considered to be immobile. For this approach to be valid the viscous forces resulting from the flowing groundwater must be insignificant relative to the capillary forces. The dimensionless capillary number (N_c) measures the ratio of these viscous effects compared to the capillary effects. The capillary number is expressed as:

$$N_c = \frac{\mu v}{\gamma} \quad (2.8)$$

where v is the average linear groundwater velocity.

When the capillary number is “small” capillary forces will dominate. Experimental evidence in porous media (Larson *et al.*, 1981) and numerical simulations conducted using rough-walled fractures (Mendoza, 1992) suggest that $N_c < 10^{-4}$ is an appropriate cut off value. Using this value for the capillary number and the parameters stated in Table 2.1 a minimum average linear velocity can be calculated. This minimum velocity is the point above which the viscous forces will dominate resulting in the remobilization of the NAPL. Using Equation 2.8 an expression for this minimum linear velocity, q , can be derived:

$$q_{min} = \frac{N_c \gamma}{\mu} \quad (2.9)$$

Solving for q_{max} leads to:

$$q_{min} = 500 \frac{m}{day} \quad (2.10)$$

The maximum values for q during the dissolution modeling are at least one order of magnitude below this minimum value; therefore, the NAPL is treated as immobile.

2.5 Aqueous Phase Transport

During dissolution mass from the NAPL is transferred to the aqueous phase. The aqueous phase mass is transported through the fracture by groundwater advection and hydrodynamic dispersion. The two-dimensional advection-dispersion equation governing aqueous phase transport in a rough-walled fracture (Sudicky and Frind, 1982) is:

$$b \frac{\partial C}{\partial t} + b v_i \frac{\partial C}{\partial x_i} - \frac{\partial}{\partial x_i} b D_{ij} \frac{\partial C}{\partial x_j} = 0 \quad i, j = x, y \quad (2.11)$$

where C is the aqueous phase concentration of the NAPL and V is the advective groundwater velocity. The hydrodynamic dispersion term, D , is a function of the dispersivity value assigned to the fracture, the groundwater velocity, and the effective diffusion coefficient.

2.6 Dissolution

There have been several models developed which describe the partitioning of NAPL to the aqueous phase. Several of these models use the assumption of “local equilibrium”. This approach assumes that the concentration of a component in one phase will be in equilibrium with its concentration in the other phase and that the concentrations may be related by a “partition coefficient” (Abriola and Pinder, 1985).

Despite frequent use in the modeling of NAPL-phase water relationships, local equilibrium has yet to be adequately demonstrated as being valid (Powers *et al.*, 1991). The local equilibrium relationship has been inferred from many lab scale experimental studies ((Fried *et al.*, 1979),(VanderWaarden *et al.*, 1971),(Hunt *et al.*, 1988a)); however, these studies have been carried out over a limited range of matrix material, organic compounds, and velocities. Also, there is laboratory evidence to support a non-equilibrium relationship for NAPL dissolution. Studies for tertiary oil recovery involving the use of surfactants have indicated that the rate of mass transfer of oil blobs is frequently not fast enough to reach a state of phase equilibrium (Lam *et al.*, 1983). Geller and Hunt (1988) showed that the concentration of some organic chemicals were below the equilibrium concentration levels immediately downstream of a NAPL source.

This study assumes NAPL dissolution is a rate-limited process. The details of this rate-limit process are discussed in the following section.

2.6.1 Mass Transfer Relationships

As previously mentioned, the transfer of NAPL from the non-aqueous to the aqueous phase is represented here as a rate-limited, mass-transfer process. Powers *et al.* (1991) have defined a rate-limited mass flux across a two-dimensional interface. This flux, F_a , is expressed as:

$$F_a = -k_t(C - C_s) \quad (2.12)$$

where k_t is an effective mass transfer coefficient, and C_s is the equilibrium concentration of the NAPL in the aqueous phase. The equilibrium concentration for a pure NAPL species is the solubility of that NAPL in water.

The rate of mass transfer from the non-aqueous to the aqueous phase is considered to be limited primarily by diffusion across a boundary layer. The mass transfer coefficient is thus directly proportional to the diffusion coefficient of the NAPL and inversely proportional to the thickness of the boundary layer. For simplicity, the mass transfer coefficient is assumed to be constant; that is, neither the thickness of the boundary layer nor the diffusion coefficient change during the dissolution process.

The mass flux (F_a), however, will be non-linear with respect to time. As NAPL dissolves, the aqueous concentration (C) increases. This increase will result in decrease in the $(C - C_s)$ term and therefore, a decrease in the mass flux across the NAPL-water contact boundary.

Fracture

To calculate a mass flux of NAPL into the fracture, Equation 2.12 must be modified to include the interfacial area of the NAPL/water contact. The resulting equation is

$$F_a = -bwk_t(C - C_s) \quad (2.13)$$

where w is the width of the aperture segment and b is the height of the aperture segment. During dissolution the value for b will change whenever a grid block of NAPL has been removed by dissolution. This will increase the non-linearity of the F_a with respect to time. Since the grid is square, the value of w does not change during the dissolution process.

Matrix

If the fracture walls are permeable, NAPL will also diffuse into the surrounding matrix. To calculate the mass flux from the NAPL to the matrix, equation 2.12 is

again modified. The resulting equation is:

$$F_a = -\phi w^2 k_t (C - C_s) \quad (2.14)$$

where ϕ is the matrix porosity. As the matrix porosity is increased, the flux into the matrix will also increase.

2.7 Numerical Formulation

A single discrete fracture is represented on a two-dimensional grid at the micro-scale. The governing flow and transport equations are discretized using the standard Galerkin finite-element formulation (Huyakorn and Pinder, 1983). Flow and transport are modeled using a triangular finite-element grid. A comparison was made between using square and triangular finite-elements grids; the triangular grid provided the least amount of numerical error so it was chosen for the flow and transport modeling. For models that incorporate matrix diffusion the surrounding matrix is modeled using one-dimensional line elements at every node on the fracture grid. This one-dimensional line element will simulate the diffusion process into the third dimension (out of the fracture plane). For simplicity, no lateral advection or diffusion takes place in the matrix. This would be reasonable where the matrix permeability is much less than that of the fracture, which is often the case.

Grid

The original aperture field and residual distribution were generated on 200x200 square grids. Using grids of coarser resolution to simulate the drainage and imbibition processes produced results that are statistically dissimilar. However, modeling flow, dissolution, and transport on 200x200 square grids was infeasible due to the amount of computing time required. For example, a single transport simulation on a 200x200 grid could take up to a week to complete. To solve this problem initial residual distributions were generated on a 200x200 grid and then scaled to a 50x50 grid for dissolution modeling.

Sixteen cells from the 200x200 distribution (4x4 segment) were reduced to one cell in the 50x50 distribution. The geometric mean of the sixteen aperture segments was used to calculate the new aperture of the smaller distribution. If seven or more of the sixteen cells contained residual, then the new cell in the 50x50 distribution would also contain residual. By experimenting with different values it is found that seven cells as the cutoff value provides the closest match in NAPL saturation to the original distribution.

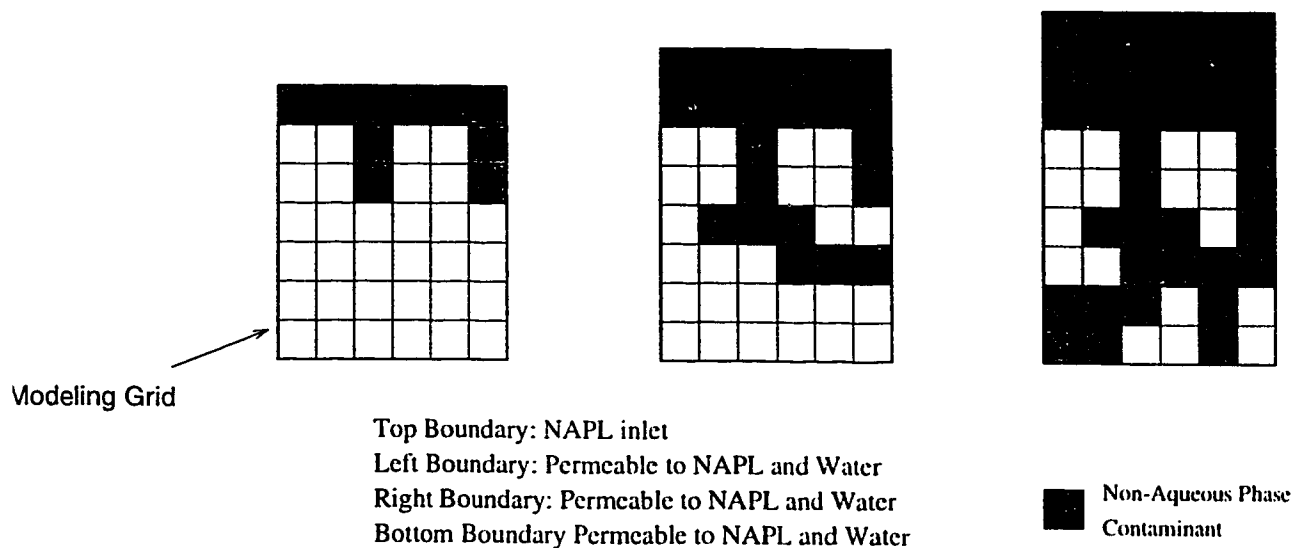
Boundary Conditions

The boundary conditions for the model change from the NAPL invasion process to the dissolution process. The invasion process is conceptualized as a separate event from the dissolution process. That is, the residual NAPL is in place before the groundwater begins to flow and dissolution takes place. The separation of these two events is physically unrealistic; however, the separation is required to perform the modeling. The invasion percolation process is not performed in discrete temporal steps; it is based on discrete capillary pressure steps. Also, starting with in NAPL residual already in place makes the dissolution model easier to construct.

Figure 2.5 illustrates the various boundary conditions used in different stages of the numerical modeling. The NAPL enters the fracture from the inlet boundary located at the top of the fracture. During the creation of the initial residual distribution the driving mechanism of the NAPL, which is the head of NAPL at the inlet boundary, is the dominating force. For drainage the NAPL enters only at the top. For imbibition the NAPL exits only at the top and bottom. The permeability of the fracture walls depends on whether the surrounding matrix is porous.

Following the invasion process, the boundary conditions are changed to simulate groundwater flow through the fracture. The left and right boundaries are specified head boundaries. The specified head boundaries are setup of so that flow is from left to right. The top and bottom boundaries now become impermeable to water flow. They can be thought of as symmetry boundaries.

NAPL Invasion Modeling



NAPL Dissolution Modeling

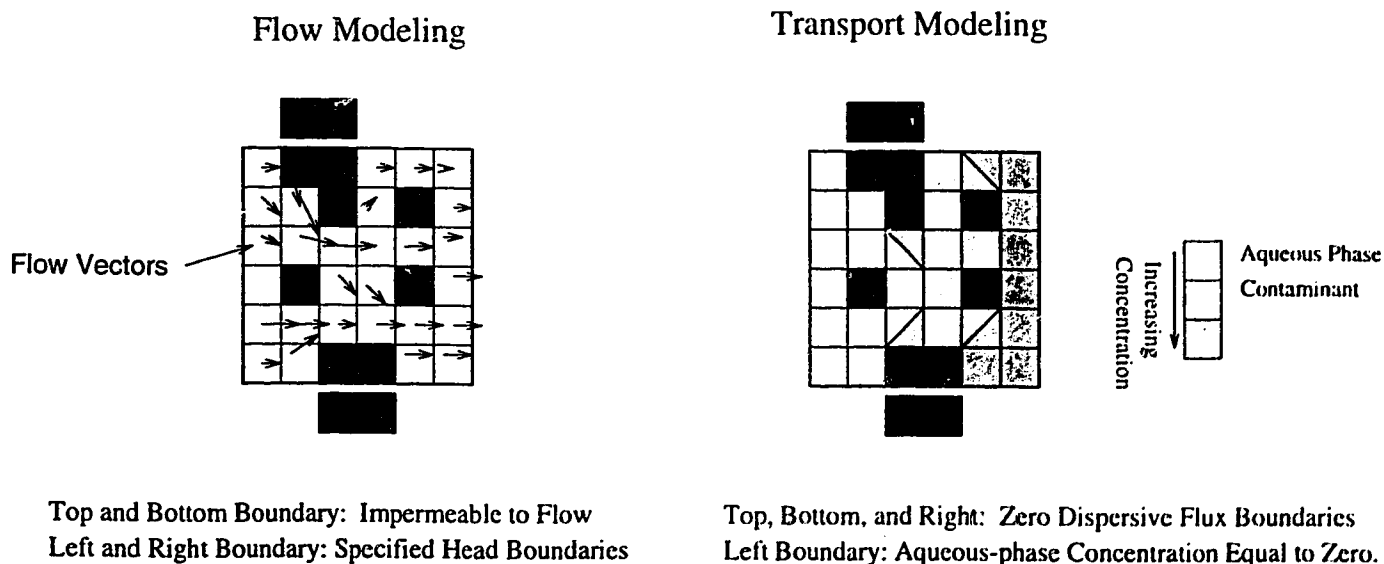


Figure 2.5: Conceptualization of processes and boundary conditions for the numerical model for various stages of the modeling.

For the transport solution the top, bottom and right boundaries are considered impermeable for dispersive transport; mass exits the right hand boundary via advective transport only. The left-hand boundary is constrained to a zero concentration, which assumes that only clean water (i.e. no aqueous-phase NAPL) is entering the system.

Dissolution Modeling

The model first calculates a groundwater flow solution through the fracture with no NAPL residual. This information is used for calculating the effective aperture and relative transmissivities during dissolution.

The residual is placed into the fracture using invasion percolation techniques and the flow solution is recalculated. The contact area between the NAPL and water for every cell is computed. The mass flux of NAPL across that interface is calculated and applied to the nodes associated with that interface. The mass fluxes at these nodes represent the dissolution process. The model now begins stepping through time, accounting for advective-dispersive transport and NAPL dissolution. The amount of NAPL removed from each cell due to dissolution is calculated. When the mass of NAPL originally in the cell is equal to the mass of NAPL that has been removed via dissolution, the cell becomes free for water to flow through. A new flow solution is then calculated and the NAPL dissolution boundaries (i.e. the nodal mass fluxes) are changed to reflect the change in the NAPL residual distribution. The transport solution now continues with the modified grid. The dissolution modeling continues until all the NAPL has been removed from the system.

2.8 Model Verification

Due to the complexity of the numerical model there is no single analytical solution that can be used to verify it. Several comparisons were made to test various aspects the numerical model. For example, comparing flow through the fracture or matrix

diffusion out of the fracture were compared to analytical solutions to verify the numerical implementation of the flow and transport equations. Following a short review of mass balance, the two most complex verifications, advective-dispersive transport and NAPL dissolution are presented.

Mass Balance

To determine whether the model is accurate and stable, a mass balance calculation is performed. A mass error term is used to quantify the amount of mass that cannot be accounted for due to numerical problems. The mass error term is defined as the mass transferred into the aqueous phase subtracted from the mass change at the boundaries and the ending aqueous phase mass in the system. A percent error is calculated by normalizing this mass error term with the original NAPL mass in the system.

Since this problem is non-linear the Peclet and Courant criteria are only used as a guide because significant errors may arise even if the criteria are fully satisfied. Increased values for longitudinal and transverse dispersivities also help increase accuracy and numerical stability without having a dramatic effect on the mass output results.

Advective-Dispersive Transport

The numerical model was used to perform a transport solution to compare with an analytical model to verify the accuracy of the advective-dispersive transport equation implementation. The simulations were performed on grids of various sizes. Parameters such as potential difference and source conditions were varied to test the robustness of the solution.

For flow calculations the left and right boundaries had constrained head values, while top and bottom boundaries were impermeable. Flow was from left to right. A uniform aperture was specified for the entire domain. A single constrained source (concentration = 1.0) in the middle of the left side boundary provided the input

| | Test 1 | Test 2 | Test 3 |
|---------------------------------------|----------------------|-----------------------|----------------------|
| Potential Difference, Δh | 9.0 | 9.0 | 99.0 |
| Grid Size (x) | 10 | 20 | 10 |
| Grid Size (y) | 10 | 20 | 10 |
| Source Thickness | 1.0 | 0.5 | 1.0 |
| Length of Model, L | 10.0 | 10.0 | 10.0 |
| Grid Spacing, ΔL | 1.0 | 0.5 | 1.0 |
| Groundwater Velocity, v | 0.075 | 0.075 | 0.825 |
| Longitudinal Dispersivity, α_l | 0.5 | 0.5 | 0.5 |
| Transverse Dispersivity, α_t | 0.5 | 0.5 | 0.5 |
| Diffusion Coefficient, D^* | 1.0×10^{-9} | 1.0×10^{-9} | 1.0×10^{-9} |
| Time Step, Δt | 1.0 | 1.0 | 1.0 |
| Total Time, t | 100.0 | 100.0 | 100.0 |
| Peclet Number(x) | 2.0 | 1.0 | 2.0 |
| Peclet Number(y) | 0.013 | 0.013 | .123 |
| Courant Number(x) | 0.075 | 0.15 | .825 |
| Courant Number(y) | 1.3×10^{-9} | 5.4×10^{-11} | 1.3×10^{-9} |
| %Error | -0.00190 | -0.00024 | -0.00588 |

Table 2.2: Parameters used in numerical model for comparison with the LINE2D analytical solution.

mass. Parameters used for these tests are shown in Table 2.2.

Each of these tests was compared to an analytical solution, LINE2D (Sudicky, 1986). The results of these comparisons are shown in Figure 2.6. The solution attained by the numerical model and analytical solution are essentially identical. Small differences result from the effects of boundary conditions and being unable to represent source conditions exactly between the two codes.

Dissolution

The numerical dissolution process was compared to an example given by Powers *et al.* (1991). Their work involved studying the dissolution of NAPLs in porous media. The NAPL in their work is represented by “blobs” in the porous media. The blobs are quantified by the interfacial contact area with the surrounding saturated media. The NAPL is dissolved using a rate-limited process. The effects of groundwater flow, transport (including dispersion), and diffusion are also included.

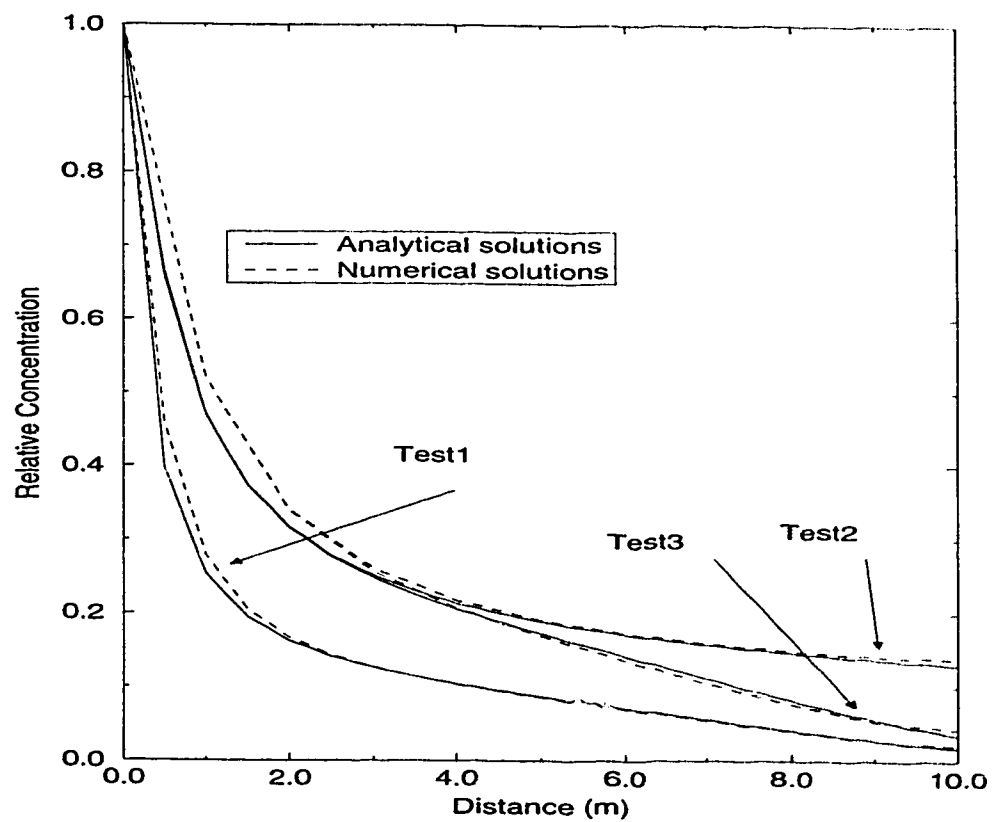


Figure 2.6: Numerical model compared to the analytical solution for a simple advection-dispersion problem.

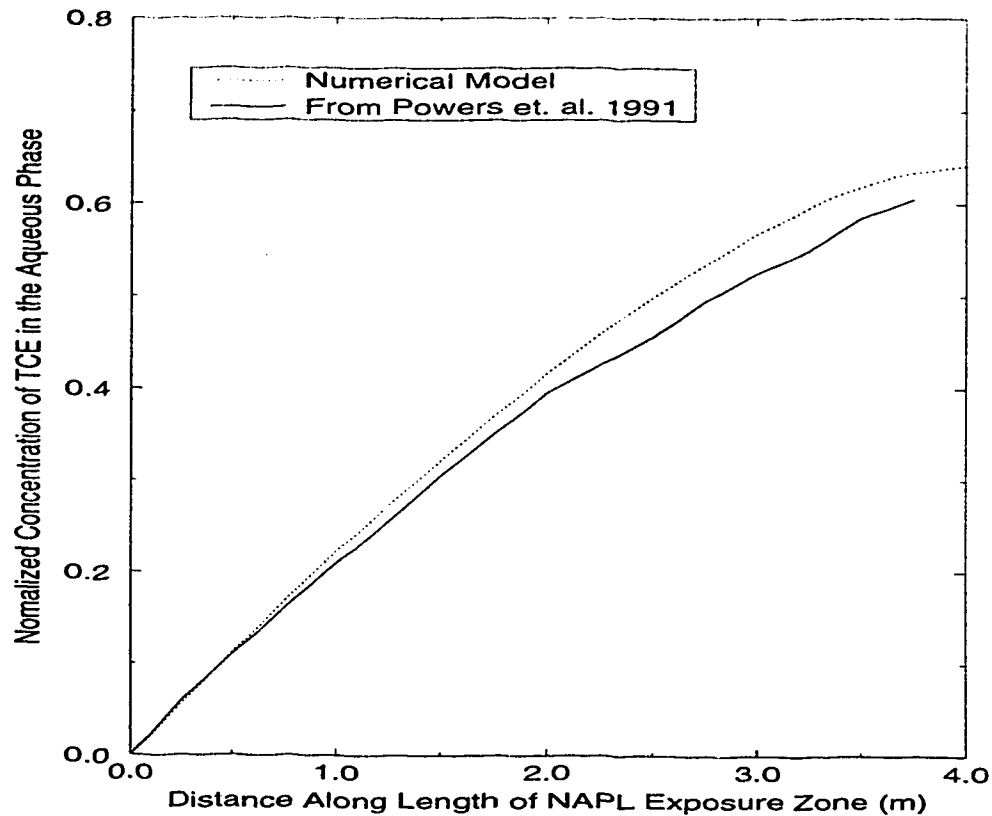


Figure 2.7: Numerical model compared the analytical solution for a simple advection-dispersion problem.

The fracture model is setup to closely resemble the scenario presented above. NAPL is distributed evenly within a fracture that has a constant aperture (i.e. for a 10% saturation every tenth cell contains NAPL residual). Parameter values such as porosity and interfacial area are matched exactly between the simulations (see Table 2.3); however, due to numerical constraints such as the effects that the boundaries have, the results cannot be matched perfectly. The results of this comparison are presented in Figure 2.7.

| | |
|---------------------------------------|-------------------|
| Aquifer Dispersivity, α | .10 <i>m</i> |
| Darcy velocity, q | 10.0 <i>m/d</i> |
| Porosity, θ | .25 |
| Residual saturation of TCE | .10 |
| Lateral extent of contaminated region | 4.0 <i>m</i> |
| Coefficient of Mass Transfer, k_t | 2.4e-6 <i>m/s</i> |

Table 2.3: Parameters used in numerical model for comparison with example from *Powers et. al.* (1991).

Chapter 3

Modeling Results and Analysis

The numerical model described in the previous chapter was applied to a number of theoretical scenarios to elucidate the dissolution behavior of NAPLs in rough-walled fractures. Most simulations were conducted using impermeable fractures walls; however, some example simulations were also run using a permeable matrix. The impermeable matrix simulations demonstrate the essential character of the dissolution process, including what factors control the dissolution process. Through comparison to the previous results, the permeable matrix simulations illustrate the potential significance of matrix diffusion on the dissolution process.

3.1 General System Behavior

This section examines the general behavior of a fracture containing NAPL residual undergoing dissolution. First, the overall character of NAPL aqueous concentration and saturation in space and time are illustrated. These are followed by an examination of changes in the mass output of the fracture, aqueous phase concentration of the NAPL, NAPL saturation and relative transmissivity of the fracture.

The small-scale perturbations in some of the curves presented here are a direct result of the discrete representation of the dissolution process whereby NAPL-occupied cells are converted to water-occupied cells. For example, when residual is removed from the fracture two effects combine to affect the dissolution process: the flow pat-

| Parameter | Value |
|---------------------------------------|----------------------------|
| Gradient Across Fracture | 0.08 m/m |
| Fracture Width, (x) | 1.25 m |
| Fracture Height, (y) | 1.25 m |
| NAPL Solubility Limit | 1100 ppm |
| Coefficient of Mass Transfer, k_t | 2.0e-6 m/s |
| Initial Mass of NAPL | 59.9 grams |
| Longitudinal Dispersivity, α_l | 0.5 m |
| Transverse Dispersivity, α_t | 0.5 m |
| Diffusion Coefficient, D^* | $1.0 \times 10^{-9} m^2/s$ |
| Time Step, Δt | 1000.0 sec |
| Total Time for NAPL Dissolution, t | 7.9 years |
| Total Mass Error, % | .13 |

Table 3.1: Parameters used in numerical model for the example simulation.

tern is changed and the amount of NAPL in contact with water changes. In most cases, removing a block of NAPL residual only marginally affects the flow pattern, yet it might dramatically increase or decrease the contact area between the water and the NAPL. This change in contact area affects the output concentration. Occasionally removing a block of NAPL may dramatically affect the fracture's transmissivity and thus change the total flow of water through the fracture. The combination of these micro-scale changes may then lead to either a spike or drop in parameters that characterize the dissolution process, such as the total downstream mass-output.

3.1.1 Simulation Description

The results in this section are from a single dissolution simulation conducted using a fracture with impermeable walls (i.e., no matrix porosity). The parameters and some basic output characteristics for this simulation are presented in Table 3.1.

The pattern of NAPL dissolution in this simulation is typical of most simulations presented later in this chapter. Figure 3.1 shows representative snapshots of the NAPL distribution and the aqueous-phase concentration within the fracture as dissolution proceeds.

Early in the dissolution process the groundwater within the fracture, which is

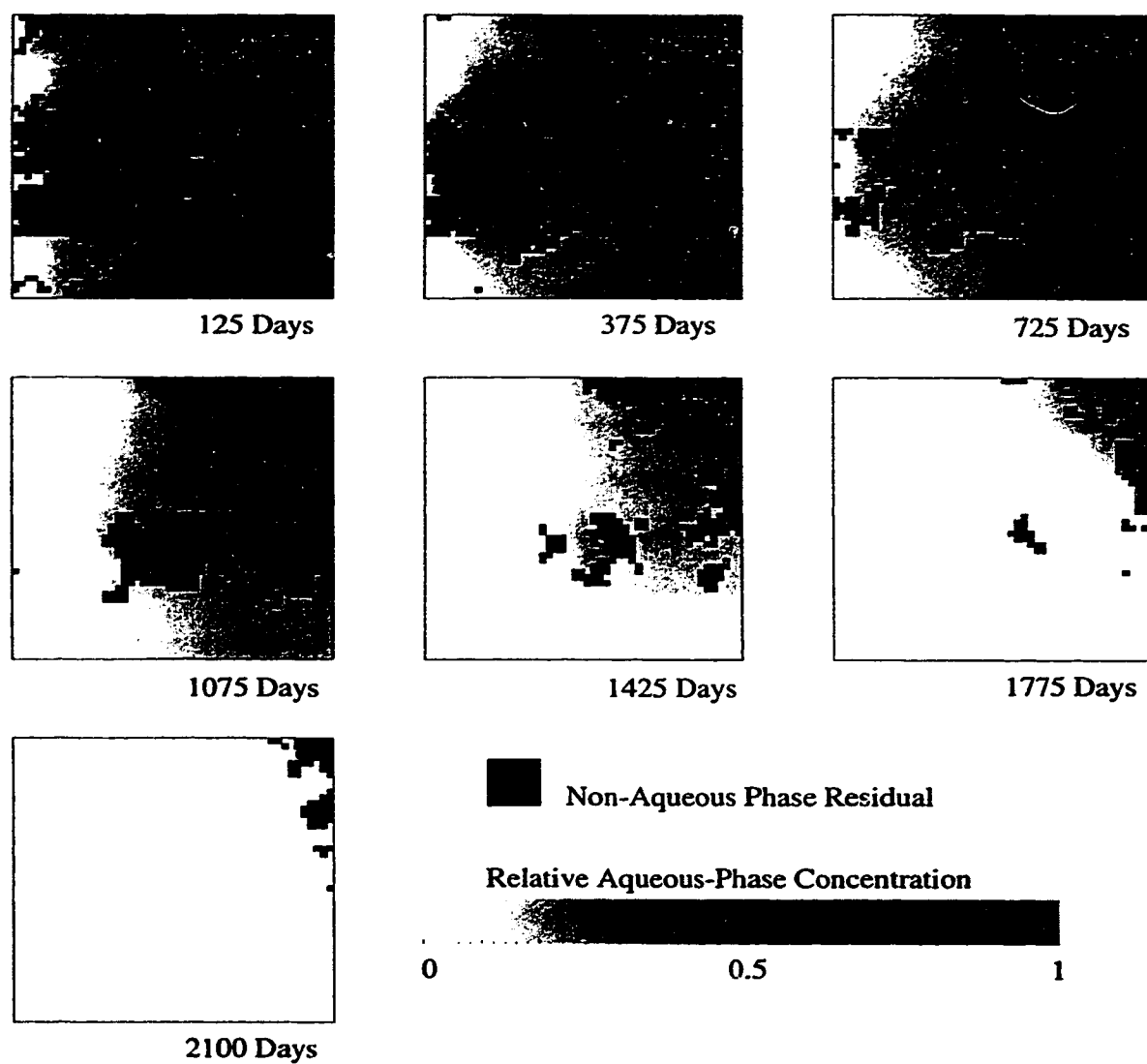


Figure 3.1: A series of snapshots showing the dissolution simulation that is discussed in this section.

moving from left to right in Figure 3.1, becomes nearly saturated with NAPL. There is a general increase in NAPL concentration from left to right; clean groundwater enters the fracture at the left and the NAPL concentration increases as water comes into contact with more NAPL residual as it passes through the fracture. The rate of NAPL dissolution at the downstream end of the fracture is slower than the upstream end because NAPL concentrations are higher near the downstream end; higher NAPL concentrations result in a slower rate of mass transfer from the non-aqueous to the aqueous phase.

3.1.2 Downstream Concentration

As shown above, the aqueous-phase concentration of NAPL varies spatially throughout the fracture. Thus, the aqueous-phase concentration in water exiting the fracture will also differ along the downstream boundary (Figure 3.1). To calculate a representative concentration of the water exiting the fracture the mass flux of NAPL at the boundary is divided by the volumetric water flux.

The average concentration of NAPL in the aqueous phase exiting the fracture falls steadily during the dissolution process (Figure 3.2). The concentration is initially close to the solubility limit and declines almost immediately. This decline is associated with the disappearance of NAPL and a greater amount of water flowing through the fracture. In other simulations where the groundwater velocity is lower than this example case, the downstream concentration may be at the solubility limit for a long period of time before the concentration begins decreasing.

3.1.3 NAPL Saturation

The amount of NAPL in the fracture is expressed in terms of its saturation. NAPL saturation is measured using both volumes and areas which are referred to as volumetric or areal saturation respectively. The specific values for volumetric and areal saturations differ because of the varying aperture distribution; however, general trends

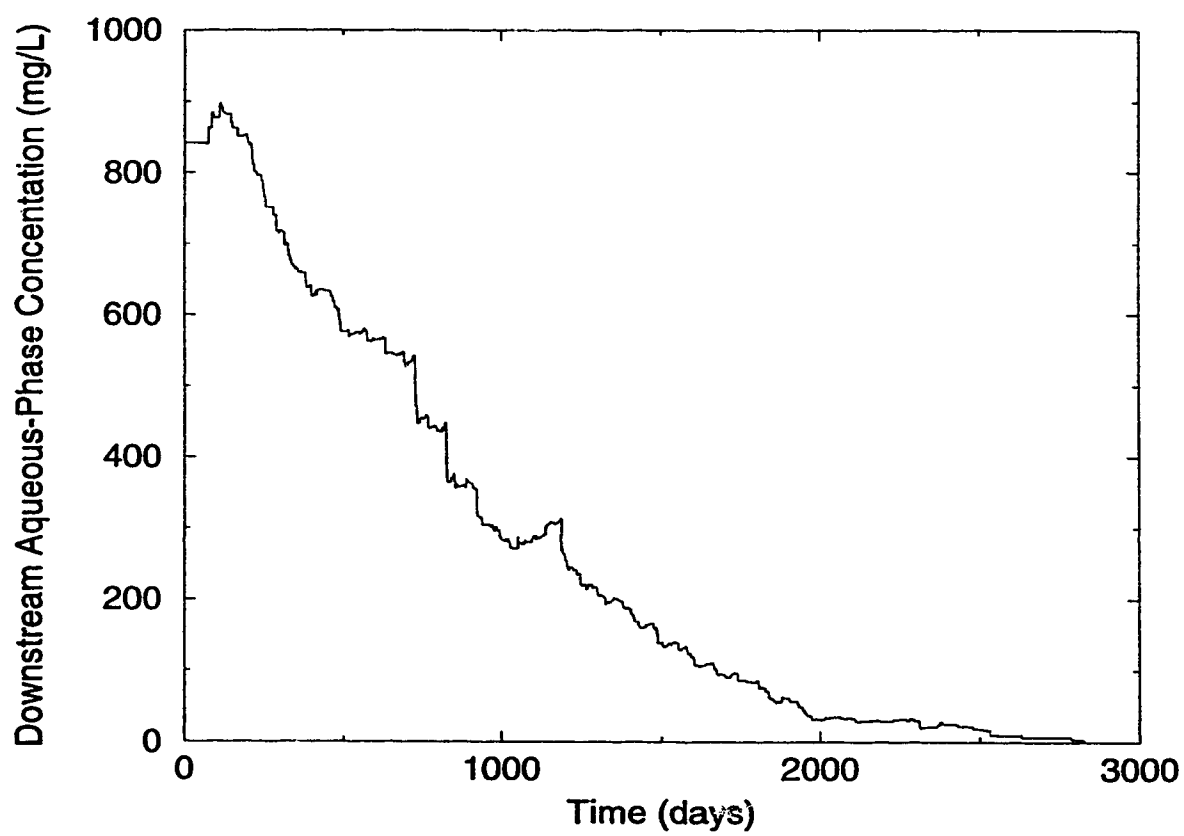


Figure 3.2: Concentration versus time curve for a single dissolution simulation.

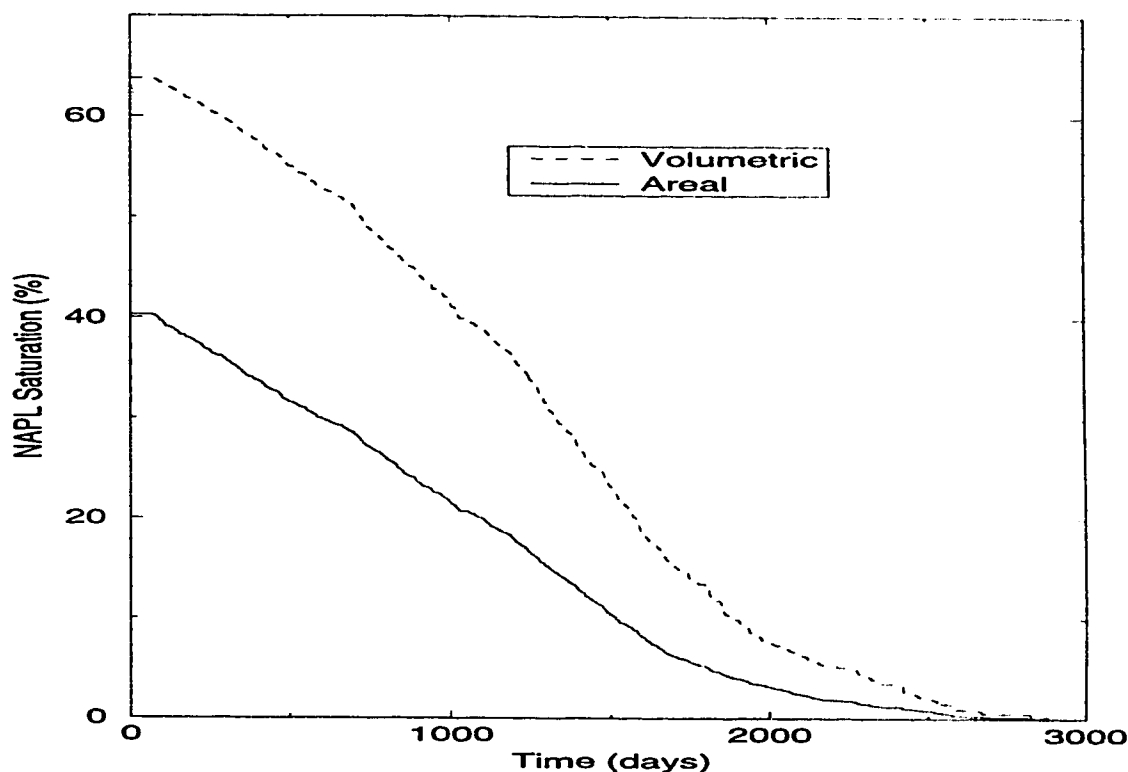


Figure 3.3: NAPL Saturation versus time curve for a single dissolution simulation.

of results are the same when these values are plotted against other parameters, such as time.

The areal saturation (as well as the volumetric saturations) decreases steadily over time during the dissolution process (Figure 3.3). The cells of NAPL disappear at a fairly constant rate; however, this rate slows near the end of the dissolution process. The cells of NAPL at later time in the model are generally the largest cells (i.e. the NAPL occupies the largest aperture segments). Since the cell contains more NAPL, it takes longer for the NAPL to disappear. This phenomenon will be discussed in more detail later.

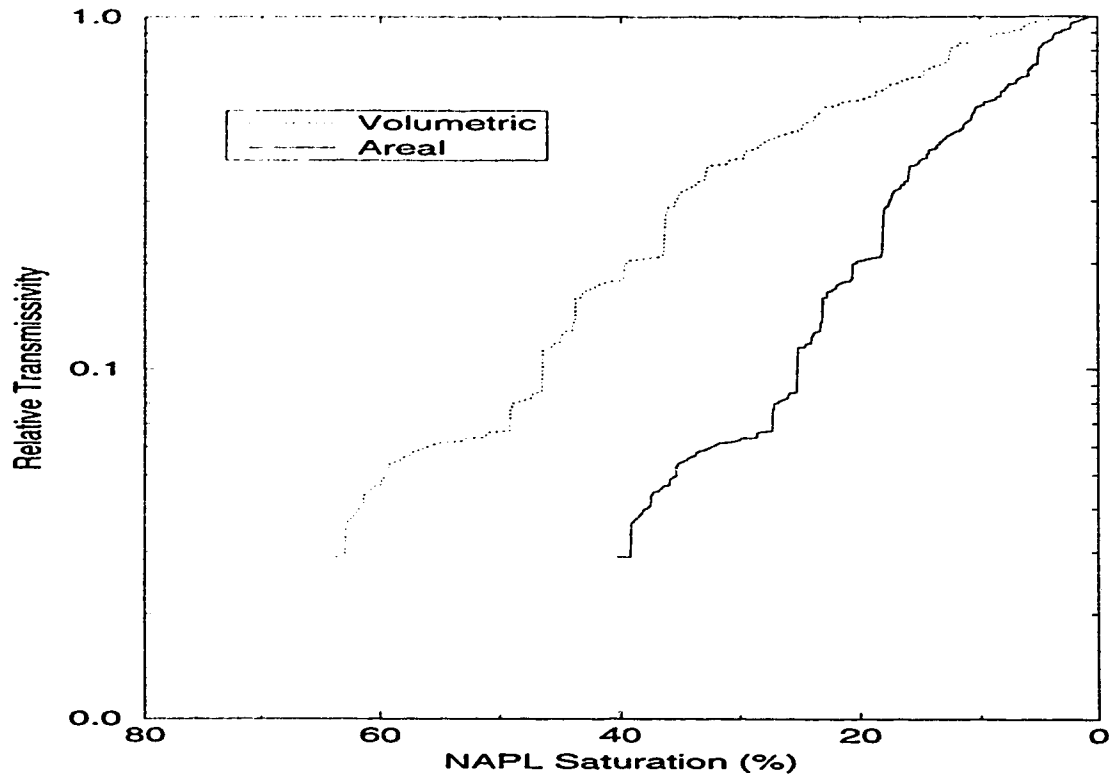


Figure 3.4: Relative Transmissivity (for water) curve for a single dissolution simulation.

3.1.4 Relative Transmissivity

The relative transmissivity of the fracture is plotted versus the areal NAPL saturation; these plots are referred to as relative transmissivity curves. As expected, the relative transmissivity of the fracture increases as the saturation of NAPL decreases (Figure 3.4). Note there are specific “jumps” in the relative transmissivity. The sudden increases occur when a cell is removed that opens a new flow path; this new flow path has a significant effect on the fracture’s relative transmissivity.

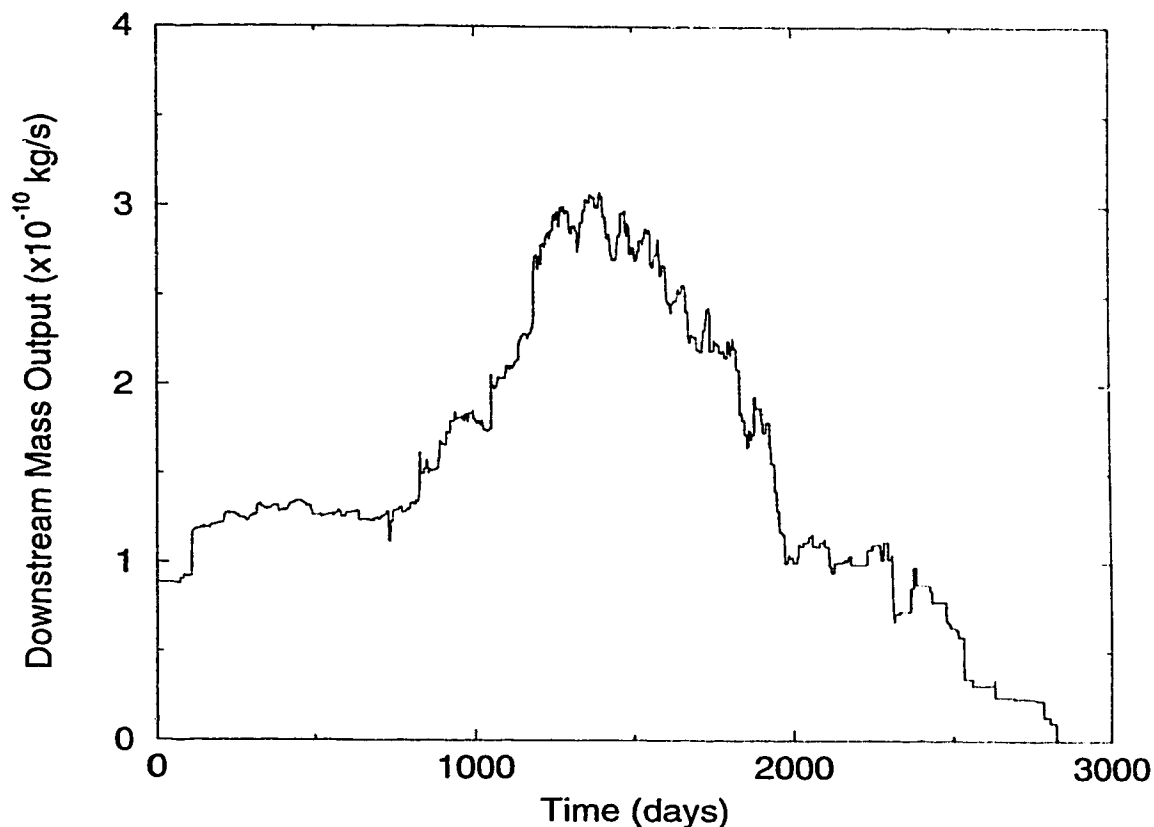


Figure 3.5: Mass-output curve for a single dissolution simulation.

3.1.5 Mass output

Figure 3.5 shows the downstream mass-output relationship versus time for the complete dissolution simulation. The overall pattern presented here is simple and similar for all other simulations: the mass-output increases gradually from an initial value to a maximum and then decreases to zero when all the NAPL has been removed. As mentioned previously, this curve represents the combined effects of variations in mass-output concentration and relative transmissivity. Note also that there is no correlation between the downstream aqueous-phase concentration and the downstream mass output (Figure 3.5) during the dissolution process.

3.2 Sensitivity Analyses

In order to determine the important controls on dissolution, a sensitivity analysis is performed on different simulation parameters. The emphasis for the sensitivity analyses is placed on the physical constraints of the system, such as NAPL location and the fracture aperture distribution.

3.2.1 NAPL Placement

Invasion Percolation

Figure 3.6 shows the mass-output for a single fracture with three different initial NAPL saturation levels created with invasion percolation methods. All other parameters, such as the gradient across the fracture and the coefficient of mass transfer for the NAPL were held constant, and the same random aperture field was used for each of the different simulations. To obtain varying initial saturations, an initial residual distribution was first created using invasion percolation techniques (Mendoza, 1992). This NAPL distribution was then artificially modified by removing or adding residual around the edges of existing NAPL residual clusters.

The curve for the low initial NAPL saturation case (20%) has a high peak or maximum mass output rate. This peak rate occurs relatively early when compared to higher initial NAPL residual saturations. Following this peak, the rate of mass output drops quickly until all the NAPL has disappeared (Figure 3.6).

The curve for the relatively high initial NAPL saturation case (44%) has a low peak mass output rate and the peak rate occurs late when compared to lower initial saturations. As well, the peak rate occurs over a greater interval of time than the lower saturation case (i.e. the curve has more of a “U” shape than a “V” shape). As would be expected, the total time for the NAPL to completely dissolve is much greater than in the lower NAPL saturation cases. This relationship between NAPL saturation and dissolution time will be discussed in more detail later.

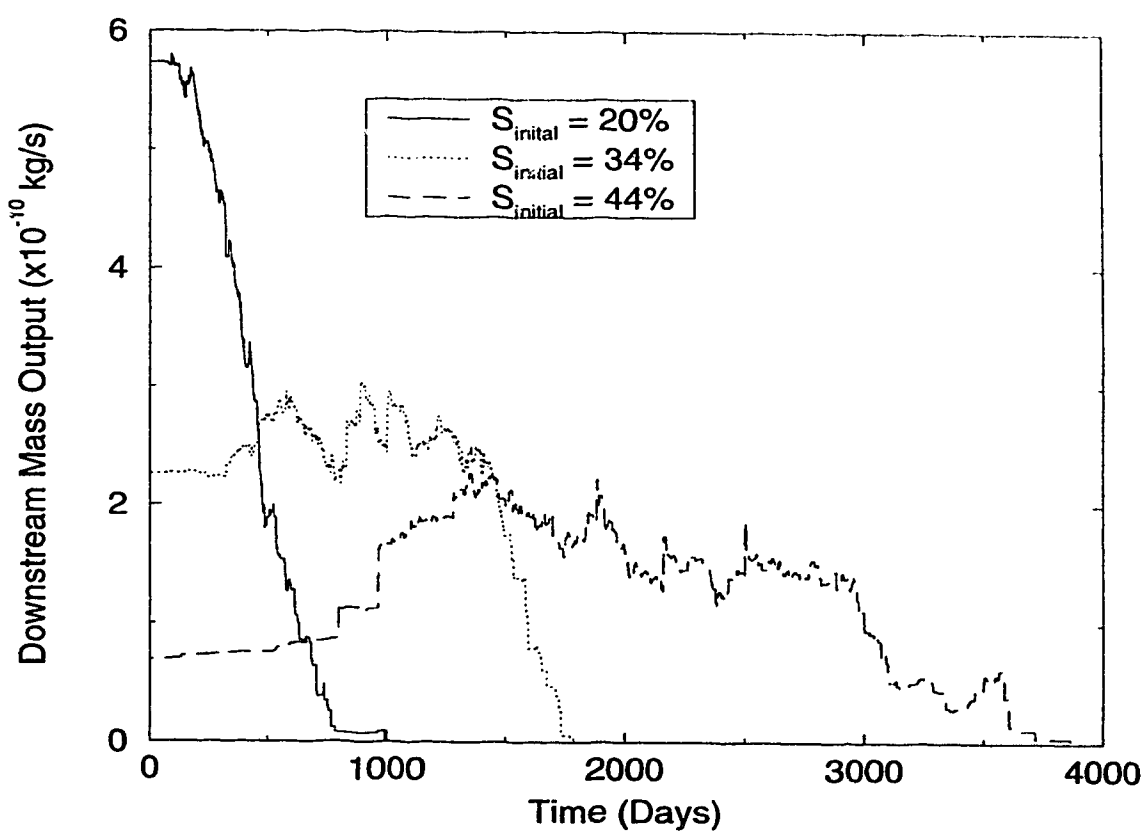


Figure 3.6: Mass-output for three saturation levels created with invasion percolation methods for a single fracture with the same aperture distribution.

Random Residual Assignment

In the previous section it was demonstrated that the initial NAPL saturation affected the mass-output curves. The position of the NAPL within the fracture will also have an effect on the mass-output curves. The location of NAPL in the fracture is controlled by the criteria controlling invasion percolation. To investigate the influence that invasion percolation has on the mass-output curves, simulations were performed where the NAPL was distributed randomly throughout the fracture. To permit direct comparisons to previous results the initial NAPL saturations were forced to be identical to the previous invasion percolation residual distributions.

The random residual assignment is produced by randomly assigning NAPL occupied cells throughout the fracture, with no consideration given to either occupancy (i.e., aperture size) or accessibility (i.e., invasion mechanism) criteria. This random residual assignment distribution of NAPL is not meant to represent any real scenario, nor is it based on an actual physical process, as is the case of invasion percolation. However, the random residual distribution does offer the chance to examine mass output curves that are independent of the process of invasion and that have a greater statistical link to the initial NAPL residual saturation. By comparing the random residual assignment results to those of invasion percolation we can identify features of the mass output curves that are a direct result of the NAPL invasion history and its position in the fracture relative to the random aperture field.

Qualitatively, the general mass-output curve shapes and trends for the random residual distributions are similar to the invasion percolation results (Figure 3.7). That is, initial lower saturations have higher peaks and the NAPL dissolves quickly, whereas higher initial saturations have lower peaks and the NAPL takes a longer time to disappear. Even though the invasion percolation distribution and random NAPL distribution mass output curves have these similarities, differences are strikingly apparent. One major difference is that the residual distributions created with invasion percolation take much longer to dissolve than the random residual distributions (note the different time scales for figure 3.6 and figure 3.7). A second significant

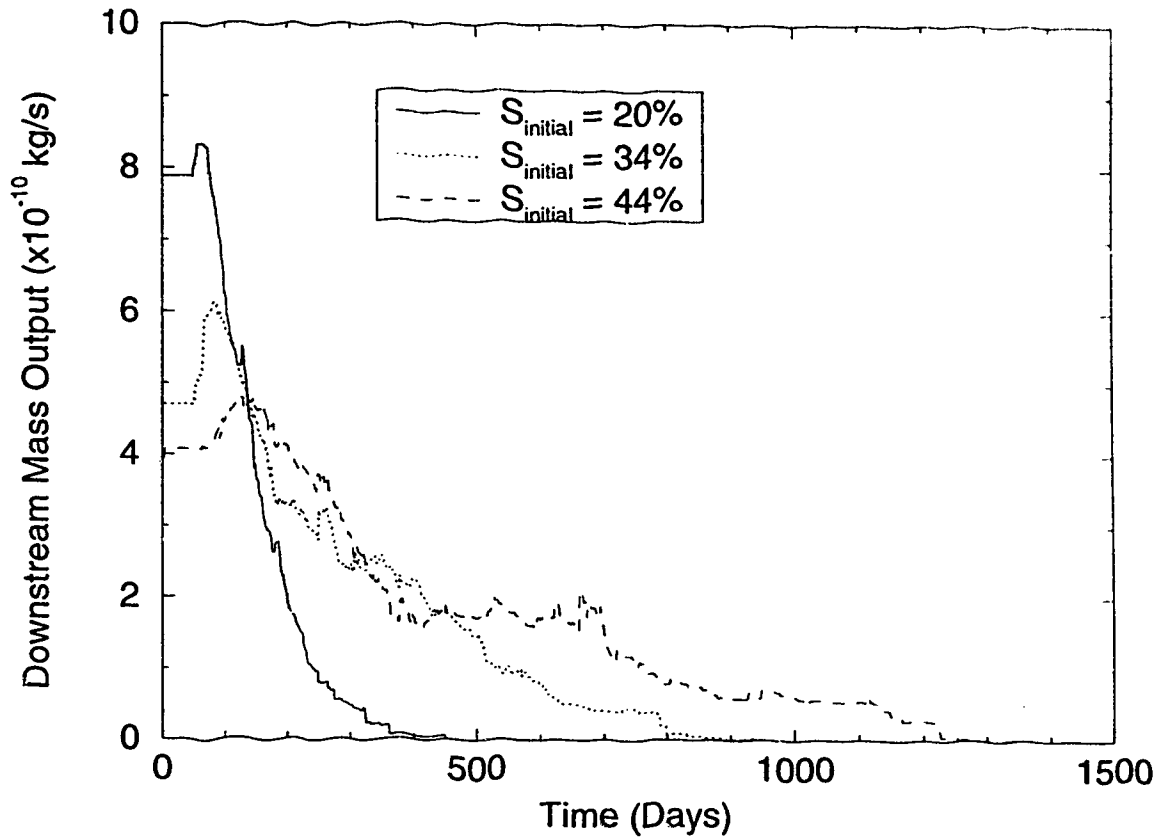


Figure 3.7: Mass-output for three saturation levels created with invasion percolation methods for a single fracture with the same aperture distribution.

difference is that the separation between the maximum peaks for the random residual distribution case is small whereas the time separation for the maximum peaks in the invasion percolation case is relatively large. Thus, invasion percolation curves are skewed far more to the right than the random NAPL distribution curves.

The underlying reason for these differences must be due to the position of NAPL within the fracture, which is directly related to the invasion process controlling the NAPL placement. Further explanation for these differences may be obtained by considering arbitrary cross-sections from both a random residual distribution and a distribution created with using invasion percolation. (Figure 3.8)

The random residual distribution has a high initial dissolution area as compared

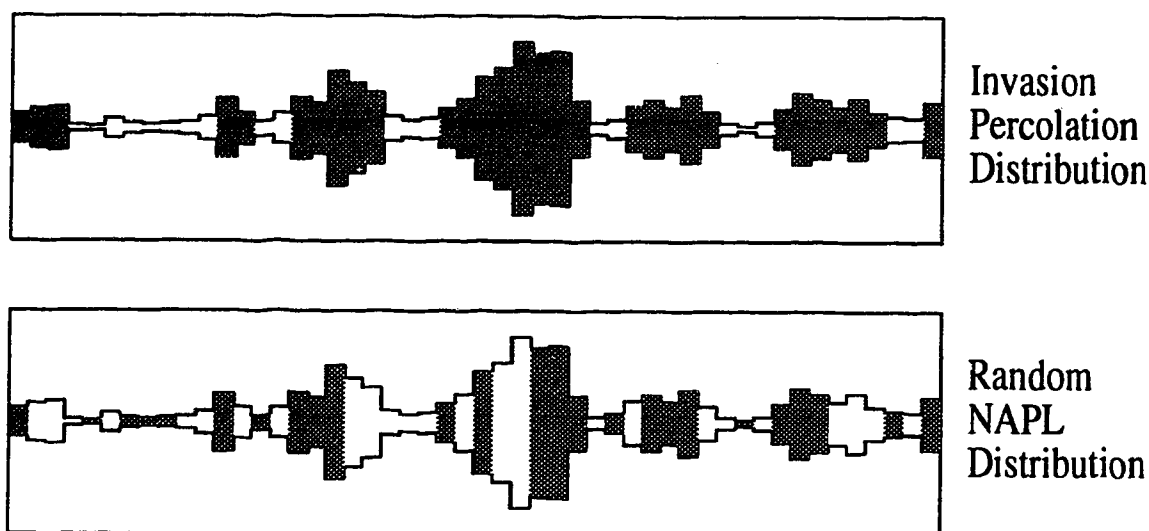


Figure 3.8: Cross-sections through a residual distribution for invasion percolation and random residual assignment. NAPL is shown in grey and water fills the rest of the fracture.

with the invasion percolation distribution. The dissolution area is simply the area of NAPL in contact with water. Even though the cross-section is a simplification of the three-dimensional case, the high initial dissolution area of the random percolation case is visually apparent. It is this high dissolution area that results in random residual distributions having a higher mass output rate than the invasion percolation distributions. Since more of the NAPL is in direct contact with water, the NAPL in random residual distributions dissolves more quickly.

A corollary to this is that the invasion percolation distribution is more continuous. The NAPL is generally located in blobs inside larger aperture spacings. As noted before, these distributions have a smaller initial dissolution area; the NAPL is more likely to be connected in groups. Since there is more NAPL-NAPL contact, there is less NAPL-water contact. Again, this is visually apparent from Figure 3.8. It is the differences in the NAPL distribution patterns that cause the differences between the random residual case and the invasion percolation case in the mass-output curves.

For the invasion scenario, the NAPL begins to dissolve from the edges of the NAPL blobs first. The initial dissolution rates would be low; hence, the initial

mass outputs are low. Once the smaller NAPL-containing cells have been removed the larger ones begin to dissolve. The dissolution of the larger aperture segments containing NAPL yield the peaks seen on the mass output graph. The peaks are generally wider (longer in time) and smaller (lower peak mass-output rate) when compared to the mass output peaks of the random residual distributions. Because of the spatial location of NAPL within the fracture, invasion percolation distributions slow the dissolution process when compared to the random residual distributions.

3.2.2 Random Field versus Saturation Effects

The previous results examined varying NAPL saturations and method of occupation (i.e., random NAPL distribution versus invasion percolation) versus the mass output for a single random aperture distribution. The random aperture distribution will also affect the mass output. To determine whether this effect is significant or predictable further simulations were conducted using a series of statistically similar, but different random aperture fields. Invasion percolation was used to create the initial NAPL residual distribution in each random field investigated. The initial NAPL saturation for every simulation was set at 40% by adding or subtracting NAPL around residual clusters until the target saturation was reached.

Figure 3.9 shows the mass output curves from two separate random field distributions. Even though both begin with an initial NAPL saturation of 40%, the time for total NAPL dissolution varies by over 2000 days. Also, the shapes of the curves vary for each distribution. Curve A has a high initial peak that occurs fairly early. This is similar to the lower saturation curves seen previously. Curve B has a lower peak mass output occurring relatively late. This curve shape is reminiscent of the higher saturations seen previously, yet both mass output curves correspond to the same initial NAPL saturation. Thus, the controlling factor causing the differences in these curves must be the character of the random field and the differences they impose on the residual distributions and flow field.

The random fields are statistically similar. The minor differences in the size

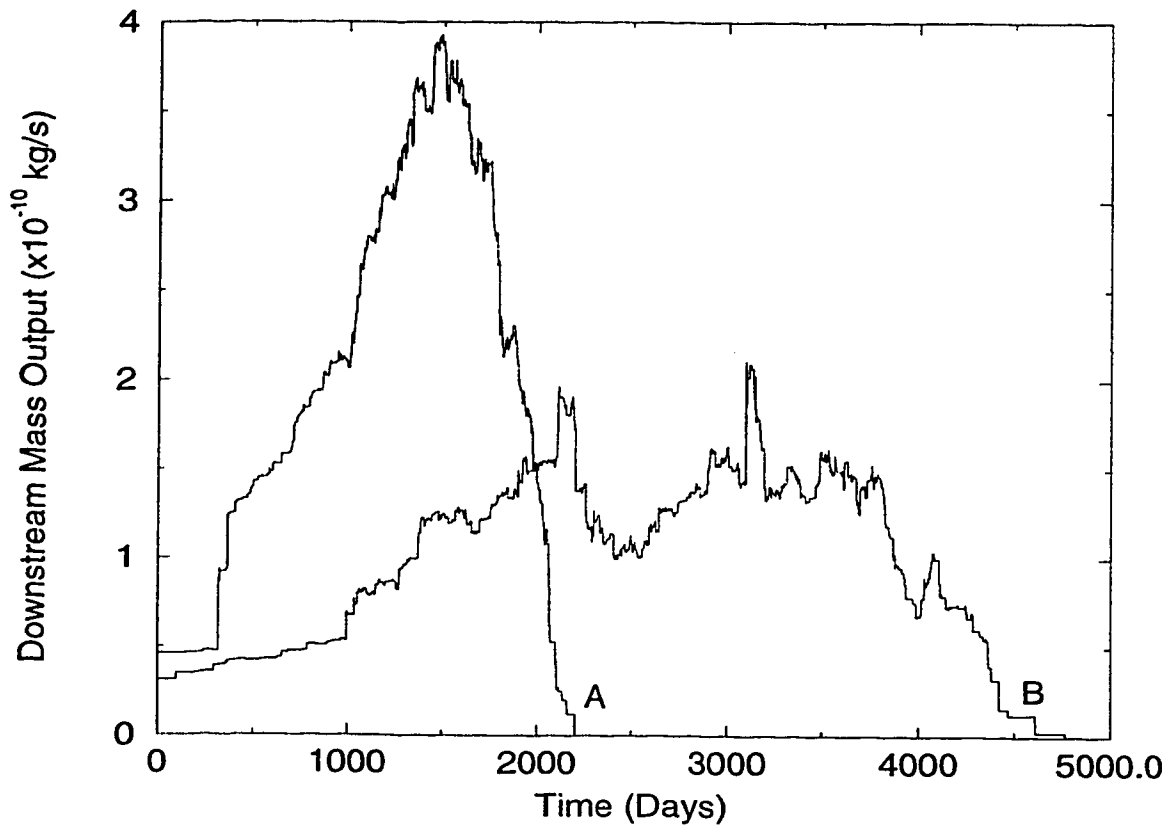


Figure 3.9: Mass output versus time for two distribution created using invasion percolation on three different random fields.

and arrangement of the initial NAPL residual with these fields play a large role in controlling the aqueous-phase mass output. More importantly, it is the series of connected pathways during the invasion process that controls the pattern of the NAPL residual. This effect, even on the conceptual level, is nearly impossible to predict beforehand.

3.2.3 Random Field Variance

The variance of the random field was modified to investigate the type of effect this would have on the mass output curves. Figure 3.10 shows cross-sections of two frac-

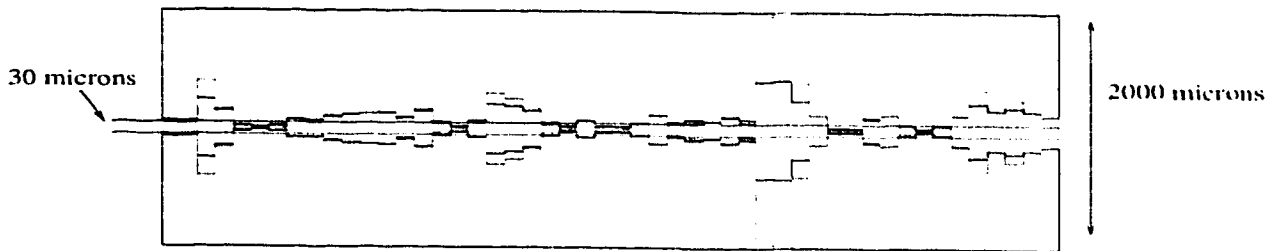


Figure 3.10: A cross-section through two fractures that share the same initial aperture distribution; however, the variance of each one has been modified. The black cross-section has a variance of 0.75 while the grey cross-section has a variance of 2.25, but both have a mean aperture of about 30 microns.

tures. The fractures started with the same aperture distributions and the apertures were modified so the overall variance of the fractures would be different. For the given mean aperture, a fracture aperture distribution with a smaller variance has larger minimum and smaller maximum apertures than a fracture with a larger variance.

The general behavior of the mass output curves after modifying the variance should be predictable. Increasing the variance of the fracture aperture distribution should have two main effects of the mass output curves. First, since the apertures surrounding the NAPL blobs are smaller the initial mass output rates should be smaller for the fractures aperture distributions with larger variances. Also, the time for the mass output peak to occur should be later. Second, the mass output peak should be larger since the peak represents the larger aperture spaces. If the variance of the aperture distribution is larger then the larger apertures space will also be large.

Figure 3.11 shows a two mass output curves for two dissolution simulations. Most of the parameters between the simulations were held constant except for the variance. The result are as exactly as predicted. These results help confirm the importance of the invasion percolation residual (i.e., blobs) in dissolution modeling. It also demonstrates that subtle changes in the nature of the random field can have a dramatic effect on the dissolution of NAPL within the fracture. Also, note that most of the peaks in the output curves can be correlated with each other. The higher value of variance has the effect of stretching the mass output curve in time.

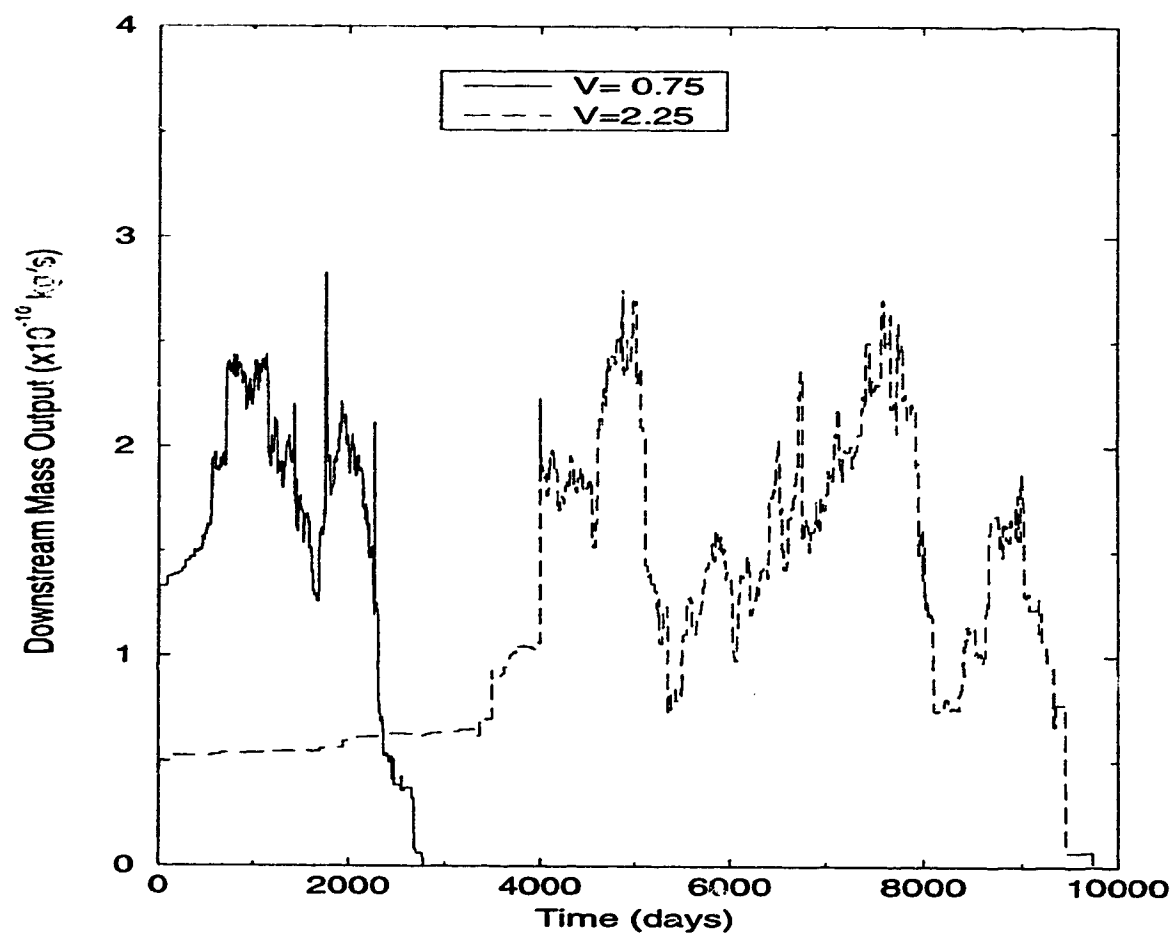


Figure 3.11: Two simulations showing the mass output of the two fractures that differ only by the variance (V) of their aperture distributions.

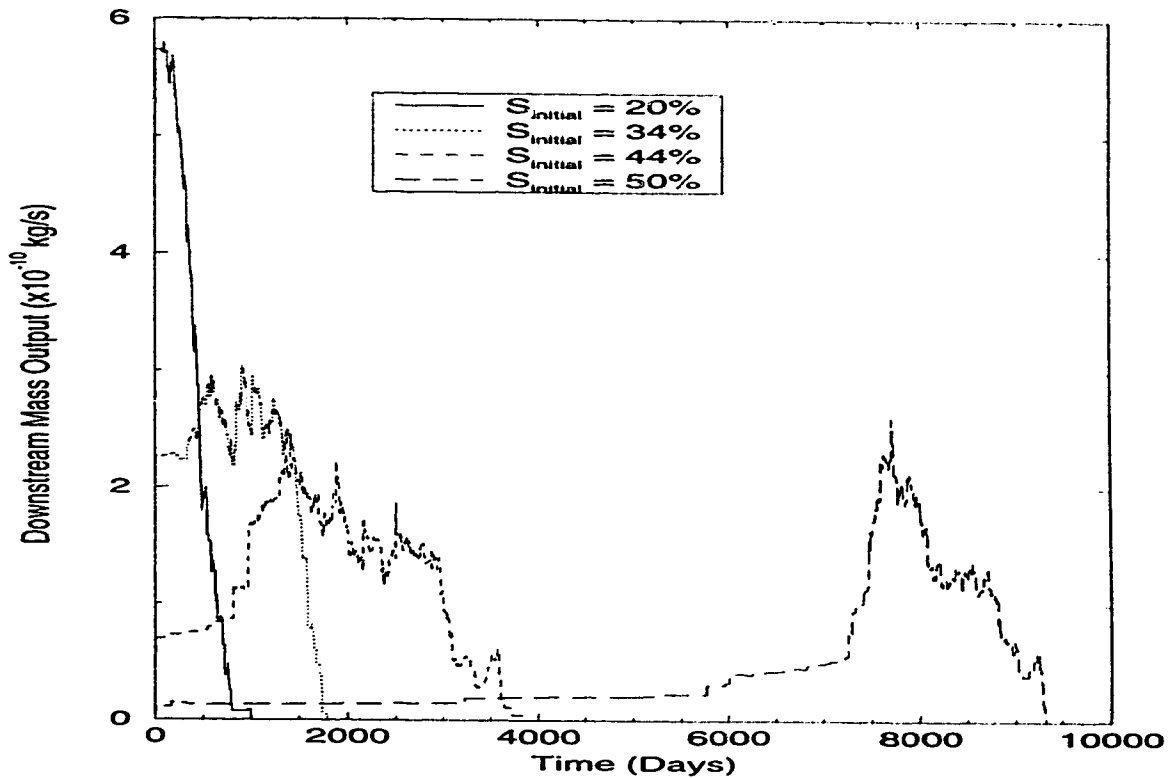


Figure 3.12: Mass-output for four saturation levels created with invasion percolation methods for a single fracture (the same aperture distribution).

3.2.4 Higher NAPL Saturations

The time for the NAPL to completely dissolve can vary by years for fractures with the same initial NAPL saturations, but with different methods of creating the initial residual distribution (e.g., distributions created using invasion percolation versus random NAPL assignment). At even higher initial NAPL saturations the effect becomes further exaggerated as demonstrated by using a NAPL saturation of 50% (compare Figure 3.12 to 3.13).

For the random residual case, increasing the initial saturation this small amount, from 44% to 50%, does not have a dramatic effect on the mass output curve. The peak

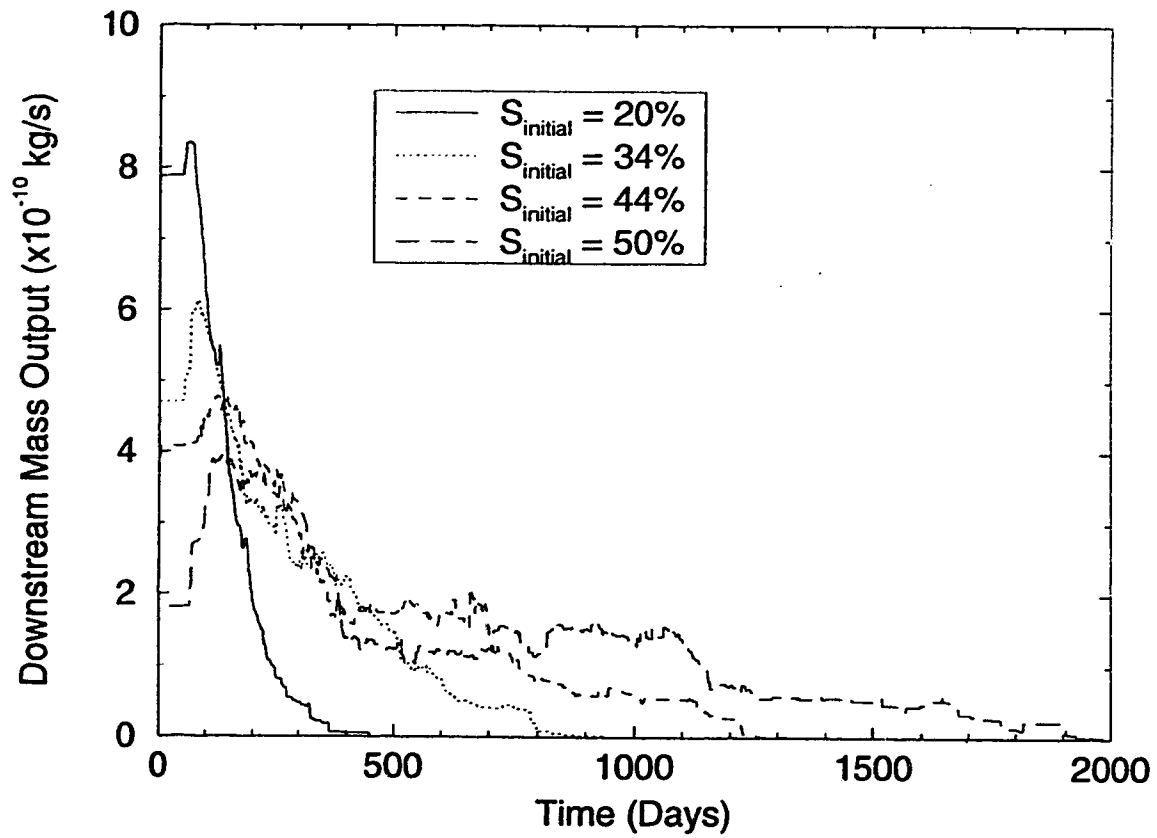


Figure 3.13: Mass-output for four saturation levels created with random percolation methods for a single fracture (the same aperture distribution).

mass output rate has declined and the overall time for complete NAPL dissolution has correspondingly increased. However, for a distribution generated using invasion percolation the mass output peak is delayed significantly where the initial saturation has been increased from 44% to 50%.

At 44% saturation most of the larger aperture segments in the invasion percolation case contain NAPL. When the saturation is increased the only additional space for the NAPL to reside is in the surrounding small aperture spaces. Since the NAPL-water contact area within these aperture cells is very small it takes a very long time for the NAPL to be removed from these smaller aperture cells. Also, the fracture has a low initial relative transmissivity because much of the fracture is filled with immobile and impermeable NAPL. Thus, the volume of water flowing through the fracture is low, which contributes to the slow dissolution rate. Once the smaller cells around the larger ones have dissolved, the mass output increases and the mass output curves have a similar peak rate curve as the lower saturation cases.

For this case there is a significant high saturation point between 44% and 50% initial NAPL saturation. This is the point where the larger aperture segments have been filled with NAPL. Once past this point (i.e. high saturations), the surrounding smaller apertures are filled. This filling of these smaller segments has a large effect on the dissolution time.

Figure 3.14 shows the relative transmissivity curve for four simulations. Each simulation is conducted with the same random aperture distribution. The NAPL residual distribution for these simulations are created using invasion percolation and are then modified to represent varying degrees of NAPL saturation. These four simulations are the same as those presented earlier in Figure 3.12

The 50% initial curve starts with the lowest relative transmissivity. This is to be expected because the NAPL is immobile and impermeable to water flow and is filling much of the fracture. However, this particular simulation continues to have lower relative transmissivities when compared to other curves at the same saturation point. For example, at the 25% NAPL saturation point, the 50% initial NAPL

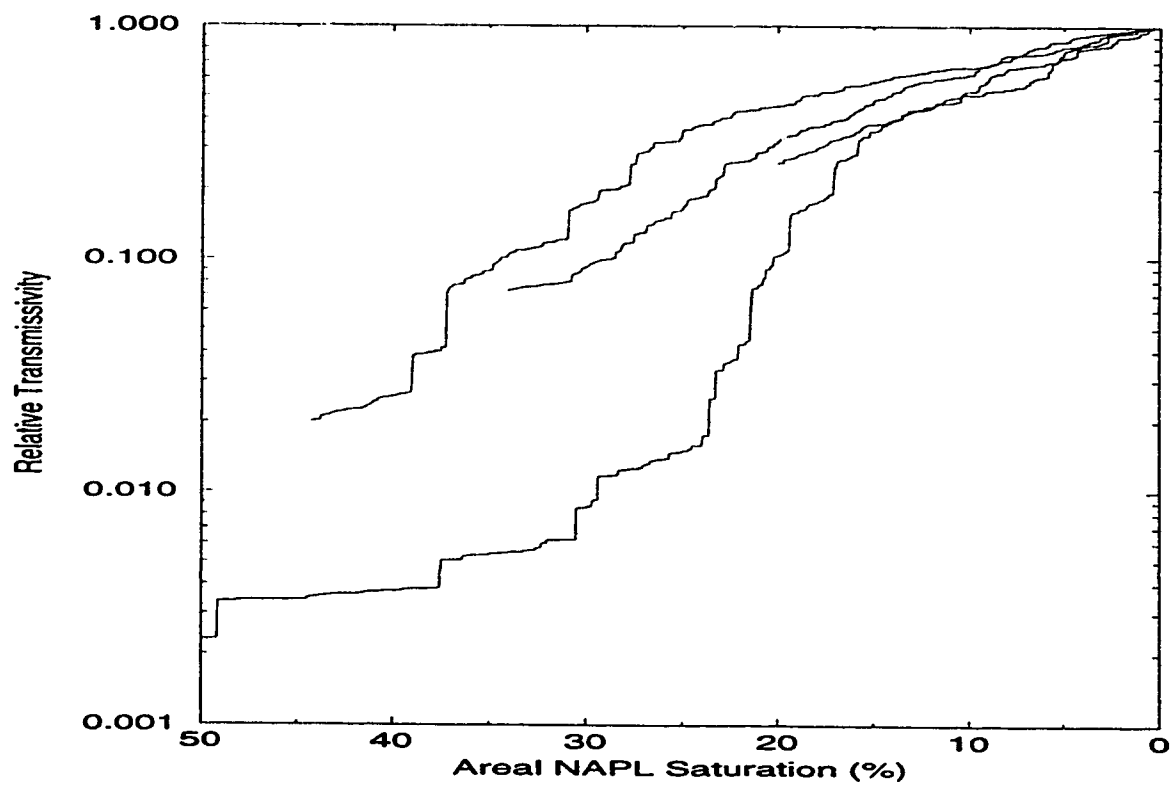


Figure 3.14: Semi-log plot of the relative transmissivity of the fracture versus the volumetric NAPL saturation. The simulations shown here used NAPL distribution created by invasion percolation.

saturation curve has a relative transmissivity of approximately 0.01, yet the curves for initial NAPL saturations of 43% and 33% have relative transmissivities that are over an order of magnitude higher.

The curves produced from the initial NAPL saturations of 20%, 33% and 44% have very similar profiles; however, the 50% saturation curve seems, for the most part, to follow a different path. This curve was differentiated earlier from these other three in the mass-output results. It was considered a “high” saturation case because the dissolution time for the NAPL jumped dramatically. Starting with a higher saturation than the other simulations has had an effect on the path this curve follows. Since the transmissivities are lower for this high saturation case, the dissolution process will take longer.

For comparison, Figure 3.15 shows the relative transmissivity curves for the random residual distributions (Figure 3.13). The overall relative transmissivity of the randomly distributed NAPL is dramatically higher. For example, the initial relative transmissivity for the 43% saturation curve is greater than 0.1. This is over an order of magnitude larger than for the same saturation created using invasion percolation. This trend is apparent throughout all the NAPL saturation levels. The reason for this again has to do with the different position of NAPL relative to the aperture distribution for the invasion percolation case versus the random residual case. The invasion percolation case has the lower relative transmissivities because the larger aperture spaces are preferentially filled. Because the relative transmissivity is directly proportional to the aperture size (Equation 2.5), the invasion percolation distributions have lower transmissivities for equal saturation of random residual distributions.

The other major difference between the invasion percolation and the random residual distribution transmissivity cases is that there is no “high” saturation distinction. The 50% curve in the random percolation case does not show any significant differences from the other curves; just as it did not show any significant differences from the trends in Figure 3.13.

The random aperture field also has an effect on the relative transmissivity curve.

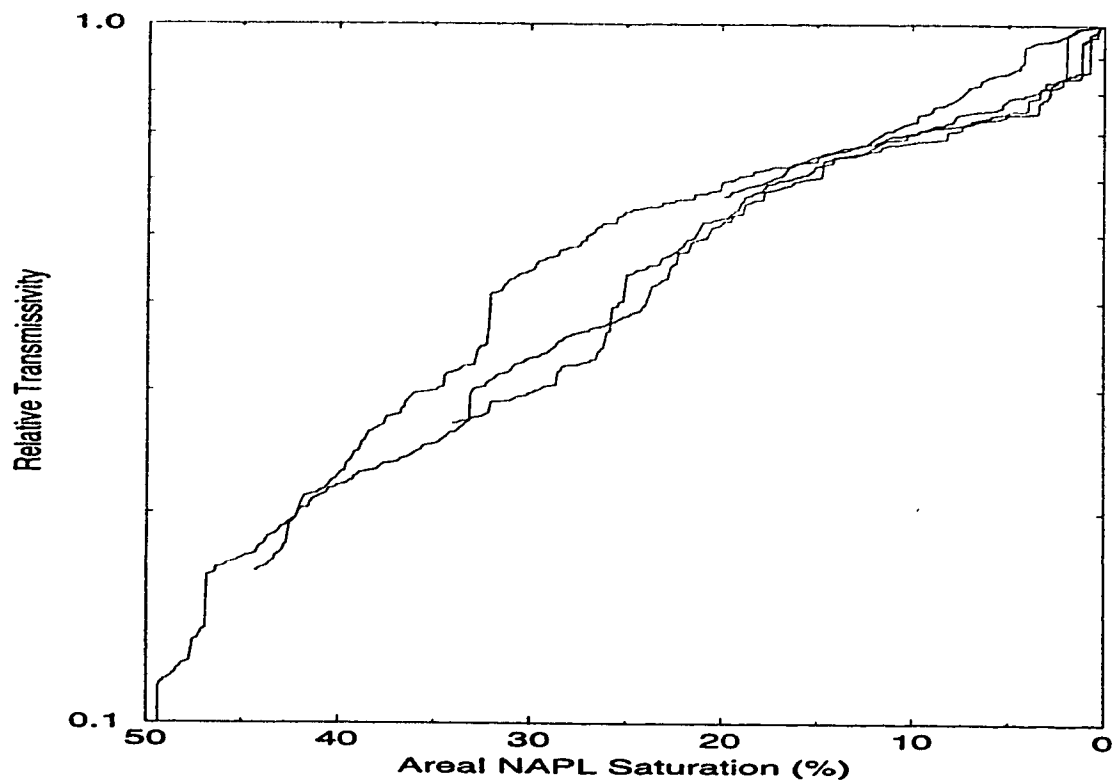


Figure 3.15: Semi-log plot of the relative transmissivity of the fracture versus the volumetric NAPL saturation. The simulations shown here used NAPL distribution created by random residual assignment.

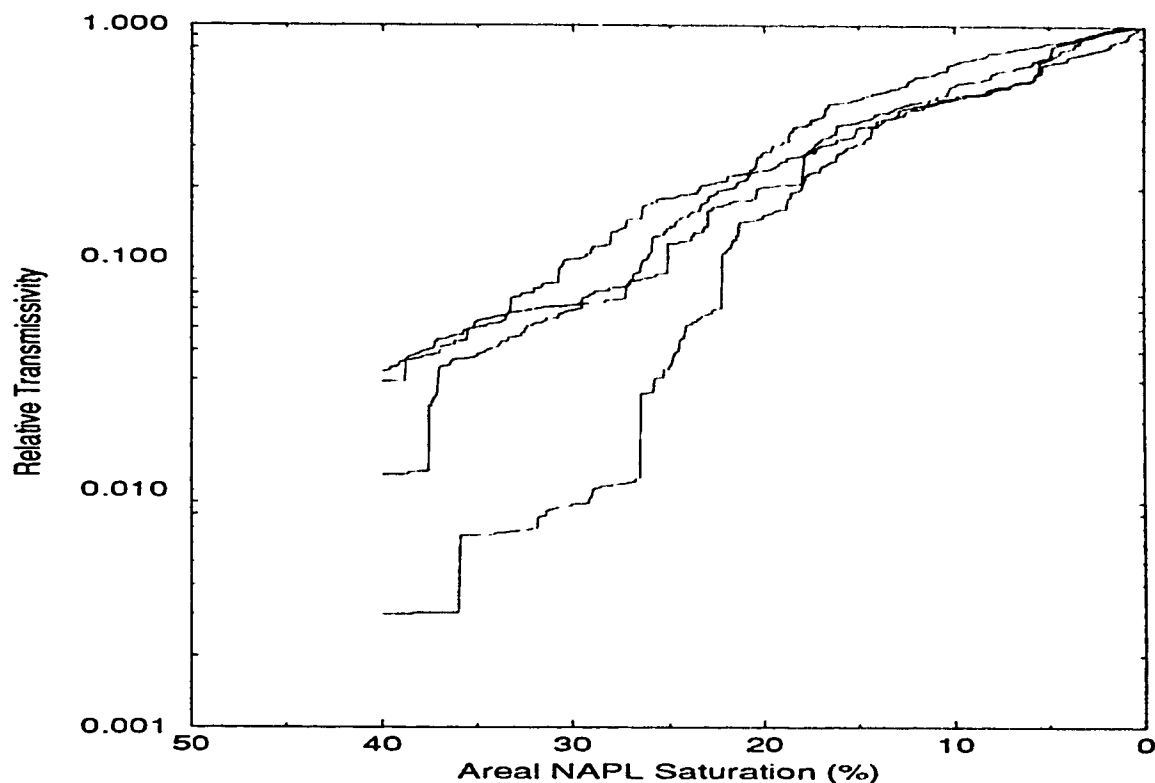


Figure 3.16: Semi-log plot of the relative transmissivity of the fracture versus the volumetric NAPL saturation. The simulations shown here used NAPL distribution created by invasion percolation and all distribution have been modified so the initial NAPL saturation is 40% in all cases.

Figure 3.16 shows the results for 4 simulations conducted with different aperture fields. Initial NAPL saturations of 40% were created using invasion percolation. The transmissivity curve for three of the simulations appear to be similar, however the fourth is lower than the rest. Since these curves are different the pattern of dissolution, and the time it takes for the NAPL to dissolve, will be different. These differences are again related to the unpredictable nature of the random fields.

The relative transmissivity curves converge when the NAPL saturation is less than about 20%. The convergence occurs when the NAPL exists only as disconnected

out the fracture. These disconnected blobs do not have a large effect on the transmissivity of the fracture when compared to higher NAPL saturations. Results were presented by *Mendoza* (1992).

Dissolution Time versus Saturation

Figure 3.14 shows the time for NAPL dissolution versus the initial NAPL saturation. It includes many of the concepts that were presented previously. This figure is constructed from the curves in Figures 3.12 and 3.13, and also with information from experiments conducted at lower saturations.

Figure 3.14 shows two curves, one representing random NAPL distributions and the other representing invasion percolation distributions. The curves are similar for saturations below 30%; however, at higher saturations the NAPL dissolution for the invasion percolation case begins to increase dramatically. As stated earlier, this is due to the larger pore spaces and the surrounding smaller ones becoming occupied with NAPL. The "high saturation point" in this case would be about 48% where the curve suddenly flattens.

Transmissivity Plots and Discussion of Boundary Effects

Figure 3.15 shows that the time for the NAPL to disappear from the fracture is different when comparing the 30% case to the 50% case. This is indicated by the different paths the transmissivity curves follow.

Figure 3.16 is a plot of the areal NAPL distribution within the fracture and shows how the distribution changes during the dissolution process. There is little difference in the distribution of the two cases early in the dissolution process; however, the NAPL in the 30% case disappears much faster and in a different order. The difference in the distribution can be explained by the difference in initial relative transmissivities. Because the initial relative transmissivity of the higher saturation case is low, there is less flow through the fracture. The aqueous-phase concentration of NAPL in the fracture reaches the solubility limit and the dissolution of NAPL slows

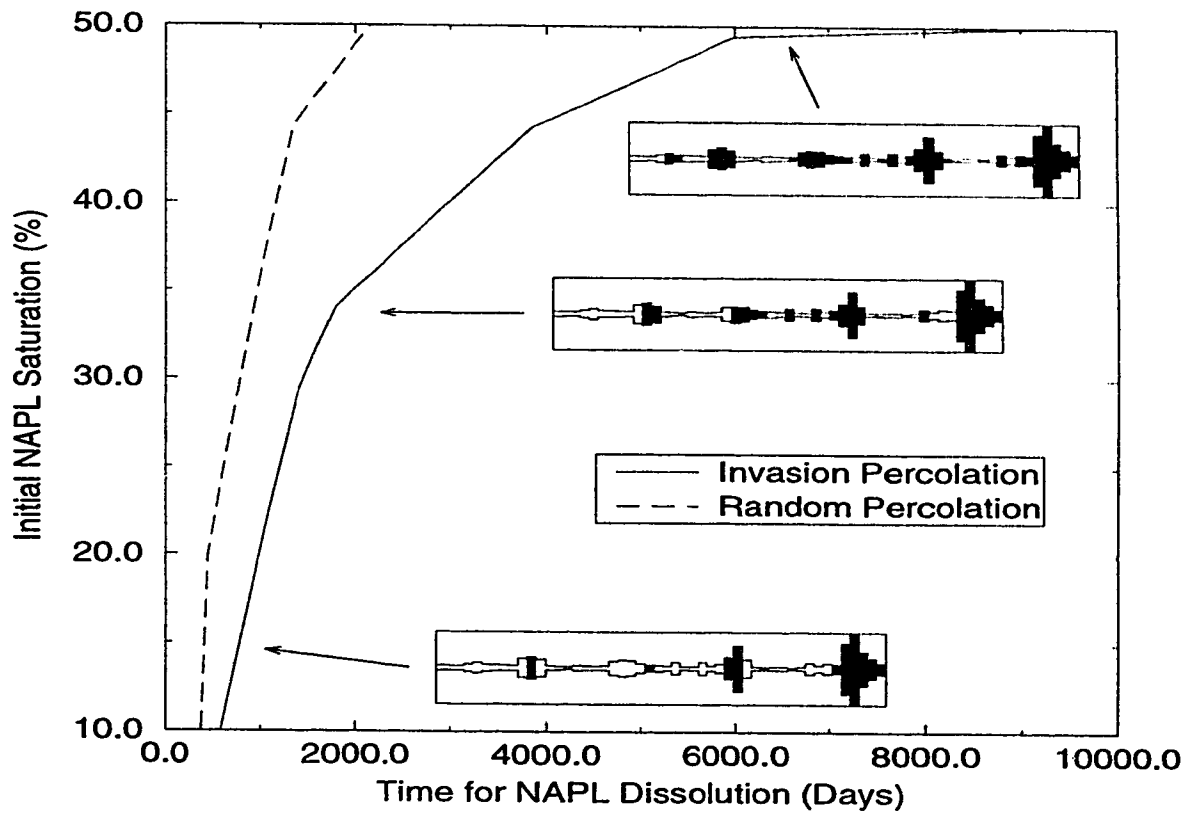


Figure 3.17: Time for NAPL dissolution versus the initial NAPL saturation. The cross sections show the NAPL position for the invasion percolation case at various points on the curve.

dramatically. The dissolution rate increases only when the transmissivity increases to the point where water can move significant amounts of aqueous-phase NAPL out of the fracture.

The pattern in which the NAPL disappears is also different. This results from the boundary conditions imposed on the simulation. For the high saturation case, very little mass is transported out of the downstream boundary, instead the NAPL slowly diffuses out the left-hand side. Until a significant pathway is opened up, this diffusion is the main mechanism for NAPL to exit the fracture. Since this process is very slow, it takes a very long time for the NAPL to dissolve. Also, the NAPL is removed along the left-hand side of the boundary as opposed to along major flow paths (such as in the lower saturation case, see Figure 3.18).

3.2.5 Groundwater Flow and Mass Transfer Coefficient

To this point only the effects of saturation, percolation method and various random fields on dissolution have been investigated. The effect that the mass transfer coefficient and groundwater velocity have on the time for the NAPL to completely dissolve is also important. If the dissolution time is long, then the NAPL residual can act as a long-term source of groundwater contamination that would be difficult or impossible to remediate. If the dissolution time is decreased, the NAPL may be able to be removed using conventional remediation technologies.

To investigate some of the effects of groundwater flow rates and the mass transfer coefficient has on the NAPL dissolution times several additional simulations were conducted. Each simulation used the same random field and the same initial residual distribution created using invasion percolation.

Groundwater Flow

The groundwater velocity through the fracture, which is related to the volume of water coming into contact with the NAPL is a controlling factor in the rate of dissolution. In the discrete fracture there is no single groundwater velocity that can be

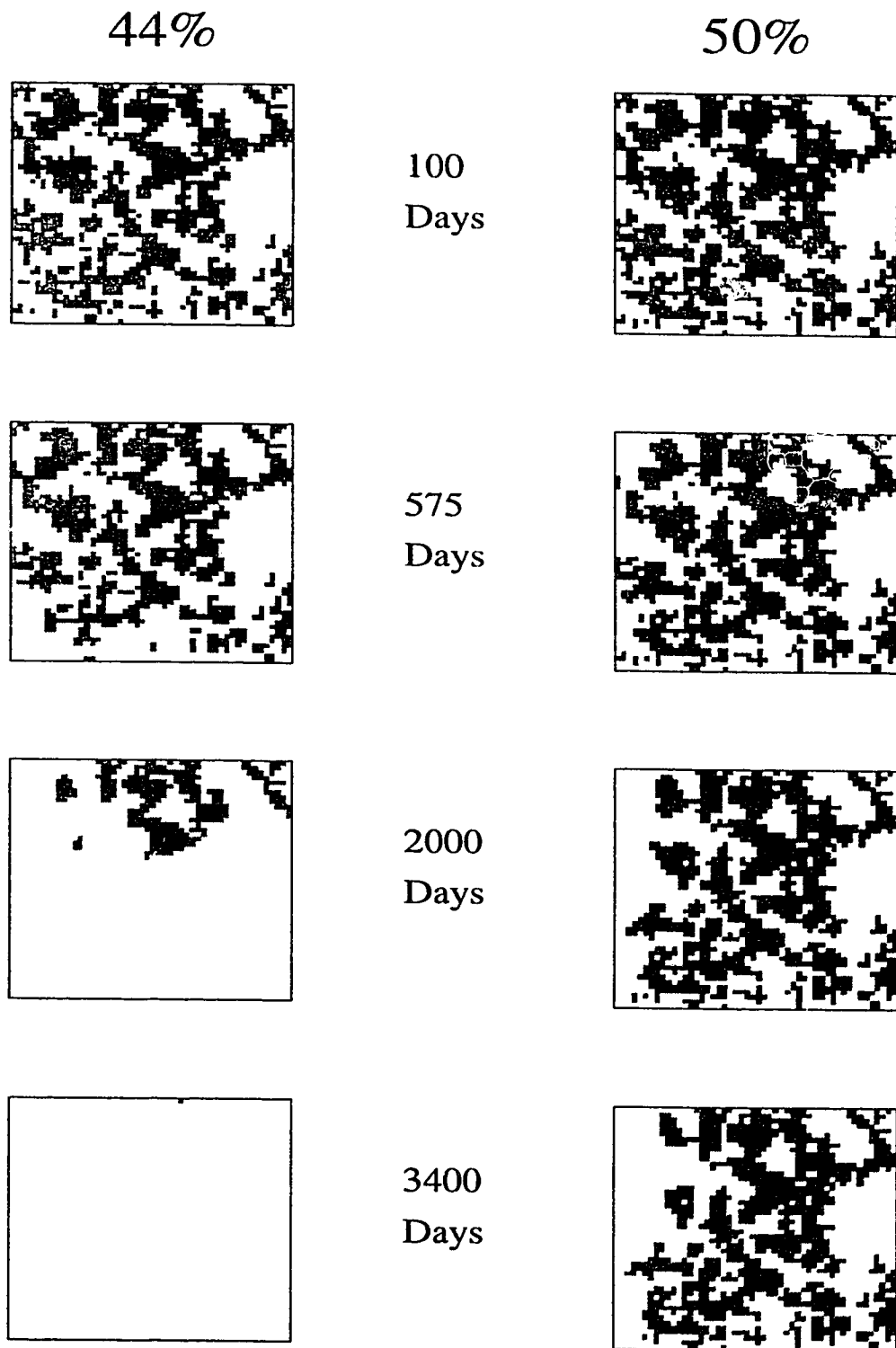


Figure 3.18: Areal saturation plots for two similar simulations with different initial areal saturations. Shading indicates NAPL.

used to characterize the flow through the fracture. Instead, the gradient across the fracture is used. An increase in the gradient directly correlates with an increase in the groundwater velocity. Of course, increasing the gradient across the fracture also increases the volume of water that passes through the fracture for a given amount of time.

Figure 3.19 shows the relationship between the gradient across the fracture versus the time for dissolution for a single residual distribution. Note the flattened part of the curve past about 7000 days. This part of the curve is mainly controlled by diffusion out of the fracture at the left-hand side. Due to the constraints of the boundary conditions for the transport model, mass can only exit via diffusion through the left hand boundary; therefore, the slope at this point in the graph may be less than expected under "real" conditions.

The effect that the groundwater flow rate has on dissolution is most dramatic in the neighbourhood of 5000 days. Here the groundwater velocity is still relatively small and the dissolution time is relatively long. However, only the smallest change in groundwater velocity produces over a 2000 day difference in the time required for NAPL dissolution. This effect is mainly a result of the right-hand boundary condition. Mass that was previously building up at the boundary and not exiting the system is now being carried across the boundary by advection. Moving this mass across the boundary lowers the concentration in the system, which increases the rate of dissolution and decreases the dissolution time.

Figure 3.19 shows that if the gradient across the fracture is increased to about 0.2 m/m , the dissolution time is around 2500 days. This difference in dissolution time is not as dramatic as in the previous step. The rate of groundwater flow is being increased; however, the rate of mass transfer from the non-aqueous to the aqueous phase remains the same. The controlling factor in the flux term controlling the dissolution is the mass-transfer coefficient (k_t) instead of the difference between the maximum solubility and the actual concentration ($C_s - C$).

When looking at higher head gradient values, such as 0.4, increasing the water

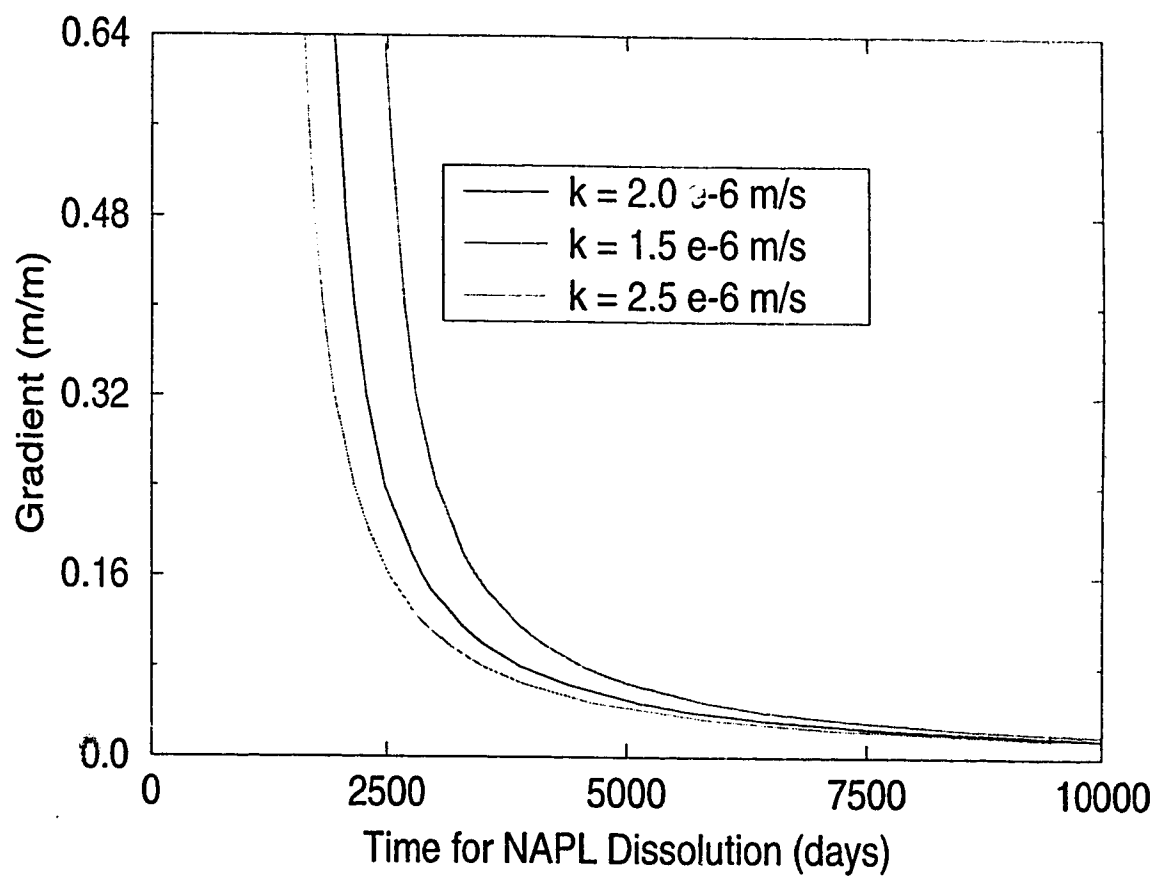


Figure 3.19: Time for NAPL dissolution versus the gradient across the fracture.

flow rate has nearly lost its effect on dissolution time. Here the water is flowing fast enough to keep mass from building up and concentrations from being high; therefore, the mass transfer coefficient is controlling the dissolution.

Mass Transfer Coefficient

Figure 3.19 also shows the effect that varying the mass transfer coefficient has on dissolution times. At low groundwater flow rates, variation in the mass transfer coefficient has little effect on the rate at which mass will be dissolving because the local concentration difference ($C_s - C$) is the controlling factor. However, when groundwater flow rates are high, differences in dissolution times due to changes in the mass transfer coefficient are more apparent. Obviously, increasing the mass transfer coefficient will result in a shorter dissolution time and vice-versa; the increase in mass transfer rates has a diminishing effect similar to increasing the rate of groundwater flow.

3.3 Monte Carlo Results

Results to this point demonstrate that the aperture field and residual distribution have large effects on the dissolution of the NAPL. However, a precise description of the effect that a certain aperture field will have on dissolution is difficult, if not impossible, to obtain. To better understand the range of dissolution behavior that different, but statistically similar, aperture fields have a Monte Carlo analysis is performed.

3.3.1 Mass output

Multiple simulations are conducted on many different initial residual distributions that were each created from a unique random aperture field. The placement of residual is generated using invasion percolation and the final residual distributions for each random aperture field following the invasion process is left unmodified. The

| | Value Used |
|-----------------------------------|------------|
| Height/Length of Fracture | 1.25 m |
| Number of Elements | 2500 |
| Average Aperture | 27.5 μ |
| Head Differential Across Fracture | 0.20m |

Table 3.2: Parameters used for Monte Carlo simulations

initial areal NAPL saturations are all within approximately 20% . The initial statistics used in generating the random aperture field, such as the average aperture, are held constant for every simulation. The random seed used to generate the random aperture distribution is the only parameter that is varied. Changing this seed will cause the random distribution of apertures to be different, which also results in a different residual distribution. Table 3.2 shows the parameters used for the generation of the aperture and residual distributions and some of the parameters used for the dissolution modeling.

Analysis of several simulations shows that the basic pattern is generally the same for all aperture/residual distributions. Figure 3.20 shows the mass output versus time results from 20 simulations. Curves that have a higher maximum mass output have been marked in black, while curves that have a lower maximum mass output have been marked in grey; this arbitrary distinction is useful for further analysis. There are curves that have profiles similar to the low saturation curves in the previous section (black curves). Also some curves have profiles similar to the high saturation curves in the previous section (grey curves). From the previous results we know that the random aperture distribution and NAPL saturation/distribution are controlling the profile of these mass-output curves. The only parameter that has been varied has been the random seed for the generation of the random aperture field. It is obvious from Figure 3.20 that the effect of the different random aperture fields is dramatic.

Figure 3.21 shows the mass-output of the fracture versus the NAPL saturation during dissolution. The curves are from the same simulations that are used in Figure 3.20, with the same black versus grey separation between high and low maximum

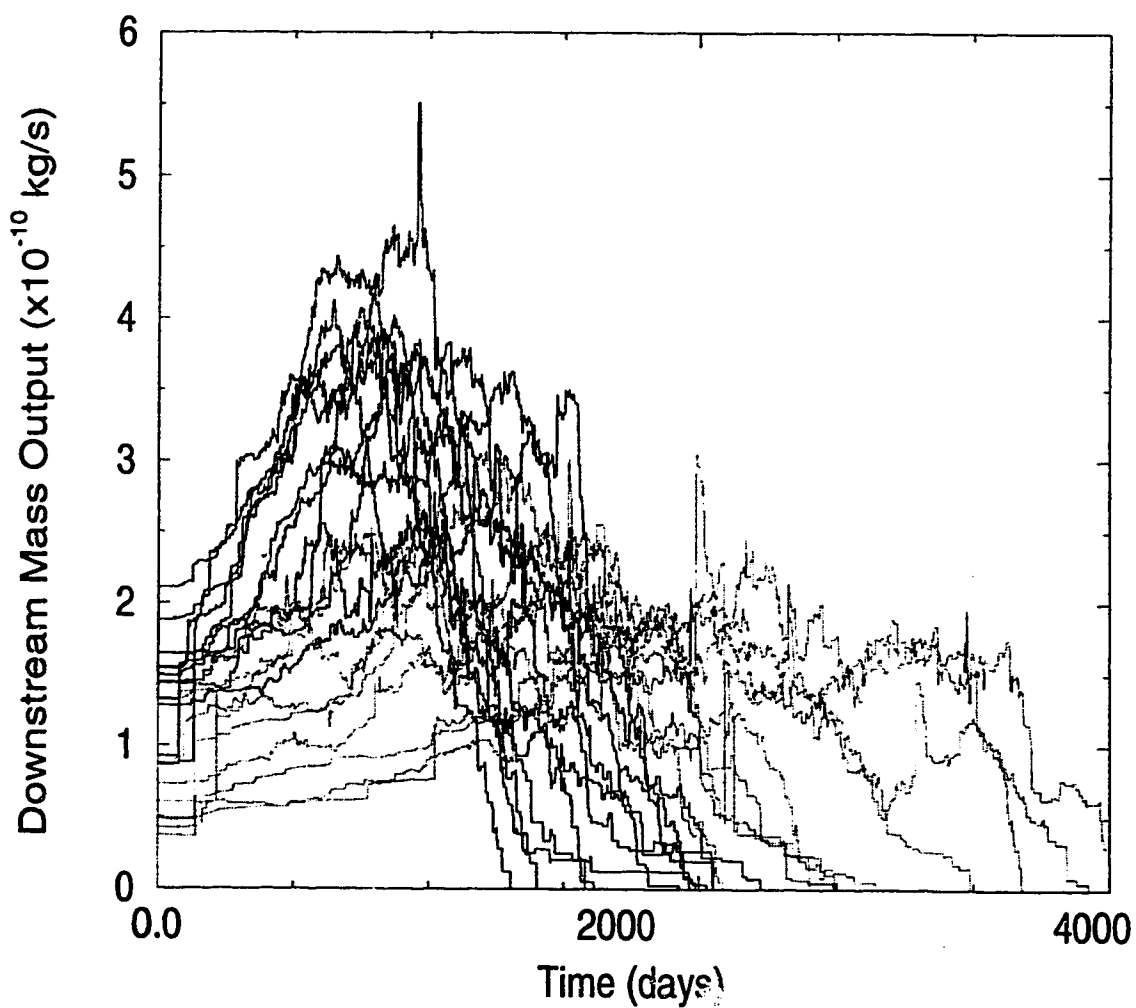


Figure 3.20: Downstream mass output versus time. Black and grey lines shown an arbitrary separation.

output values being used. The curve shape between each simulation is similar except for the maximum mass-output rate. This maximum rate occurs around 20% to 40% volumetric saturation of NAPL. Note that there is a correlation between the initial volumetric saturation of the wetting phase and the maximum downstream mass output; higher initial wetting-phase volumetric saturation (lower NAPL saturation) generally results in higher downstream mass outputs.

The curves that have a high mass output result from NAPL being trapped in larger aperture segments. This results in a larger area of NAPL in contact with water; dissolution time is decreased and the rate of mass output is increased. Curves that have a lower mass output result from NAPL being trapped in small aperture segments. This results in a smaller area of contact with water; dissolution time is increased and the rate of mass output is decreased. This concept, which has been discussed previously, is illustrated in Figure 3.22

Some of the mass-output profiles appear to be produced by saturations similar to case A while some appear to be produced by saturations similar to case B. A high mass output case and a low mass output case will be examined. Figures 3.23 and 3.24 show the previous results with two individual examples of a high output case and a low output case highlighted.

The highlighted residual cluster in the cross-section of case A (Figure 3.26) shows the NAPL in a larger set of aperture segments. The surface area of NAPL in contact with the surrounding water is relatively high. This results in a greater mass flux of NAPL from the non-aqueous to the aqueous phase. Compare this to the highlighted section in the cross-section of case B (Figure 3.26). Here, most of the NAPL is trapped in segments which are relatively small, except for the centre of the residual cluster. The area in contact with water is relatively low, therefore the mass flux during dissolution is also low. Since the mass flux is low, the residual cluster will take a longer time to disappear than the cluster in case A. When the smaller segments around case B cluster have dissolved, the center part will disappear relatively quickly with high mass fluxes into the water leading to the rapid decline in mass output at

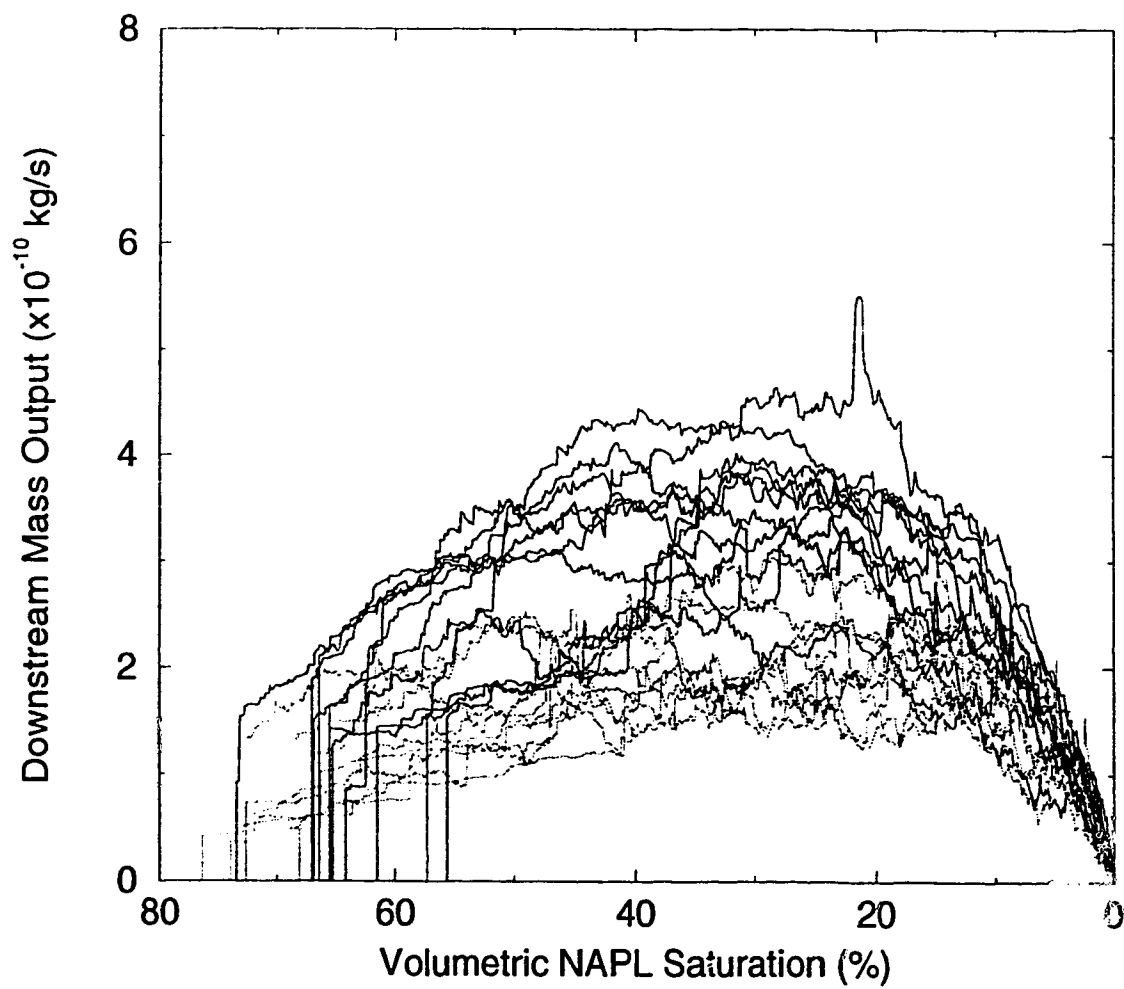


Figure 3.21: Downstream mass output versus volumetric saturation of the wetting phase. Black and grey lines shown an arbitrary separation.

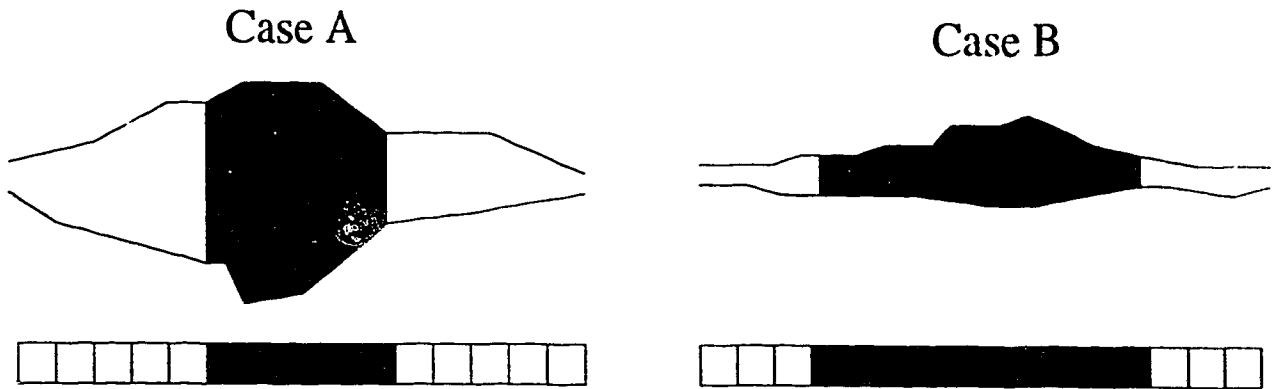


Figure 3.22: Two conceptual cases on how NAPL is located within a fracture. The bottom grid shows what the areal saturation would look like in plan view.

the tail end, similar to case A.

The cluster in case A (Figure 3.26) is surrounded by smaller aperture segments. If these segments were filled with NAPL the pattern of dissolution for the cluster would be more similar to case B. Generally, NAPL is trapped in larger aperture segments. Naturally, these larger aperture segments are surrounded by smaller aperture segments. If these surrounding aperture segments contain no NAPL the dissolution patterns (such as mass output over time) will be similar to case A. If these surrounding aperture segments contain NAPL, then the dissolution pattern will be similar to case B.

The initial residual distribution patterns cannot all be simply identified as case A or case B type initial residual clusters. On the contrary, when looking at other cross-sections of case A, case B type residual cluster distributions can be found and vice-versa. The controlling factor is how many case A residual distributions there are compared to how many case B residual distributions. It is the relative distribution of these two cluster types that will determine which case the mass output will resemble. Because there is a spectrum of distribution types (i.e., some distributions have more case A distributions and some have less) there is a distribution of the mass output curves from type A to type B.

Despite the fact that the above behavior and their causes have been clearly identified, identifying a priori whether a residual pattern will produce a type A or type

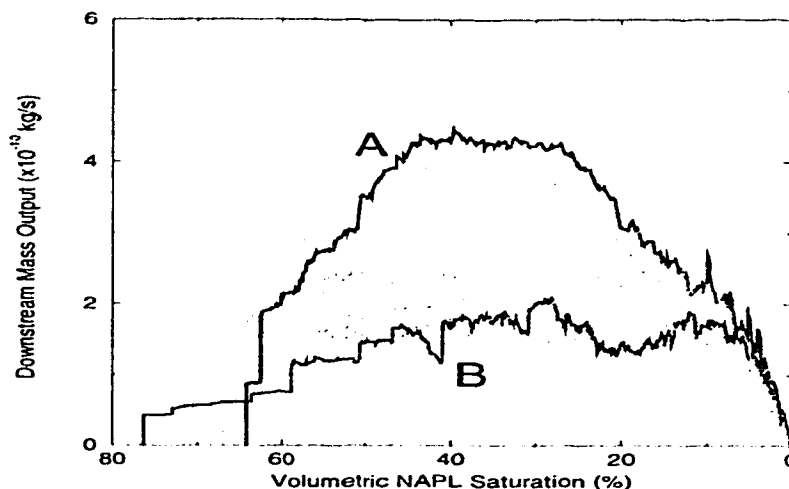


Figure 3.23: Downstream mass output versus volumetric saturation of the wetting phase. Two example realizations are highlighted.

B mass output result is difficult. It is especially difficult in these simulations since the random aperture distribution is the only real variable. There is some indication given by the initial NAPL saturation. For example, Figure 3.25 shows the two initial residual distribution for simulations that produced the A and B mass-output curves. Residual distribution B does have a greater saturation. However, in the scope of these simulations, the effect of the random field is just as important as the areal saturation of the initial residual NAPL.

3.3.2 Relative Transmissivity

Figure 3.27 shows the relative transmissivity curves for the 20 Monte Carlo simulations discussed above. The same distinction between the high mass-output curves and low mass-output curves (black versus grey) has been made. There is no apparent distinction in the paths the relative transmissivity curves follow between these two cases. In general, the grey curves (i.e., corresponding to simulations that have relatively longer dissolution times) have lower starting relative transmissivities similar to the example shown in Figure 3.14.

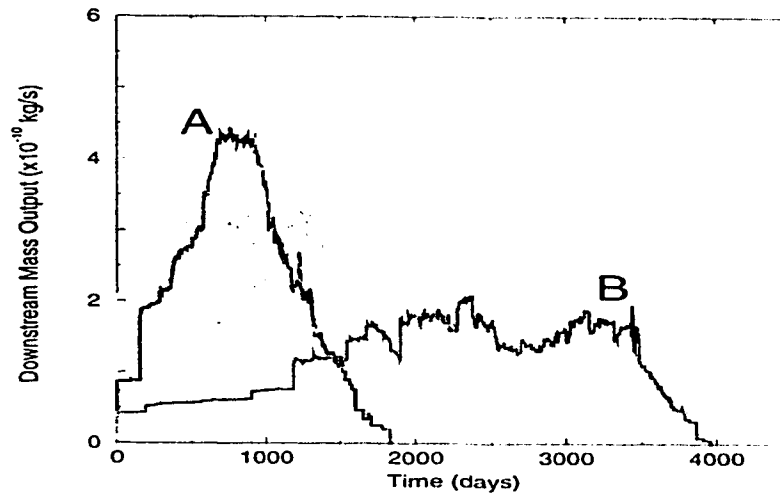


Figure 3.24: Downstream mass output versus time. Two example realizations are highlighted.

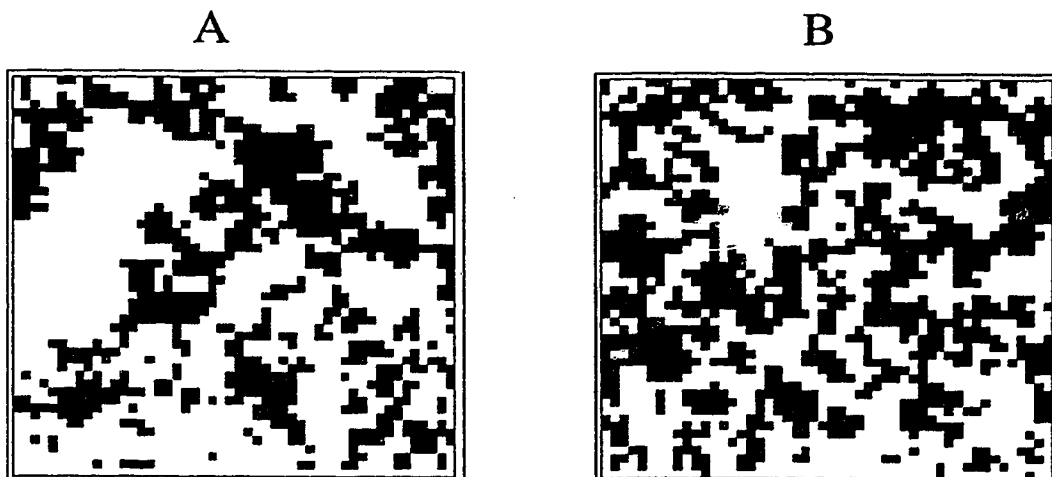


Figure 3.25: Initial residual distribution for cases A and B.

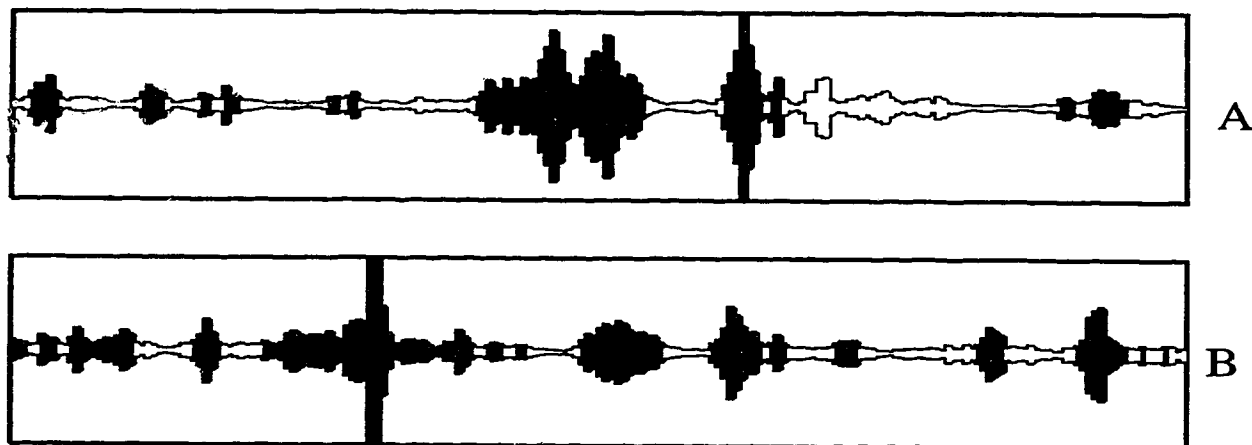


Figure 3.26: Cross sections taken through cases A and B.

These curves depend not only on the original placement of the NAPL as the mass output results do but, they also depend on the order of disappearance of NAPL. That is, when one cell containing NAPL is removed the transmissivity of the entire fracture will change accordingly. A cell may be right near a flow channel and affect the transmissivity dramatically when it disappears or it may have little effect on the relative transmissivity when it is removed.

Figure 3.28 shows the effect of varying the mass transfer coefficient and the average groundwater velocity on the relative transmissivity curves. Simulations were conducted on one random aperture field with the same initial invasion percolation distribution. The gradient was modified from $8 \times 10^{-5} m/m$ of water head to about $0.4 m/m$ of water head across the fracture. The mass transfer coefficient was modified from $1.5 cm/s$ to $2.5 cm/s$. The results show very little difference in the relative transmissivity curves which suggests that the NAPL is being dissolved in nearly the same order for every case, even though dissolution times can vary dramatically.

The one dotted curve in Figure 3.28 corresponds to a very low gradient case. Here the NAPL does dissolve in a slightly different order. This is due to the limiting right-hand boundary condition. The limitation of this boundary is that mass can only cross that boundary via groundwater advection. Because the groundwater velocity is low, more NAPL diffuses out the left hand-side boundary than exits at the right.

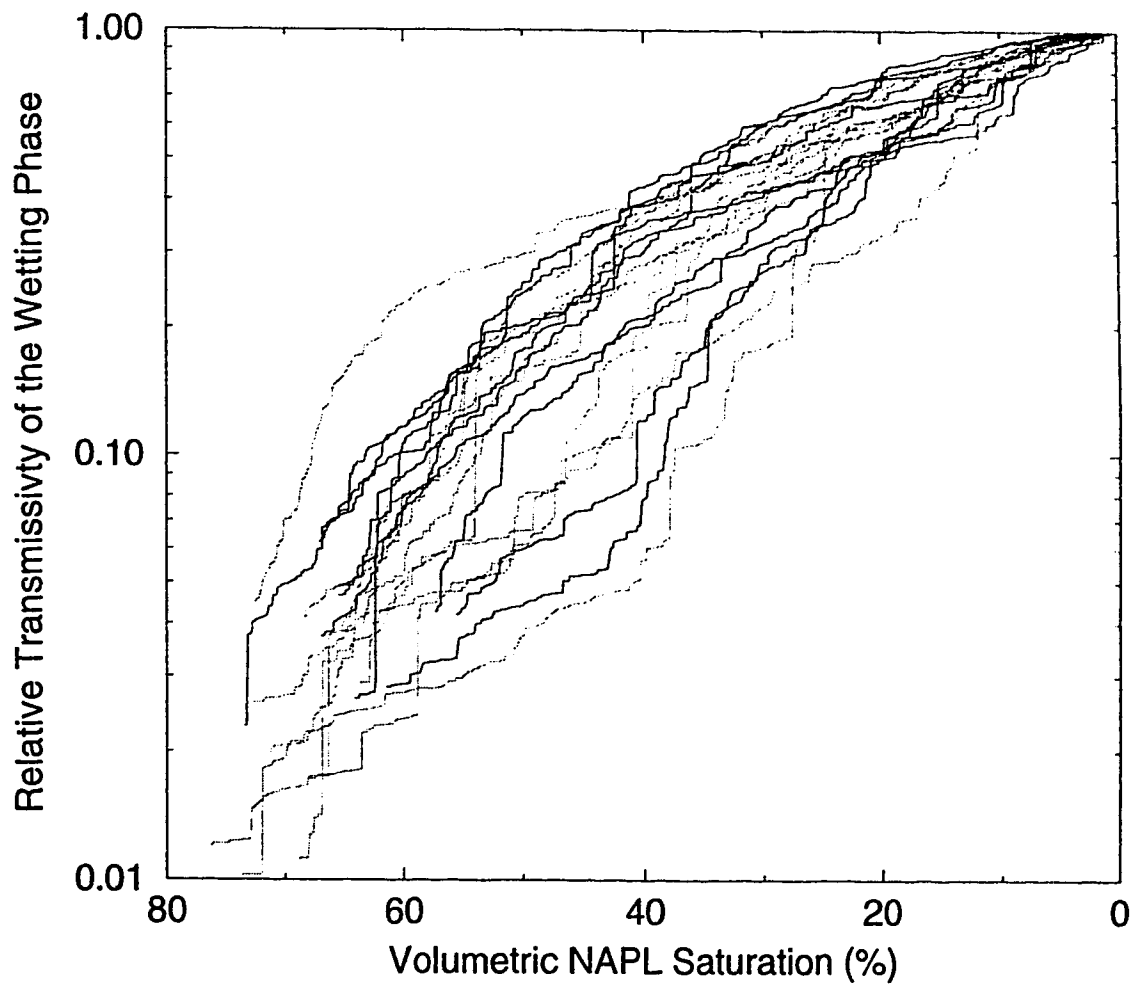


Figure 3.27: The relative transmissivity curve from the Monte Carlo analysis. The same black and grey separation of the curves is used.

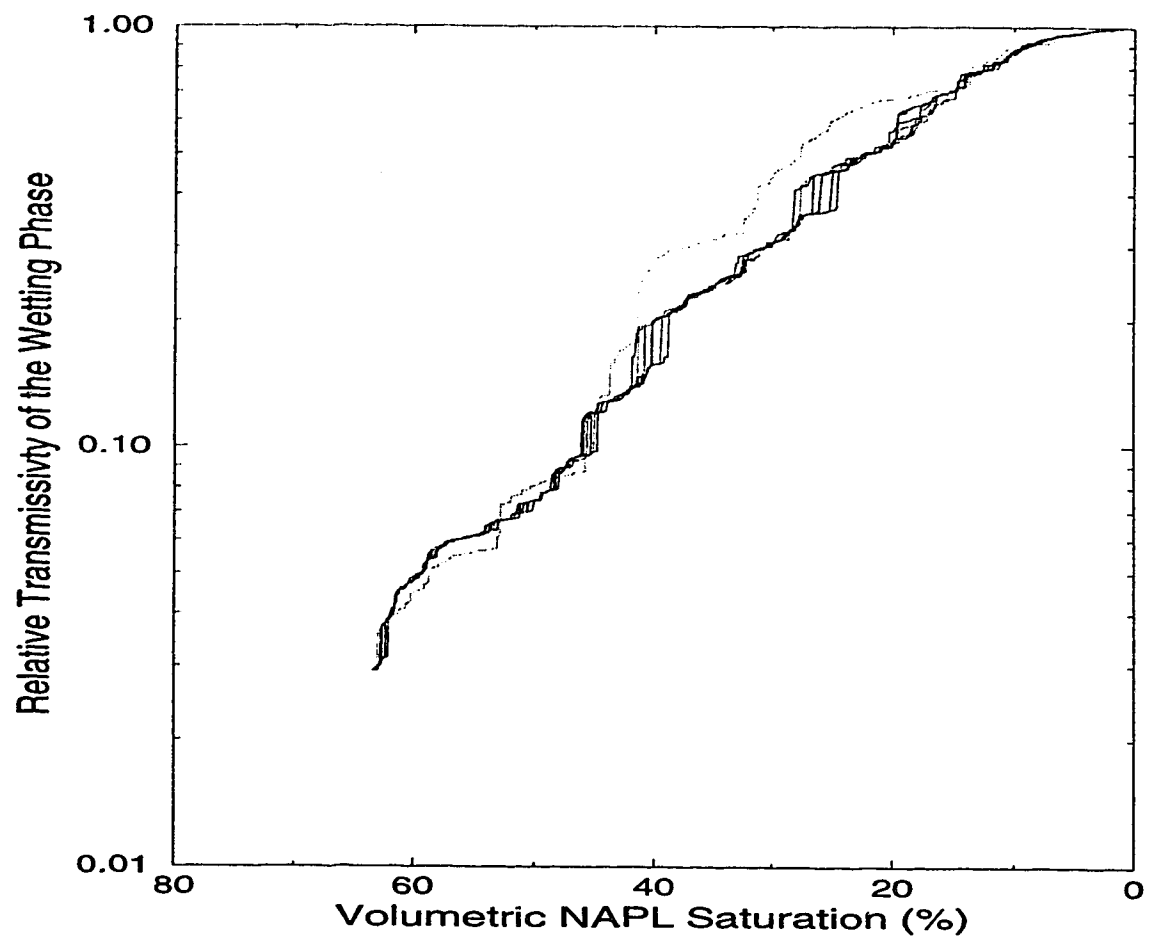


Figure 3.28: Relative transmissivity curves where the groundwater velocity and mass transfer coefficients are varied.

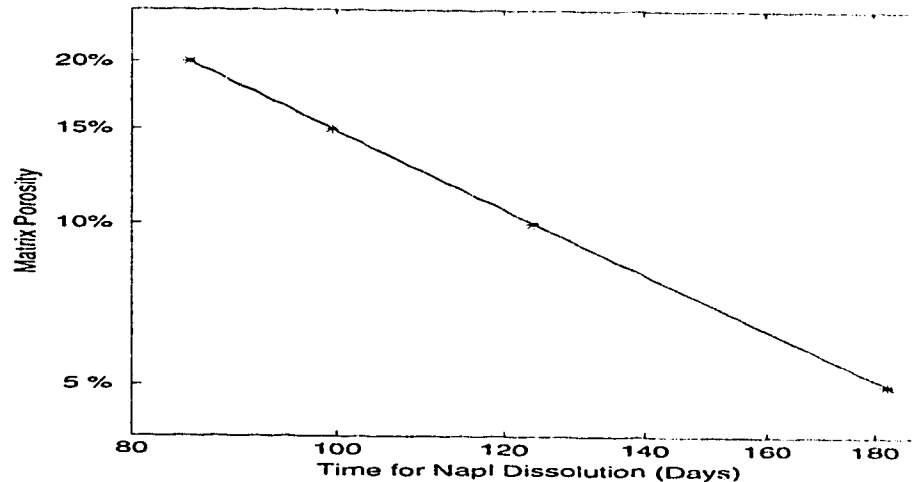


Figure 3.29: Plot of NAPL dissolution time versus matrix porosity.

3.4 Permeable Matrix

The results presented to this point have all dealt with fractures that have impermeable walls (i.e., the surrounding matrix has no porosity). However, recent research (Parker *et al.*, 1994) has indicated that a permeable matrix can have a large effect on NAPL dissolution time; a sample of this effect on dissolution is presented here.

Figure 3.29 shows a plot of the NAPL dissolution time versus the matrix porosity (note the plot is on a log-log scale). The simulations represented on this plot were conducted on a constant aperture field with the same invasion percolation N distribution. The grid used is smaller (25X25) than the previous sections; this was necessary because of the extra computational requirements involved in modeling both the fracture and the matrix. Each simulation was conducted with a different value for matrix porosity. The overall effect on the dissolution time is dramatic.

Matrix porosity is critical because the surface area available for NAPL-water contact with matrix water is much greater than the NAPL-water contact area with the fracture. Even though diffusion is a relatively slow process, much of the NAPL can migrate into the surrounding matrix. If the matrix is permeable, then the NAPL

of the dissolution time and output concentrations become even more complex. Material that is stored in the matrix will begin to slowly diffuse back into the fracture and act as a low-level, long-term source of groundwater contamination.

Chapter 4

Conclusions

This study modeled physical processes at the micro scale to investigate the dissolution of non-aqueous phase liquids in single, discrete, rough-walled fractures. The results indicate that micro-scale features, in particular the random aperture distribution of the rough-walled fracture, have large effects on the dissolution process.

Predicting NAPL dissolution times and concentrations for fractured material has been extremely elusive. A porous media analogue can be used to represent the contaminated fractured material. A conceptual porous media scenario usually involves blobs of NAPL (usually spheres) distributed through the porous media (e.g. *Powers* (1991)). However, porous media analogues do not account for the effects that the fractures have on the distribution and dissolution of NAPL. For accurate simulation of dissolution in field scale models, effects that the fracture system has on dissolution must be incorporated into the models. Because these effects are generally ignored (not to mention difficult or impossible to predict) accurate dissolution estimates may be difficult to produce.

In general, the results of the dissolution modeling are very sensitive to the aperture distribution within a rough-walled fracture. This sensitivity is particularly evident from examining the aqueous-phase mass output over time and the time necessary for complete dissolution of the residual NAPL: simulations using aperture distributions that are statistically similar can produce very different results. These results are closely related to the amount and spatial distribution of NAPL within the frac-

ture; however, the NAPL distribution is the result of invasion percolation which is ultimately controlled by the random aperture distribution. Because the results are extremely sensitive to an essentially random parameter (i.e., random aperture distribution) there is appreciable uncertainty.

As a result of the invasion percolation process, blobs of NAPL are located in the larger aperture spaces and are surrounded by smaller aperture spaces. The control this spatial arrangement has on the dissolution process is particularly evident in the mass-output curves, which in turn are a function of the output concentration and average relative transmissivity. A low dissolution rate occurs initially when the smaller NAPL cells are dissolving, while a mass output peak occurs when the larger, inner NAPL cells begin dissolving. The mass output then decreases at later time when only a few isolated zones of residual are present. Comparisons with random NAPL distributions further emphasize the importance of modeling the NAPL position within the fracture using a physically realistic scenario (i.e., invasion percolation). Low initial NAPL saturations will produce high rates of mass output over a short period of time whereas high initial NAPL saturations will produce low rates of mass output over a much longer period of time. The random aperture field and the NAPL distribution within the field also can have a significant effect on the mass-output results. Fractures with similar characteristics and initial NAPL saturations can have very different mass-output curves.

Following an initial rapid buildup, the average concentration exiting the fracture generally decreases steadily during the dissolution process. This decrease correlates with a decrease in the NAPL saturation, which decreases the water-NAPL contact area and an increase in the relative transmissivity, which increases the water flow rate through the fracture. In the field, low concentrations are generally interpreted to mean there is little or no NAPL free-phase contaminant present. Results from this study support this interpretation; however, it is important to acknowledge that even though the NAPL concentration is decreasing, the mass output of NAPL out of the fracture may be increasing due to increased water flow rates.

Relative to an assumption of phase equilibrium, the use of a rate-limited mass transfer process reduces the effect that increased groundwater velocity has on the time for NAPL dissolution. Remediation schemes using dissolution to remove residual contaminant may be improved by studying this relationship between the mass-transfer coefficient and the groundwater velocity.

The initial relative transmissivity of a fracture is highly dependent on the initial NAPL residual distribution; however, the change in relative transmissivity during the dissolution process is generally insensitive to the groundwater velocity and mass-transfer coefficient. In other words the NAPL disappears in roughly the same sequence regardless of the groundwater gradient or the mass-transfer coefficient.

An exception occurs for cases with very high initial saturations. In this case the initial effective transmissivities are so low that diffusion is the primary transport mechanism. The consequences of this are that the dissolution process is initially very slow and the relative transmissivity curve may follow a different path than for initial residual saturations in the same fracture. Of course, because transport by diffusion is generally very slow the dissolution time for the NAPL in the fracture increases substantially.

NAPL can rapidly diffuse into the surrounding matrix if it is porous. This matrix diffusion process adds to the complexity in predictions involving NAPL and fractured material. Aqueous-phase NAPL that is stored in the matrix can begin to diffuse back into the fracture once the original NAPL residual has completely dissolved. This reverse matrix diffusion would cause the fracture to continue to output low concentrations of NAPL over a long period of time; this is consistent with field observations (Kennedy and Lennox, 1995).

4.1 Implications

Results here have shown that predicting the dissolution character of a single fracture may be very difficult, or even impossible, given the usual lack of specific information about the fracture aperture distributions and corresponding NAPL saturation.

However, the general prediction of NAPL dissolution over an entire site still may be possible. By using a fracture network model, the individual mass outputs of single fractures may become less important and an average value of mass output and dissolution rate may be enough to make general predictions. This may be particularly true in fractured, porous media where the uptake of the dissolved-phase into the matrix will tend to integrate and smooth results.

The time required for NAPL in a fracture to completely dissolve is quite long; simulations conducted for the impermeable case averaged about seven years for the NAPL to completely dissolve (with clean water flowing into a 1 m square fracture). Extrapolating this to the field scale (i.e., a network model) would be difficult; however, it would be expected that NAPL dissolution at this scale would take a much longer time, possibly tens of years.

One limitation of the approach taken here, where only a single fracture is considered, is that the model does not account for flow bypassing the fracture containing NAPL. If the fracture has an appreciable NAPL saturation it will have a low transmissivity. Thus, water may bypass the fracture through either the surrounding matrix or adjacent fractures that do not contain NAPL. If this occurs then the mass output of the fracture system would be over-predicted, leading to a gross under-prediction of the required dissolution time. Another limiting feature of the modeling is that the water flowing into the fracture is assumed to be clean: that is, it contains no aqueous-phase NAPL. If it does contain some aqueous-phase NAPL then the dissolution time for the fracture segment under consideration would be increased since the mass transfer rate from the non-aqueous to the aqueous phase would be lower. Thus, the overall dissolution time for a fracture network would increase since water entering fractures downstream contains aqueous NAPL.

References

- Abriola, L. M., and Pinder, G. F. 1985. A Multiphase Approach to the Modeling of Porous Media Conamination by Organic Compounds 1. Equation Development. *Water Resources Research*, 21(1), 11–18.
- Brusseau, M. L. 1992. Rate-Limited Mass Transfer and Transport of Organic Solutes in Porous Media that Contains Immobile Immiscible Organic Liquid. *Water Resources Research*, 28(1), 33–45.
- Flick, E. W. 1985. *Industrial Solvents Handbook*. Third edn. Park Ridge, New Jersey, USA: Noyes Data Corporation.
- Fried, J. J., Muntzer, P., and Zillox, L. 1979. Groundwater pollution by transfer of oil hydrocarbons. *Ground Water*, 17(6), 586–594.
- Geller, J. T., and Hunt, J R. 1988 (July). *Non-aqueous phase organic liquids in the subsurface: dissolution kinetics in the saturaed zone*. Presented at the International Symposium on Processes Governing the Fate of Contaminants in the Subsurface Environment, Int. Assoc. of Water Pollut. Res. and Control, Stanford, Calif.
- Hardisty, P. E., Ross, S. D., Dabrowski, T.L., and Brown, A. 1995. Remediation of LNAPL in Fractured Rock: Theory and Application. *In: Solutions '95 International Congress XXVI*. International Association of Hydrogeologists, Edmonton, Alberta, Canada.

- Hunt, J. R., Sitar, N., and Udell, K. S. 1988a. Nonaqueous Phase Liquid Transport and Cleanup 1. Analysis of Mechanisms. *Water Resources Research*, 24(8), 1247–1258.
- Hunt, J. R., Sitar, N., and Udell, K. S. 1988b. Nonaqueous Phase Liquid Transport and Cleanup 2. Experimental studies. *Water Resources Research*, 24(8), 1259–1269.
- Huyakorn, P.S., and Pinder, G.F. 1983. *Computational Methods in Subsurface Flow*. San Diego, California, USA: Academic.
- Imhoff, P. T., Jaffe, P. R., and Pinder, G. F. 1993. An experimental study of complete dissolution of a nonaqueous liquid in a saturated porous media. *Water Resources Research*, 20(2), 307–320.
- Kennedy, C. A., and Lennox, W. C. 1995. A control volume model of solute transport in a single fracture. *Water Resources Research*, 31(2), 313–322.
- Lam, A. C., Schecter, R. S., and Wade, W.H. 1983. Mobilization of residual oil under equilibrium and non-equilibrium conditions. *Soc. Petrol. Enq. J.*, 23(6), 781–790.
- Larson, R. G., Davis, H. T, and Scriven, L. E. 1981. Displacement of residual non-wetting fluid from porous media. *Chemical Engineering Science*, 36, 75–85.
- Lowry, M. I., and Miller, C. T. 1995. Pore-scale modeling of nonwetting-phase residual in porous media. *Water Resources Research*, 31(3), 455–494.
- Mackay, D. M., Roberts, P. V., and Cherry, J. A. 1985. Transport of organic contaminants in groundwater. *Environ. Sci. Technol.*, 19(5), 364–392.
- Mendoza, C. A. 1992. *Capillary Pressure and Relative Transmissivity Relationships Describing Two-Phase Flow Through Rough-Walled Fractures in Geologic Materials*. Ph.D. thesis, University of Waterloo, Waterloo, Ontario, Canada.

- Parker, B. L., Gillham, R. W., and Cherry, J. A. 1994. Diffusive Disappearance of Immiscible-Phase Organic Liquids in Fractured Geologic Media. *Ground Water*, 32(5), 805–820.
- Pennell, K. D., Jin, M., Abriola, L. M., and Pope, G. A. 1994. Surface enhanced remediation of soil columns contaminated by residual tetrachloroethylene. *Journal of Contaminant Hydrogeology*, 16, 35–53.
- Powers, S. E., Loureiro, C. O., Abriola, L. M., and W. J. Weber, Jr. 1991. Theoretical Study of the Significance of Nonequilibrium Dissolution of Nonaqueous Phase Liquids in Subsurface Systems. *Water Resources Research*, 20(4), 463–477.
- Powers, S. E., Abriola, L. M., and W. J. Weber, Jr. 1994. An experimental investigation of nonaqueous phase liquid dissolution in saturated subsurface systems: Transient mass transfer rates. *Water Resources Research*, 30(2), 321–332.
- Robin, M. J. L., Gutjahr, A. L., Sudicky, E. A., and Wilson, J. L. 1993. Cross-Correlated Random Field Generation With the Direct Fourier Transform Method. *Water Resources Research*, 29(7), 2385 – 2397.
- Schwille, F. 1981. Groundwater Pollution in Porous Media by Fluids Immiscible with Water. *The Science of the Total Environment*, 21, 173–185.
- Schwille, F. 1988. *Dense Chlorinated Solvents in Porous and Fractured Media*. Chelsea, Michigan, USA: Lewis Publishers. Translated by James F. Pankow.
- Snow, D. T. 1970. The frequency and apertures of fractures in rock. *Int. J. Rock Mech. Min. Sci.*, 7(23).
- Sudicky, E. A., and Frind, E. O. 1982. Solute Transport in Fractured Porous Media. *Water Resources Research*, 18(6).
- Sudicky, E.A. 1986. *LINE2D*. Institute for Groundwater Research, University of Waterloo, Canada. Unpublished FORTRAN code.

- VanderKwaak, J. E. 1993. *Numerical Simulation of DNAPL Dissolution and Aqueous Phase Contaminant Transport in Discretely Fractured Porous Media*. M.Phil. thesis, University of Waterloo, Waterloo, Ontario, Canada.
- VanderLeeden, F., Troise, F.L., and Todd, D.K. 1990. *The Water Encyclopedia*. Second edn. Chelsea, Michigan, USA: Lewis Publishers.
- VanderWaarden, M., Bridie, L. A. M., and Groenewoud, W. M. 1971. Transport of mineral oil components to groundwater. *Water Res.*, 5, 213–226.